# ASSOCIATIONS BETWEEN CHLOROPHYLL AND WIND FORCING IN THE GULF OF MEXICO DERIVED FROM SATELLITE OBSERVATIONS

A Dissertation

by

MAUREEN C. TRNKA

BS, DePaul University, 2003
MS, Nova Southeastern University, 2008

Submitted in Partial Fulfillment of the Requirements for the Degree of

DOCTOR of PHILOSOPHY

in

COASTAL AND MARINE SYSTEM SCIENCE

Texas A&M University-Corpus Christi
Corpus Christi, Texas

August 2015

August 2015

# ASSOCIATIONS BETWEEN CHLOROPHYLL AND WIND FORCING IN THE GULF OF MEXICO DERIVED FROM SATELLITE OBSERVATIONS

A Dissertation

by

MAUREEN C. TRNKA

This dissertation meets the standards for scope and quality of
Texas A&M University-Corpus Christi and is hereby approved.

Alberto M. Mestas-Nuñez, PhD
Chair

Paul Zimba, PhD
Co-Chair

Thomas C. Shirley, PhD
Committee Member

Andrew Thomas, PhD
Committee Member

Magesh Thiyagarajan, PhD
Graduate Faculty Representative

August 2015

# ABSTRACT

The Gulf of Mexico supports many industries that rely on its natural resources. The standing stock of phytoplankton is important for the health of the ecosystem. Chlorophyll-*a* concentration is an effective indicator of phytoplankton biomass. Ocean color satellites make it possible to measure chlorophyll over large geographic areas; however, an individual sensor has limits. The GlobColour project merges observations from multiple satellites into one product. The purpose of this study is to use GlobColour and QuikSCAT to investigate the seasonal and non-seasonal associations between chlorophyll and wind from 2000-2008 in the Gulf of Mexico.

Chapter II provides an overview of the Gulf of Mexico's physical setting, circulation, and main features. The Gulf is divided into regional areas based on topographic features. Basin-wide phytoplankton biomass is discussed in the context of nutrient-transport mechanisms including coastal upwelling, Ekman pumping, horizontal advection, and vertical turbulent mixing.

In Chapter III, seasonal associations are evaluated between chlorophyll and wind using Empirical Orthogonal Functions and Singular Value Decomposition. Chlorophyll has strong variability over the shelves. The interior variability of chlorophyll and wind speed is in-phase with annual periodicity, increasing in winter and decreasing in summer. Strong winter winds increase the upward turbulent transport of nutrients into the mixed layer. The northern chlorophyll variability has a dipole with increased anomalies over the Western Shelf and decreased anomalies around the Mississippi mouth; associated with intensified easterly winds.

In Chapter IV, non-seasonal anomalies of chlorophyll and wind are similarly investigated. Increases in wind speed are associated with chlorophyll increases over the Campeche Bank, Bay of Campeche, and West Florida Shelf; the mechanism is upward

entrainment of nutrients by turbulent mixing. Northerly winds are associated with coastal upwelling in the Bay of Campeche, offshore advection in the west, and a chlorophyll dipole across the Mississippi mouth. The coupled patterns are predominantly intraseasonal and spatially coherent with interannual modulations.

This study is the first to apply a merged ocean color product to research in the Gulf of Mexico. Overall, this project provides baseline information on the seasonal and non-seasonal variability of chlorophyll and winds, identifies statistical associations, and proposes dynamical mechanisms.

# DEDICATION

This dissertation is dedicated to my seventh grade science teacher in Illinois, Mr. John Figlewicz. Mr. Fig is the most passionate and enthusiastic teacher I have ever encountered. His love of science is contagious. He was the first person to teach me the scientific method and helped me to create my very first research project. The excitement I felt at that time is what inspired me to pursue a career in science. My heartfelt gratitude goes out to Mr. Fig.

ACKNOWLEDGEMENTS

I acknowledge Dr. Alberto Mestas-Nuñez for his time and encouragement as my advisor and teacher. Dr. Paul Zimba was a helpful and thoughtful reviewer that provided excellent insights that I greatly appreciated. I offer sincere thanks to Dr. Thomas Shirley and Dr. Andrew Thomas for their expert knowledge in my area of research and for their editorial support. Thank you to Dr. Magesh Thiyagarajan, for dedicating his time and providing me with excellent professional advice and direction. I thank Patricia Rodriguez for her administrative assistance throughout my years as a student and instructor. I am indebted to Frank Kelly, my peer and friend, for teaching me MatLab and answering my seemingly endless number of questions. Frank, this project would not have been possible without you. I would like to acknowledge the professors of the CMSS program and the diverse educational experiences they provided. I would like to thank my friends near and far and my fellow students at TAMUCC who were my emotional support and confidants. Lastly, I am so grateful to my family for their continued support and patience while I have pursued my educational goals. I love you Mom, Dad, Monica, Bridgid, and Katie.

TABLE OF CONTENTS

LIST OF FIGURES

FIGURES PAGE

LIST OF TABLES

TABLES PAGE

# CHAPTER I: An introduction to the Gulf of Mexico and ocean remote sensing

## Introduction

The Gulf of Mexico is an ecotone of unique natural resources in the western hemisphere. Wetland areas surrounding the Gulf are an important source for both the seafood and shellfish industries, while offshore waters support commercial and recreational fisheries. Eddies and meanders that form from dynamic instabilities of the Loop Current are important in biological retention and recruitment. Lee et al. (1994) correlated the presence of the "Tortugas Gyre", a cold cyclonic recirculation that forms when the Loop Current enters the Florida Strait, with increased food supply, local retention, and shoreward transports for increased recruitment of spawned snapper and grouper species in the Florida Keys. In 2010, according to the National Marine Fisheries Service, the commercial fish and shellfish harvest from the five U.S. Gulf states (Texas, Louisiana, Mississippi, Alabama, and Florida) was estimated to be 1.3 billion pounds valued at $639 million. The Gulf of Mexico yields more finfish, shrimp, and shellfish annually than the south-Atlantic, mid-Atlantic, Chesapeake, and New England areas combined. The Gulf houses four of the top seven fishing ports domestically by weight and eight of the top twenty fishing ports by dollar value (Burkett and Davidson 2012).

The Gulf of Mexico is also a major source for oil and natural gas which are the main contributors to the geologically derived wealth of the basin (Nehring 1991). Oil accumulation controlled by salt uplifts is varied along with the geometry of salt structures themselves (Halbouty 1967). The Gulf basin is one of the largest petroleum reserves in the world and by the end of 1987 had a known recovery of 112.7 billion barrels of crude oil, 22.5 billion barrels of natural gas liquids, and 523.8 trillion $ft^3$ of natural gas, for a total of 22.5 billion barrels of oil equivalent (Nehring 1991). The Gulf of Mexico contains approximately 9% of the world's known recovery of crude oil and natural gas liquids, and approximately 11% of the world's

known recovery of natural gas. Only the Arabian-Iranian province contains more petroleum liquids, and only the Arabian-Iranian province and West Siberian provinces contain more natural gas (Nehring 1991).

Previous oceanographic research in the Gulf of Mexico has mostly focused on its two unique features: the Loop Current, and the Mississippi River plume (e.g., Sturges and Leben 2000, Rabalais et al. 2002a, 2002b). Along with these topics, episodic events like the passage of a major hurricane, (e.g., Katrina or Rita, see Day Jr. et al. 2007), or an oil spill (e.g., 2010 Deepwater Horizon; Malakoff 2012, Dietrich et al. 2014), spark new research interest in the area. With growing knowledge about the value of the Gulf's natural resources, more recent research has focused on issues such as local circulation and wind patterns (e.g., Sturges and Lugo-Fernandez 2005), fisheries (e.g., de Mutsert et al. 2008), and harmful algal blooms (e.g., Stumpf et al. 2003); all which affect the health and sustainability of the entire Gulf of Mexico system.

Since the late 1970s, remote sensing has been a valuable tool to study and monitor large oceanographic areas. Sea surface temperature has been monitored for over three decades by the use of thermal infrared and passive-microwave satellite sensors (e.g., Parkinson and Cavalieri 2008) while ocean color and altimetric sea level have existed globally for more than a decade (e.g., McClain 2009). The sampling pattern of satellite missions is designed to provide the maximum possible coverage in time and space. The data stream from one sensor alone, however, typically results in a product with gaps between swaths depending on the swath width of the sensor. One way to ameliorate these sampling problems is to merge datasets from multiple missions to improve data coverage in one unified product.

While merging of data from multiple sources has been used for sea surface temperature and altimetry, it is a rather new development for ocean color. Ocean color merging efforts have

recently taken place under NASA or ESA programs (e.g., Gregg and Conkright 2001, Kwiatkowska and Fargion 2002, Maritorena and Siegel 2005). The merging of ocean color datasets can result in improved, diverse data projects with fewer uncertainties (Maritorena et al. 2010). A good merging product should account for difference among the individual datasets, without creating bias, discontinuity or artifacts in the product it generates. The ESA GlobColour Project applies a model for ocean color data merging. The GSM01 model used for GlobColour chlorophyll data was described by Garver and Siegel (1997) and updated by Maritorena et al. (2002). This merged product uses data from SeaWiFS, AQUA, and MERIS daily water-leaving radiances for a time period common to all three sensors. The use of the GlobColour product has increased in recent years, however most studies apply the data on a global scale (e.g., Kahru et al. 2010, Maina et al. 2011, Cole et al. 2012). Application of the GlobColour product on smaller, regional areas has yet to be fully explored.

Research on remotely-sensed surface chlorophyll variability in the Gulf of Mexico has generally received less attention than other regions of the world ocean. In the U.S. coastal waters, ocean color research has focused highly productive areas such as the California Current System (e.g., Nezlin and Li 2003, Espinosa-Carreon et al. 2004, Venegas et al. 2008, Thomas et al. 2009). The 2010 Deepwater Horizon oil spill has brought national attention back to the Gulf of Mexico, in part because of the negative impacts of the spill on the natural resources the Gulf provides to the country. Previous studies of chlorophyll variability in the Gulf of Mexico have used single-sensor data (Martínez-López and Zavala-Hidalgo 2009, Salmerón-García et al. 2011). In addition, most previous studies of the Gulf of Mexico's response to surface wind forcing have focused on ocean currents (Cochrane and Kelly 1986, Oey 1995, Dubranna et al. 2011), with little effort devoted to relating the wind-driven responses by phytoplankton biomass.

The purpose of this study was to use remotely sensed monthly chlorophyll and wind forcing data from 2000-2008 to characterize their individual and coupled variability in the Gulf of Mexico. This study addresses the seasonal and non-seasonal components of the variability and applies, for the first time, a merged satellite dataset (i.e., GlobColour) to the Gulf of Mexico basin. Overall, this project provides baseline information on the variability of surface chlorophyll concentrations and wind stress forcing, identifies statistical associations between these two remotely sensed biological and physical variables, and proposes dynamic mechanisms that are consistent with these associations.

References

Burkett VR, Davidson MA (eds) (2012) Coastal impacts, adaptation, and vulnerabilities: A technical input to the 2013 national climate assessment. Cooperative Report to the 2013 National Climate Assessment, Island Press, 150 pp

Cochrane JD, Kelly FJ (1986) Low-frequency circulation on the Texas-Louisiana continental shelf. J Geophys Res 91:10645-10659

Cole HS, Henson S, Martin A, Yool A (2012) Mind the gap: The impact of missing data on the calculation of phytoplankton phenology metrics. J Geophys Res 117:C08030, doi:10.1029/2012JC008249

Day Jr. JW, Boesch DF, Clairain EJ, Kemp GP, Laska SB, Mitsch WJ, Orth K, Mashriqui H, Reed DJ, Shabman L, Simenstad CA, Streever BJ, Twilley RR, Watson CC, Wells JT, Whigham DF (2007) Restoration of the Mississippi Delta: lessons learned from Hurricane Katrina and Rita. Science 315:1679-1684

Dietrich, DE, Bowman, MJ, Korotenko, KA, Bowman, MHE (2014) Oil Spill Risk Management: Modeling Gulf of Mexico Circulation and Oil Dispersal. John Wiley & Sons, 240 pp

Dubranna J, Pérez-Brunius P, López M, Candela J (2011) Circulation over the continental shelf of the western and southwestern Gulf of Mexico. J Geophys Res 116:C08009, doi:10.1029/2011JC007007

Espinosa-Carreon TL, Strub PT, Beier E, Ocampo-Torres F, Gaxiola-Castro G (2004) Seasonal and interannual variability of satellite-derived chlorophyll pigment, surface height, and temperature off Baja California. J Geophys Res 109:C03039, doi:10.1029/2003JC002105

Garver SA, Siegel DA (1997) Inherent optical property inversion of ocean color spectra and its biogeochemical interpretation: I. Time series from the Sargasso Sea. J Geophys Res

102:18607-18625

Gregg WW, Conkright ME (2001) Global seasonal climatologies of ocean chlorophyll: Blending in situ and satellite data for the coastal zone color scanner era. J Geophys Res 106:2499-2516

Halbouty MT (1967) Salt domes, Gulf region-United States and Mexico. Gulf Publishing, Houston, 425 p

Kahru M, Gille ST, Murtugudde R, Strutton PG, Manzano MS, Wang H, Mitchell BG (2010) Correlations between winds and ocean chlorophyll. J Geophys Res 115:C12040, doi:10.1029/2010JC006500

Kwiatkowska EJ, Fargion GS (2002) Merger of ocean color data from multiple satellite missions within the SIMBIOS project. Proc SPIE symp - Remote sensing of the atmosphere, ocean, environment and space. Ocean remote sensing and applications. Hangzhou, China. 4892:168-182

Lee TN, Clarke ME, Williams E, Szmant AF, Berger T (1994) Evolution of the Tortugas gyre and its influence on recruitment in the Florida Keys. Bull Mar Sci 54:621-646

Maina J, McClanahan TR, Venus V, Ateweberhan M, Madin J (2011) Global gradients of coral exposure to environmental stresses and implications for local management. PLoS One 6:e23064, doi:10.1371/journal.pone.0023064

Malakoff D (2012) BP criminal case generates record payout for science and restoration. Science 338:1137, doi:10.1371/journal.pone.0023064

Maritorena S, Fanton d'Andon OH, Mangin A, Siegel DA (2010) Merged satellite ocean color data products using a bio-optical model: Characteristics, benefits, and issues. Remote Sensing Env 114:1791-1804

Maritorena S, Siegel DA, Peterson A (2002) Optimization of a semi-analytical ocean color model for global scale applications. Appl Opt 41:2705-2714

Maritorena S, Siegel DA (2005) Consistent merging of satellite ocean color data sets using a bio-optical model. Remote Sensing Env 94:429-440

Martínez-López B, Zavala-Hidalgo J (2009) Seasonal and interannual variability of cross-shelf transports of chlorophyll in the Gulf of Mexico. J Mar Sys 77:1-20

McClain CR (2009) A decade of satellite ocean color observations. Ann Rev Mar Sci 1:19-42

de Mutsert K, Cowan Jr. JH, Essington TE, Hilborn R (2008) Reanalyses of Gulf of Mexico fisheries data: Landings can be misleading in assessments of fisheries and fisheries ecosystems. Proc Natl Acad Sci 105:2740-2744

Nehring R (1991) Oil and gas resources. In: Salvador A (ed) The Gulf of Mexico Basin. Geological Society of America, The Geology of North America, Boulder, CO, p 445-494

Nezlin NP, Li B-L (2003) Time-series analysis of remote-sensed chlorophyll and environmental factors in the Santa Monica-San Pedro Basin off Southern California. J Mar Sys 39:185-202

Oey L (1995) Eddy and wind-forced shelf circulation. J Geophys Res 100:8621-8637

Parkinson CL, Cavalieri DJ (2008) Artic sea ice variability and trends, 1979-2006. J Geophys Res 113:C07003, doi:10.1029/2007JC004558

Rabalais NN, Turner RE, Dortch Q, Justic D, Bierman Jr. VJ, Wiseman Jr. WJ (2002a) Nutrient-enhanced productivity in the northern Gulf of Mexico: past, present and future. Hydrobiologia 475/476:39-63

Rabalais NN, Turner RE, Wiseman Jr. WJ (2002b) Gulf of Mexico hypoxia, aka "the dead zone". Annu Rev Ecol Syst 33:235-263

Salmerón-García O, Zavala-Hidalgo J, Mateos-Jasso A, Romero-Centeno R (2011) Regionalization of the Gulf of Mexico from space-time chlorophyll-a concentration variability. Ocean Dynamics 61:439-448

Stumpf RP, Culver ME, Tester PA, Tomlinson M, Kirkpatrick GJ, Pederson BA, Truby E, Ransibrahmanakul V, Soracco M (2003) Monitoring *Karenia brevis* blooms in the Gulf of Mexico using satellite ocean color imagery and other data. Harmful Algae 2:147-160

Sturges W, Leben R (2000) Frequency of ring separations from the Loop Current in the Gulf of Mexico, a revised estimate. J Phys Oceangr 30:1814-1819

Sturges W, Lugo-Fernandez A (eds) (2005) Circulation in the Gulf of Mexico: observations and models. Geophys Monogr Ser. AGU, Washington, DC, 161:360 pp

Thomas AC, Brickley P, Weatherbee R (2009) Interannual variability in chlorophyll concentrations in the Humboldt and California Current Systems. Prog Oceanogr 83:386-392

Venegas RM, Strub PT, Beier E, Letelier R, Thomas AC, Cowles T, James C, Soto-Mardones L, Cabrera C (2008) Satellite-derived variability in chlorophyll, wind stress, sea surface height, and temperature in the northern California Current System. J Geophys Res 113:C03015, doi:10.1029/2007JC004481

# CHAPTER II: A synopsis of the physical setting, general circulation, primary productivity, and nutrient transport of the Gulf of Mexico

Abstract

An overview of the physical setting, general circulation, primary productivity, and nutrient transport of the Gulf of Mexico is presented. The formation of the Gulf of Mexico in the Late Triassic era led to a distinctive basin with dynamic features. General knowledge about the Gulf has grown over the years to include more detailed accounts of the Loop Current and its eddies, nutrient inputs and movement, as well as phytoplankton biomass patterns. Based on topographic features, the Gulf is divided into regional areas of interest: Interior Basin, located in the central region; West Florida Shelf, including the Alabama-Mississippi Shelf to east and northeast; Louisiana-Texas Shelf, to the north and northwest; Tamaulipas-Veracruz Shelf, to the west; Bay of Campeche, to the southwest; and Campeche Bank, to the south. The physical characteristics of each area are reviewed along with a discussion of their respective circulation patterns. Basin-wide phytoplankton biomass is presented in the context of coastal upwelling, Ekman pumping, horizontal advection of nutrient-rich waters, and vertical mixing and turbulence.

## Introduction

The Gulf of Mexico (GoM) is a circular basin with a diameter of approximately 1,500 km (Salvador 1991) and two openings to adjacent bodies of water, namely the Yucatan Channel and the Florida Strait (Fig. 2.1). Although the Gulf is semi-enclosed, it contains many of the circulation features that are found in larger ocean basins (Hofmann and Worley 1986). It is bounded on the north, northeast and northwest by the United States, on the southeast by Cuba, and on the south and southwest by Mexico.

The area of the Gulf basin is approximately 1.5 million km² and almost half of this area consists of continental shelf waters with depths shallower than 200 m (Fig. 2.1) (Salvador 1991). The deepest part of the Gulf is found at the Sigsbee Deep, an irregular trough more than 560 km long in the southwestern region with depths exceeding 4,300 m (Liddell 2007). The whole basin contains a volume of roughly 2498 quadrillion liters ($2.5 \times 10^6$ km$^3$) of water with a mean depth of ~1,615 m (Turner 1999). The Gulf of Mexico originated in the Late Triassic (c. 220 Ma) with the rifting of Pangea and separation of the North American, South American, and African plates (Liddell 2007). Subsiding rift basins were filled with volcanic rocks and extensive salts were deposited while shelves were established around the basin margins (Liddell 2007).

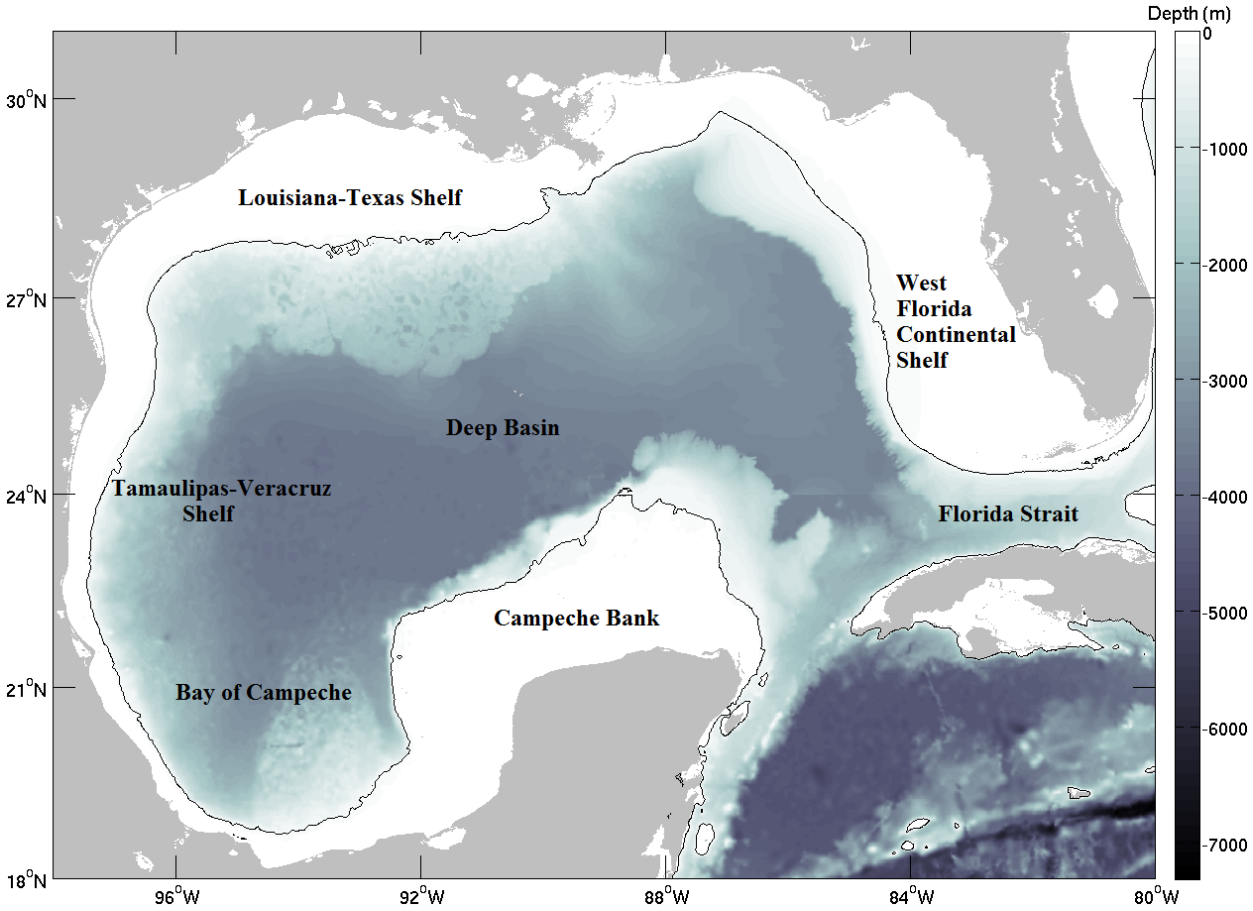


Fig. 2.1 Topography of the Gulf of Mexico with the 200 m isobath defining the continental shelf break (solid black line).

The floor of the Gulf of Mexico rises steeply to the east and south along the Florida and Campeche escarpments. Throughout the rest of the basin, the floor rises more gently and smoothly towards the coast through generally well-defined slope and continental shelf physiographic provinces (Salvador 1991). Based on the main coastal and topographic features, the Gulf of Mexico can be divided into six major regional areas: (a) Interior basin, located in the deep central region; (b) West Florida Shelf, including the Alabama-Mississippi Shelf to the east and northeast; (c) Louisiana-Texas Shelf, to the north and northwest; (d) Tamaulipas-Veracruz Shelf, to the west; (e) Bay of Campeche, to the southwest; and (f) Campeche Bank, to the south (Fig. 2.1).

Climatologically, the Gulf of Mexico is in a transitional area between the tropical and subtropical zones at midlatitudes (18°N to 30°N). High-pressure atmospheric cells alternate on short and seasonal timescales in the Gulf, which affects the air masses present over the land and their circulation surrounding the basin. This seasonality has a major impact on the climate over the Gulf of Mexico; frontal intrusions and the presence of cold air may have increased frequency during winter months (De Velasco and Winant 1996).

## 2.1 Physical Description of the Gulf of Mexico

### 2.1.1 Interior Basin

The interior basin of the Gulf is divided into three parts: the continental rise, the Sigsbee Abyssal Plain, and the Mississippi Cone (Antoine 1972). The continental rise was created by a build-up of sediments that were transported north toward the basin by tectonic movements. The lack of sediment input from the south and east is evidenced by the lack of rises abutting the steep escarpments of Florida and the Campeche Bank (Antoine 1972). The Sigsbee Abyssal Plain,

located northwest of the Campeche Bank, has a deep, relatively flat topography. The only topographic irregularities in this area of the Gulf are the Sigsbee Knolls and other small salt domes (Antoine 1972). The Mississippi Cone is characterized by soft sediments and extends to the southeast from the Mississippi Trough, merging with other sediment types in the central basin. The Mississippi cone is located between the DeSoto Canyon to the east and the Mississippi Trough to the west (Ewing et al. 1958).

The term "hurricane heat potential" was first defined as the integrated vertical temperature from the sea surface to the depth of the 26° isotherm by Leipper and Volgenau (1972). They found that hurricane heat potential the Gulf of Mexico varies geographically and interannually. In four summers, heat potential ranged from 700 cal $cm^{-2}$ north of the Yucatan to 31,600 in the central east Gulf. To know the hurricane heat potential, the vertical structure of the water must be considered in conjunction with the sea surface temperature patterns (Leipper and Volgenau 1972).

### 2.1.2 West Florida Shelf

The northeastern Gulf of Mexico can be defined as the region that extends from east of the Mississippi mouth, eastward up to the eastern side of Apalachee Bay of Florida. The DeSoto canyon is off the coast of the Florida-Alabama border and is an indentation in the Florida Shelf. In the east, sediments from the Mississippi River cover the western edge of the Florida Carbonate Platform. The Florida Platform is separated from the Gulf Basin by the Florida Escarpment and forms the southeastern side of the DeSoto Canyon. It has been suggested that the DeSoto canyon was formed by erosion possibly caused by Loop Current circulation (Nowlin 1971).

The South Florida continental shelf and slope is a submerged section of the larger Florida Peninsula. This region extends from Apalachee Bay to the Straits of Florida and includes the Dry Tortugas and Florida Keys. Carbonate-based sediments are present in this area and progress from north to south with thicker sediments along the southern region of Florida. The area of south of the Florida peninsula was closed toward the east during the Cretaceous time by a barrier reef (Antoine and Ewing 1963, Ewing et al. 1966, Sheridan et al. 1966). The Jordan Knoll in the Florida Straits appears to be remnants from this ancient barrier reef system. Historically, this reef may have extended across the straits and adjoined Florida with northern Cuba (Antoine 1972).

### 2.1.3 Louisiana-Texas Shelf

The Louisiana-Texas Shelf (LATEX) includes the shelf region from the Rio Grande to the Mississippi Delta with a shelf break in depths of about 75 to 100 m. One major structural element of this area is the Gulf Coast Geosyncline (Antoine 1972). Major salt deposits throughout the northern Gulf region were deposited in the Middle Jurassic and gave rise to salt diapers, such as the Flower Garden Banks (Liddell 2007). A major portion of the geosyncline offshore of Texas and Louisiana are characterized by buried salt deposits. On the continental shelf the diapiric salt structures are subsurface, however on the continental slope they appear as topographic features (Antoine 1972).

The LATEX coast is arcuate and concave to the southeast. The Rio Grande the shelf is narrow, about 85 km in width; widens to about 200 km off Cameron, Louisiana and then disappears at the Mississippi Delta. In its central portion, the shelf is fairly wide and flat. Near the Mississippi Delta is a submarine canyon. A number of reefs are found along the outer edge

of the shelf (i.e., The Flower Garden Banks). In contrast to the shelf, the topography of the continental slope is quite complex. The LATEX Shelf is considerably more shallow and wider than the shelf off the Pacific coast of the United States, and it is comparable in depth to the West Florida Shelf with an average depth of ~25 meters (Zavala-Hidalgo et al. 2003b).

### 2.1.4 Tamaulipas-Veracruz Shelf

Located between the Mexican state of Veracruz to the south and the Rio Grande to the north, the Tamaulipas-Veracruz Shelf spans the entire eastern shore of Mexico. Major topographic features are the gentle folds that parallel the shore. These folds have a wave length of 5-6 miles and a total relief of 12-1500 feet (Antoine 1972). Along the western Gulf, high rainfall delivers fine-grained terrigenous sediments to Gulf waters (Liddell 2007). Despite heavy sediment input, reefs do occur in these waters.

Reefs occur near the shelf edge (i.e., Tuxpan Reef system and Veracruz Reef System), approximately 100-200 km from the Yucatán Peninsula coastline (Liddell 2007). Reefs are absent north of Tampico, because of the upwelling of cold winter water (Glynn 1973). No reefs are present to the south of the Veracruz Reef System because of upwelling (Ferré-D'Amaré 1985).

### 2.1.5 Bay of Campeche

The Bay of Campeche is an isthmian embayment that extends west from the Campeche Bank to the offshore regions east of Veracruz, bounded on the south and southwest by the Sierra Madre Oriental with a maximum depth of ~55 m (Antoine 1972). The coastal plain of the Bay is low, poorly drained and swampy, similar to the Texas-Louisiana coastal plain (Antoine 1972).

The offshore topography is complex and distinguished by long parallel ridges that running along the outside of the basin. Bay of Campeche contains salt domes, and the upward migration of salt through overlaying sediments contributes to complex bottom profiles (Worzel et al. 1968). Both the northern Gulf and Bay of Campeche physiographic settings are similar and are both characterized by deep thicknesses of Tertiary clastic sediments (Antoine 1972).

### 2.1.6 Campeche Bank

The Yucatán Platform includes the exposed Yucatán Peninsula and the submerged shelf of the Campeche Bank. The platform has flat-lying carbonate sediments of 3-4 km depths that date back to the Late Cretaceous period (Liddell 2007). The Campeche Bank is the site of numerous bank reefs with atoll structures (i.e., Cayos Arcas, Triángulos, Cayo Arenas, and Alacrán Reef). It is bounded to the west by the Yucatán Escarpment, to the north by the Yucatán Terrace, and to the east by the Yucatán Strait (Bryant et al. 1991). The western border of the Campeche Bank is similar to the DeSoto Canyon transition zone in the northern Gulf as the carbonate sediments are replaced by terrigenous clastics (Antoine 1972).

The Campeche shelf is broad to the north and west, approximately 240 km in width, and narrows to the east along the Caribbean boundary with an average depth of ~50 m. Minimal surface drainage and limited sediment transport are present in the Campeche Bank waters because of a lack of land run-off (Liddell 2007).

## 2.2 Circulation of the Gulf of Mexico

### 2.2.1 Interior Basin

The general circulation in the interior Gulf (north of the Bay of Campeche) is dominated by two semi-permanent large-scale features: (1) the very energetic Loop Current in the eastern half; a component of the Gulf Stream current system, and (2) a large, weaker anticyclonic gyre in the western half, with its characteristic Western Boundary Current (Behringer et al. 1977). The Loop Current flows clockwise connecting the Yucatan Current which flows into the Gulf through the Yucatan Strait, and the Florida Current which flows out of the Gulf through the Florida Straits (Hofmann and Worley 1986). The Loop Current forms large meanders that can penetrate deep into the northern Gulf and separate forming large anticyclonic eddies (Fig. 2.2) (Beringher et al. 1977). The Loop Current can also intrude onto the west Florida continental shelf (Huh et al. 1981). A near surface velocity field in the GoM using drifter data from 1989-1999 was described by Dimarco et al. (2005). An anticyclonic gyre-like circulation was found in the upper water layer throughout deep-water regions of the western GoM (~22-26°N). The anticyclonic flow pattern had a defined northward boundary current structure in the western Gulf, attributed to forcing from eddies and wind. A profile of $^{129}I$ in the waters of the western Gulf of Mexico was presented by Schink et al. (1995). They found that the upper waters are enriched in $^{129}I$ approximately sixty-fold over the natural deep water values. The build-up of new $^{129}I$ in the upper waters confirms the rapid transport of waters from the northern North Atlantic through the Caribbean and into the Gulf.

The eddy field created by the Loop Current affects most aspects of the circulation patterns of the entire GoM (Sturges and Leben 2000). As anticyclonic warm-core eddies are shed from the Loop Current, they propagate into the western Gulf while cyclonic features can

cleave these anticyclonic rings into smaller eddies (Biggs et al. 1996). An IR satellite dataset from 1973-1993 (Sturges 1994) demonstrated the time between ring shedding events had two modes; one at 8-9 months and one at 13-14 months. These modes were the amount of time it took for the ring to separate from the Loop Current after formation had occurred. Sturges and Leben (2000) used an updated and expanded dataset to revise these previous findings. They examined maps of sea surface topography and corrected TOPEX data while following a similar method used by Sturges (1994) to compile ring-separation events from 1973-1999. They found that ring separations occurred at 6 months and 11 months after formation with a smaller peak at 9 months. No statistically significant power existed at the annual frequency of 12 months. This research was expanded by Leben (2005) to find that eddy separation interval varies from a couple weeks up to ~18 months. Separation intervals cluster near 4.5-7, 11.5, and 17-18.5 months; suggesting a length of 6 months between occurrences. Several proposed mechanisms exist to explain why the Loop Current and its shedding process act in a semi-erratic manner. The erratic nature of eddy shedding intervals occurred at the lowest eddy viscosity was noted by Hurlburt (1986). Oey's (1996) model yielded irregular separation times because of the local unpredictable behavior of the Loop Current, and later Oey et al. (2003) proposed an "upstream influence", with conditions dependent on the Caribbean Sea and flow transports from the Atlantic and Greater and Lesser Antilles Passages. The relationship between separation interval and the latitude of the Loop Current at the time separation affects the shedding process was suggested by Leben (2005).

In general, anticyclonic eddies have diameters of 200-400 km and maximum surface current speeds of 1-2 m/s (Huh and Schaudt 1990, Cooper et al. 1990, Forristall et al. 1992). They move westward and will collide with the continental shelf slope, lose energy, then usually

move northward towards the LATEX shelf (Lewis and Kirwan 1985, Vidal et al. 1992). Cold-core cyclonic eddies have diameters of 50-150 km and are usually formed from the interaction of anticyclonic rings with the shelf (Lewis et al. 1989, Hamilton 1992). When these rings encounter the shelf, cyclonic-anticyclonic eddy pairs are formed that affect surface current variability along the outer edge of the continental shelf (Brooks and Legeckis 1982, Oey 1995). The time scales of energy transfer from large eddies to smaller ones with phytoplankton growth was studied by Platt and Denman (1980). They found that eddies of the order of 100 km may be characterized by the time taken for transfer of half of their kinetic energy to eddies of half the original size. When this is less than the generation time of phytoplankton, they suggest patches are destroyed and where it is more, patches persist. The critical dimension in the ocean is around 1 km and larger eddies which have diameters of 200-300 km retain their phytoplankton for as long as they persist.

Although the upper layer mean flow in the central and northwestern Gulf is anticyclonic, DeHaan and Sturges (2005) found that the average flow near the edges of the GoM below approximately 2000 m is cyclonic. Their reasoning to explain the deep cyclonic flow was based on rectification of deep topographic Rossby waves by bottom friction. Mizuta and Hogg (2004) found divergence of the vertically integrated Reynolds stress was caused by bottom friction, which in turn induces a mean along-slope flow direction cyclonically (i.e., shallower water on the right going down-current). The process of Ekman pumping links the mean current flow with the Reynolds stresses associated with the wave field. The surface flow in the western Gulf is pumped down to depth and leaves the Gulf via deep flow through the Yucatan Channel and Straits of Florida (Sturges and Kenyon 2008).

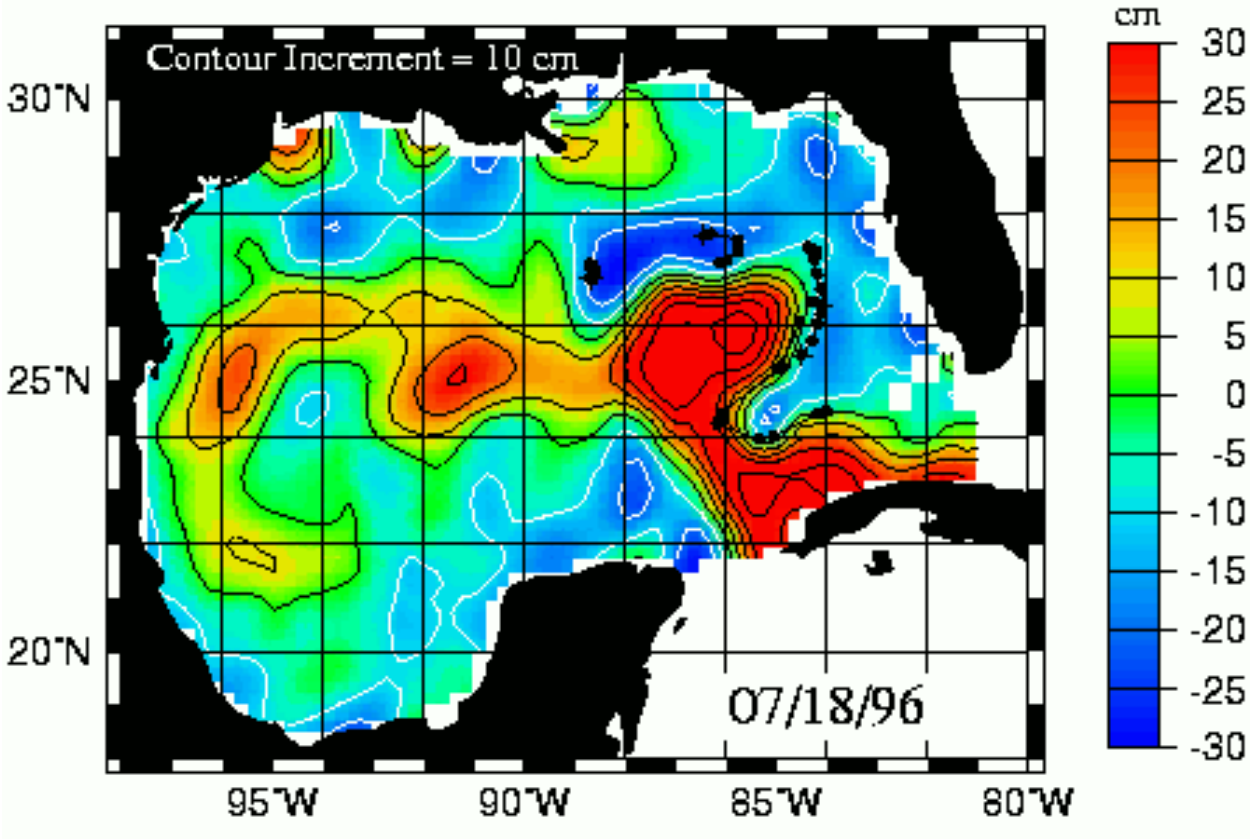


Fig. 2.2 Blended ERS-2/TOPEX dynamic topography in the Gulf of Mexico for July 18, 1996, from surface drifter data with the location of the Loop Current and eddies. Image modified from earth.esa.int.

A shelf break separates the wide continental shelves of the Gulf from the deep ocean circulation. The Loop Current and the eddies that shed from it dominate the surface circulation within the central Gulf basin. Eddy detachment may occur after the Loop Current is pinched-down or necked-down by cyclones. However, not every necking-down occurrence results in a detachment. Sea surface height maps have examples of strong reattachment events, where a previously detached eddy is reattached to the Loop Current (Schmitz et al. 2005). These features have depth ranges of several hundred to one thousand meters (Mooers and Maul 1998) and because of vorticity conservation, tend to remain offshore beyond shelf areas. However, they interact with the shelf water at the shelf break resulting in water exchange between the shelf edge and the deep ocean (Vidal et al. 1992). No annual cycle exists for these eddies or the Loop

Current, but there are preferential locations for cross-shelf water exchange. Continental shelf waters are strongly influenced by local surface forcing and the influx of fresh water from rivers. Therefore, the properties of shelf waters exhibit strong seasonal variability (Morey et al. 2005).

### 2.2.2 West Florida Shelf

The West Florida Shelf is one of the broadest continental shelves in North America. In general, shelf circulation is driven forcing from deep ocean and shelf waters. Local forcing is typically driven by surface momentum from winds and buoyancy fluxes from land-derived fresh water fluxes while deep forcing and fluxes are transported along the shelf break. The West Florida Shelf geometry is that of a steadily sloping inner shelf that is separated from the slope edge by a large shelf width (Weisberg et al. 1996).

Over the Florida shelf, a weak counterclockwise flow exists which is related to the penetration of the Loop current. Long-term observations of the West Florida Shelf have circulation forced by tides, winds, and Loop Current interactions varies on scales from semi-diurnal to inter-annual (Weisberg et al. 1996). The interaction of surface and bottom Ekman layers on the inner shelf produce an across-shelf sea level slope and a geostrophic interior flow. The inner shelf is separated from the shelf break because of the large shelf width. Farther northwest on the shelf, the width decreases and the inner shelf extends beyond the shelf break (Weisberg et al. 1996).

Strong forcing magnitudes affect deep ocean waters by allowing them to broach the shelf break and be advected to the southeast (due mostly to the bottom Ekman layer). During "normal" conditions, there is separation in the south between the inner and outer shelves resulting in the inner shelf being insulated from the deep ocean waters while upwelling-favorable

winds recycle nutrient-depleted inner shelf water. However, during anomalous conditions, the deep ocean properties can flow directly from the shelf break to the land (Weisberg et al. 2005).

The physical mechanisms of the region are include the formation of a cyclonic meander/eddy in the spring between the Loop Current to the west and the Florida Escarpment to the east (Vukovich and Maul, 1985). The Loop Current has cold, biologically rich, upwelling features that can develop into cyclonic, cold-core eddies. In this region, Bluefin tuna catch inside a cold-core meander was three times higher than in the central Gulf (Maul et al. 1984).

### 2.2.3 Louisiana-Texas Shelf

Louisiana-Texas (LATEX) shelf circulation is driven by the slope eddy field and regional wind field (e.g., Ohlmann and Niiler 2005). Surface circulation on the inner shelf (< 30 m water depth), is predominantly driven by the wind (Walker 2005). Wind stress toward the west results in flow in the same direction on the inner Louisiana shelf along the Texas coast (Cochrane and Kelly 1986, Cho et al. 1998). The term "downcoast" refers to flow from Louisiana towards Mexico and "upcoast" refers to the flow from Mexico towards the mouth of the Mississippi. The Mississippi and Atchafalaya Rivers flow on the Louisiana shelf with an average discharge of 18,400 $m^3 s^{-1}$ and sediment input of 210 million tons annually (Milliman and Meade 1983). The annual cycle of the discharge has increased flow during the spring and decreased flow in the late summer and autumn (Walker 1996). Enhanced down-coast flow along the Louisiana coast occurs from the buoyancy flux-produced pressure gradients that are balanced by the Coriolis force (Walker 2005). The dominant pattern on the LATEX shelf is a cyclonic circulation with a wind-driven downcoast jet (flow from Louisiana towards Mexico) and a weak northeastward current on the outer shelf (Cochrane and Kelly 1986, Oey 1995, Li et al. 1996, Cho et al. 1998).

The LATEX shelf has cyclonic circulation, except during the summer when the flow towards the east (Zavala-Hidalgo et al. 2003b). Seasonal currents along the LATEX shelf are wind-driven, with direction determined by the concave eastern coastline and orientation of the wind relative to this littoral. Regions of strong convergence of along-coast wind stress occur on the LATEX shelf in spring and summer (Zavala-Hidalgo et al. 2006).

### 2.2.4 Tamaulipas-Veracruz Shelf

On the Tamaulipas-Veracruz (TAVE) shelf, there is a seasonal current reversal of northward from May-August and southward from late September-March (Zavala-Hidalgo et al. 2003b). Seasonal currents in the western Gulf are mainly wind-driven (Cochrane and Kelly 1986, Zavala-Hidalgo et al. 2003b). The TAVE shelf has upwelling favorable winds from April to August with a peak in July when southeasterly winds are dominant in the area and cold sea surface temperature anomalies associated with upwelling are present (Zavala-Hidalgo et al. 2006).

### 2.2.5 Bay of Campeche

A semi-permanent gyre-like circulation exists in the Bay of Campeche. Vazquez de la Cerda et al. (2005) updated the understanding of the general circulation in this region and found evidence of a time-dependent cyclonic circulation. Average surface current vectors for the cyclonic gyre are to be westward intensified. Near-surface drifter data was coherent with a seasonal cycle in the wind stress curl. Poor communication occurs with the western Gulf in the upper 800 m of the Bay of Campeche with a Gulf-wide exchange in the deeper layers going from north to south (Vazquez de la Cerda et al. 2005).

### 2.2.6 Campeche Bank

Cyclonic eddy generation takes place on the northeastern Campeche Bank. Sea-surface height anomaly data (Topex-Poseidon) from January 1993 to March 2000, Zavala-Hidalgo et al. (2003a) reported the formation of eight cyclonic eddies located on the northeastern Campeche Bank. These eddies were always generated in the same region, were not periodic, but had a timed relationship with the formation of anticyclonic eddies that were pinched off from the Loop Current (Zavala-Hidalgo et al. 2003a). Upwelling on the eastern side of the Campeche Bank is produced by a dynamic uplift associated with the Yucatan Current. However, the upwelled cold shelf water does not reach the surface and remains along the bottom, except along the coast of the Yucatan where it is found at the surface. The mean circulation on the Campeche Bank is upcoast throughout the year with upwelling favorable winds (Zavala-Hidalgo et al. 2006).

## 2.3 Primary Productivity

Ocean primary production is important because it is the base of the ocean food chain and half the world's oxygen is produced by phytoplankton (Lin et al. 2003). Primary production occurs in the top 50-150 m of the water column where there is sufficient light for photosynthesis (Lin et al. 2003). Primary production, or the rate of phytoplankton production, is usually measured as carbon newly incorporated into organic matter. The pigment system within the phytoplankton absorbs light energy in the visible spectrum and converts it to chemical energy necessary for cell growth. Over land, the main factors limiting primary production are availability of water and temperature. In the ocean, the availability of light and nutrients are the main environmental factors regulating primary production.

Chlorophyll *a* is the key light-absorbing pigment involved in photosynthesis. The concentration of chlorophyll-*a* is an effective indicator of phytoplankton biomass in the water because it is present in photosynthetic organisms (Cullen 1982). Chlorophyll concentration is relatively easy to measure *in situ*: phytoplankton are removed from a known volume of water with a filter, then chlorophyll is extracted and quantified or a spectrophotometer or fluorometer may be used to measure absorbance/fluorescence on whole water. However, when it comes to measuring chlorophyll in a larger geographic area, for example, the GoM, these on-site techniques are not practical.

The influence of phytoplankton on the color of seawater has been studied for many decades. Chlorophyll *a*, the primary photosynthetic pigment in phytoplankton, absorbs more blue and red light than green, so the spectrum of backscattered sunlight or color of ocean water shifts from deep blue to green as the concentration of phytoplankton increases (Yentsch 1960). Because phytoplankton are such a major contributor to ocean color, remote measurements are an accurate way to quantify chlorophyll concentrations (standing stock) when non-algal contribution to absorption and backscatter are minimal (e.g., Yentsch 1960, Smith and Baker 1978, Platt and Sathyendranath 1993, Behrenfeld and Falkowski 1997, O'Reilly et al. 1998).

Remote sensing has been used to measure chlorophyll concentrations in the water column since the launch of the Coastal Zone Color Scanner (CZCS) in 1979. Coastal chlorophyll concentrations are highly variable both spatially and temporally. In general, remote sensors that measure ocean color estimate chlorophyll concentrations over the first optical depth, typically defined as one secchi depth (Gordon and McCluney 1975). Satellite ocean color data provide the only practical means for monitoring the spatial and seasonal variations of near-surface

phytoplankton, information essential for the study of the standing stock of phytoplankton, which has implications for global carbon and other biogeochemical cycles (O'Reilly et al. 1998).

## 2.4 Mechanisms for transporting nutrients

### 2.4.1 Coastal Upwelling

The connection of wind forcing to ocean circulation has been studied since the pioneering work by Ekman 1902. According to Ekman theory, wind driven surface currents in the Northern Hemisphere flow at about 45° to the right of the surface wind direction, because of the Coriolis force. Water underneath the surface layer is not directly forced by the wind, but its movement is affected by the friction through shear with the topmost layer. As a result, this lower layer has a flow that is weaker and further to the right of the topmost layer. Similarly, successive deeper layers experience weaker flows at more extreme angles to the right of the surface wind direction. At a sufficiently deep layer, the water flows in the opposite direction of the surface wind. However, the direction of the overall depth-integrated flow of the wind-driven layer, known as Ekman transport, is 90° to the right of the surface wind direction in the northern hemisphere.

Smith (1968) was the first to cite wind forcing as the most important driving force for coastal upwelling. A typical example of coastal upwelling is the California Current having strong seasonality in wind forcing and high levels of primary production (Abbott and Zion 1985, Abbott and Barksdale 1991, Enriquez and Friehe 1995, Thomas et al. 2001, Thomas et al. 2003, Thomas et al. 2009, Venegas et al. 2008). In the winter, the monthly mean surface wind stress over the northern California Current is north, driving surface waters onshore and resulting in downwelling favorable conditions. In contrast, during the summer the winds are predominantly southerly which drives offshore Ekman transport and thus induces upwelling of cold nutrient-

rich water (Strub et al. 1991). The upwelled water supports elevated coastal phytoplankton concentrations (Thomas et al. 2001).

In the Gulf of Mexico, Walker (2005) described the LATEX shelf coastal upwelling that resulted from a summer up-coast flow. From May-August, southerly winds across the LATEX shelf cause a reversal in shelf water circulation from down-coast to up-coast. Resulting currents flow northward on the Texas shelf and eastward on the Louisiana shelf. The near isothermal shelf temperatures of spring were replaced with cooler upwelled water along the LATEX and northern Mexican coasts. The combination of up-coast currents, wind stress towards the south, and Ekman dynamics result in northward and northeastward movement of the upwelled waters along the shelf. Walker's findings were further confirmed by Zavala-Hidalgo et al. (2006) who observed colder water on the LATEX and northern Mexican shelves from May to August with a peak in July. The current reversal along the Western Shelf was also observed as northward in the summer (May-August) and southward in the autumn and spring (September-March).

### 2.4.2 Ekman Pumping

In addition to the previously mentioned coastal upwelling because of Ekman transport near a coast, wind-driven upwelling can also result from Ekman pumping in the ocean interior. Ekman pumping is the vertical flow generated by surface divergence or convergence of the surface Ekman flow. For instance, a low pressure system with cyclonic surface winds, generates surface divergence which leads to upwelling. Conversely, anti-cyclonic surface winds in high pressure system generate net convergence and downwelling. Ekman pumping, which is associated with positive wind stress curl in the northern hemisphere, may induce nutrient

upwelling which can lead to increased concentrations of phytoplankton in surface waters (Fiechter and Moore 2009).

Ekman pumping has been well documented in the California Current System (e.g., Pickett and Paduan 2003). Halpern (2002) investigated Ekman transport and Ekman pumping off the coast of Peru during the 1997-1998 El Niño. Under normal conditions, upwelling occurred from Ekman pumping and Ekman transport. El Niño conditions resulted in Ekman downwelling four times faster than the normal speed of Ekman upwelling and offshore Ekman transport doubled. The conclusion was that the increased downwelling was the source for a deepened coastal thermocline during the El Niño. Gaube et al. (2013) examined eddy-induced Ekman pumping in the South Indian Ocean and its effects on chlorophyll. The South Indian Ocean has unique eddies in the region, in particular anticyclones with very high chlorophyll content. For Ekman upwelling to sustain phytoplankton concentrations within an anticyclone, high concentrations of phytoplankton and nutrients must be entrained in the eddy during its formation.

In 1995, Hurricane Opal passed through the Gulf of Mexico over a 14-hour period and encountered a warm core ring that was shed by the Loop Current. Prior to the passage of Opal over the ring, surface height anomalies exceeded 30 cm with an estimated depth of the 20°C isotherm between 175-200 m. During the passage over the ring, surface winds increased from 35 to over 60 m $s^{-1}$ and the radius of maximum wind decreased from 40 to 25 km. Following the passage of the storm, the 20°C isotherm decreased to 50 m which suggested upwelling under the storm because of Ekman divergence from the wind (Shay et al. 2000).

### 2.4.3 Horizontal advection of nutrient-rich waters

Nutrients in various forms are important for phytoplankton growth and production. Nitrogen is considered a more dominant influence than phosphorus in estuarine and marine communities (Valiela 1984) however, not all coastal systems are nitrogen-limited (Howarth and Marino 2006).

The Mississippi River is the major contributor of freshwater, nutrients, sediments, and pollutants to the northern Gulf of Mexico shelf and slope. These river inputs have important impacts on all aspects of continental shelf oceanography in the northern Gulf of Mexico (Fig. 2.3). Primary production on the Louisiana shelf is enhanced by the nutrient outflow from the Mississippi River (Riley 1937). Riley (1937) was the first to describe elevated chlorophyll concentrations coinciding with the mixing of phosphorus-laden river water into the Gulf of Mexico. Lohrenz et al. (1997) found a temporal relationship between riverborne nutrient fluxes and primary production on continental shelf waters of the northern Gulf of Mexico. Primary production was significantly correlated with nitrate and nitrite concentrations over a 6 year period.

Of the rivers and streams between Galveston Bay (Texas) and the Mississippi River delta, the Mississippi and Atchafalaya Rivers flows account for 96% of the annual freshwater discharge; 98.5% of the total nitrogen load, and 98% total phosphorus (Dunn 1996). Sources of nutrients from groundwater discharge and upwelling are presumed to be minimal based on geologic and physical features of the system, but data on exchange of nutrients from these potential sources are limited (Rabalais et al. 1999).

Fig. 2.3 A true-color image of the Mississippi River plume has the sediment from the river mixing with the dark blue water of the Gulf two days after a rainstorm. Image acquired and modified from MODIS sensor on NASA's Terra satellite collected on March 5, 2001.

Guo et al. (1994) used water samples from the shelf and slope in the northern Gulf to analyze the dissolved organic carbon (DOC), colloidal organic carbon (COC), and apparent oxygen utilization (AOU). The DOC concentrations varied from 131 µM near-shore (~20 m depth) and 83 µM offshore (~1550 m depth). A linear correlation was found between DOC and AOU at offshore stations, however correlations were lower than expected based on Redfield stoichiometry. They found water mixing to be the most important factor affecting the distribution of DOC and the significant correlation between DOC and AOC. Concentrations of COC (>1000 Dalton) ranged from 20 to 69 µM which comprised ~45% of the initial DOC. COC (>10,000 Dalton) ranged from 4 to 16 µM and was ~11% of the study area. In the Gulf, COC concentration and COC/DOC ratios decreased from surface waters to deep waters.

2.4.4 Vertical mixing and turbulence

Vertical mixing in the water column leads to the deepening of the mixed surface layer, a thin layer of water with nearly uniform temperature, salinity, and dissolved gases (Fig. 2.4). Density cycles in the water column, usually resulting from seasonal temperature changes, can result in changes of the depth of the mixed layer (Müller-Karger et al. 1991). Walsh et al. (1989) used a complex coupled physical-biological numerical model to determine that the single most important factor controlling seasonal variation of chlorophyll concentrations in offshore waters of the Gulf of Mexico was the depth of the mixed layer embodying both light limitation and nutrient availability. These findings were supported by a model that had phytoplankton concentrations at their highest when the mixed layer was deepest (125 m) and reached a minimum with the shallowest mixed layer (20 m) (Müller-Karger et al. 1991). Pigment concentrations did not increase until the mixed layer was deeper than 50 m, typically in the fall when the tropical storm and hurricane season commenced.

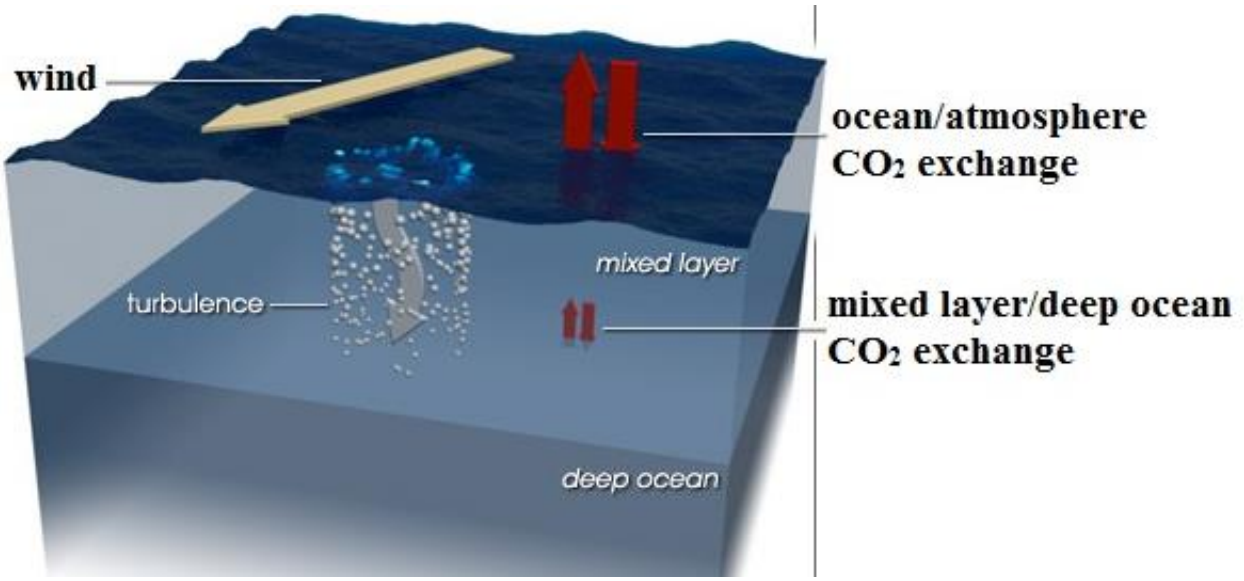


Fig. 2.4 Atmospheric carbon dioxide is absorbed into the mixed layer at the ocean's surface. The mixed layer has uniform temperature, salinity and dissolved gases and is maintained by wind-driven turbulence. Exchange between the deep ocean and mixed layer allows carbon dioxide to reach deep ocean waters. Image from earthobservatory.nasa.gov

Summary

The Gulf of Mexico is an ecologically diverse system with distinguishing features such as its climate, topography, and nutrient inputs. First, the location of the Gulf in a transitional area of the tropical and subtropical climactic zones makes for distinctive weather patterns such as hurricanes, dynamic wind systems, and pressure systems that converge from the south, west, and north. Second, the physical topography of the Gulf allows for large scale and small scale circulation features including the Loop Current, eddies, and other deep water and coastal circulation patterns. And lastly, primary productivity levels and nutrient loads affect the total biological productivity which in turn affects the many marine-related industries that are dependent on the Gulf. Connecting the physics to the biology of the Gulf can help towards managing the natural resources towards sustainability in the future.

References

Abbott MR, Barksdale B (1991) Phytoplankton pigment patterns and wind forcing off central California. J Geophys Res 96:14649-14667

Abbott MR, Zion PM (1985) Satellite observations of phytoplankton variability during an upwelling event. Cont Shelf Res 5:661-680

Antoine JR (1972) Structure of the Gulf of Mexico. In: Rezak R, Henry VJ (eds) Texas A&M University Oceanographic Studies, Volume 3: Contributions on the geological and geophysical oceanography of the Gulf of Mexico. Gulf Publishing Company, Houston, TX, 303 p

Antoine JW, Ewing JI (1963) Seismic refraction measurements on the margins of the Gulf of Mexico. J Geophys Res 68:1975-1996

Behrenfeld MJ, Falkowski PG (1997) Photosynthetic rates derived from satellite-based chlorophyll concentration. Limnol Oceaogr 42:1-20

Behringer DW, Molinari RL, Festa JF (1977) The variability of anticyclonic flow patterns in the Gulf of Mexico. J Geophys Res 82:5469-5476

Biggs DC, Fargion GS, Hamilton P, Leben RR (1996) Cleavage of Gulf of Mexico loop current eddy by a deep water cyclone. J Geophys Res 101:20,629-20,641

Brooks DA, Legeckis RV (1982) A ship and satellite view of hydrographic features in the western Gulf of Mexico. J Geophys Res 87:4195-4206

Bryant WR, Lugo J, Cordova C, Salvador A (1991) Physiography and bathymetry. In: Salvador A (ed) Gulf of Mexico Basin. Volume J of The Geology of North America. Geological Society of America, Boulder, CO, p 13-30

Cho K, Reid RO, Nowlin Jr WD (1998) Objectively mapped stream function fields on the Texas-

Louisiana shelf based on 32 months of moored current meter data. J Geophys Res 103:10377-10390

Cochrane JD, Kelly FJ (1986) Low-frequency circulation on the Texas-Louisiana continental shelf. J Geophys Res 91:10645-10659

Cooper C, Forristall GZ, Joyce TM (1990) Velocity and hydrographic structure of two Gulf of Mexico warm-core rings. J Geophys Res 95:1663-1679

Cullen JJ (1982) The deep chlorophyll maximum: Comparing vertical profiles of chlorophyll *a* Can J Fish Aquat Sci 39:791-803

DeHaan CJ, Sturges W (2005) Deep cylclonic circulation in the Gulf of Mexico. J Phys Oceangr 35:1801-1812

De Velasco GG, Winant CD (1996) Seasonal patterns of wind stress and wind stress curl over the Gulf of Mexico. J Geophys Res 101:18127-18140

DiMarco SF, Nowlin Jr. WD, Reid RO (2005) A statistical desciption of the near-surface velocity field from drifters in the Gulf of Mexico. In: Sturges W, Lugo-Fernandez A (eds) Circulation in the Gulf of Mexico: observations and models. American Geophysical Union, Washington, DC, p 101-10

Dunn DD (1996) Trends in nutrient inflows to the Gulf of Mexico from streams draining the conterminous United States 1972-1993. U.S. Geological Survey, Water-Resources Investigations Report p 96-4113

Enriquez AG, Friehe CA (1995) Effects of wind stress and wind stress curl variability on coastal upwelling. J Phys Oceangr 25:1651-1671

Ewing M, Ericson DB, Heezen BC (1958) Sediments and topography of the Gulf of Mexico. In: Weeks E (eds) Habitat of Oil. Am Assoc Petroleum Geologists, Tulsa, p 995-1053

Ewing JI, Ewing M, Leyden R (1966) Seismic profiler survey of Blake Plateau. Am Assoc Petroleum Geologists Bull 50:1948-1971

Ferré-D'Amaré AR (1985) Coral reefs of the Mexican Atlantic: A review. In: Gabrie C, Harmelin VM (eds) Proceedings of the Fifth International Coral Reef Congress, Tahiti, 27 May-1 June 1985. Moorea, French Polynesia: Antenne Museum-Ephe, 6:349-354

Fiecheter J, Moore AM (2009) Interannual spring bloom variability and Ekman Pumping in the coastal Gulf of Alaska. J Geophys Res 114:C06004

Forristall GZ, Schaudt KJ, Cooper CK (1992) Evolution and kinematics of a Loop Current eddy in the Gulf of Mexico during 1985. J Geophys Res 97:2173-2184

Gaube P, Chelton DB, Strutton PG, Behrenfeld MJ (2013) Satellite observations of chlorophyll, phytoplankton biomass, and Ekman pumping in nonlinear mesoscale eddies. J Geophys Res 118, 6349-6370, doi:10.1002/2013JC009027

Glynn PW (1973) Aspects of the ecology of coral reefs in the western Atlantic region. In: Jones OA, Endean R (eds) Biology and Geology of Coral Reefs. Academic Press, New York, p 271-342

Gordon HR, McCluney WR (1975) Estimation of the depth of sunlight penetration in the sea for remote sensing. Appl Opt 14:413-416

Guo L, Coleman Jr. CH, Santschi PH (1994) The distribution of colloidal and dissolved organic carbon in the Gulf of Mexico. Mar Chem 45:105-119

Halpern D (2002) Offshore Ekman transport and Ekman pumping off Peru during the 1997-1998 El Niño. Geophys Res Lett 29(5), 10.1029/2001GLO14097

Hamilton P (1992) Lower continental slope cyclonic eddies in the central Gulf of Mexico. J Geophys Res 97:2185-2200

Hofmann EE, Worley SJ (1986) An investigation of the circulation of the Gulf of Mexico. J Geophys Res 91:14221-14236

Howarth RW, Marino R (2006) Nitrogen as the limiting nutrient for eutrophication in coastal marine ecosystems: Evolving views over three decades. Limnol Oceanogr 51:364-376

Huh OK, Schaudt KJ (1990) Satellite imagery tracks currents in the Gulf of Mexico. Oil Gas J 88:70-76

Huh OK, Wiseman Jr WJ, Rouse LJ (1981) Intrusion of Loop Current waters onto the west Florida continental shelf. J Geophys Res 86:4186-4192

Hurlburt HE (1986) Dynamic transfer of simulated altimeter data into subsurface information by a numerical ocean model. J Geophys Res 91:2372-2400

Leben RR (2005) Altimeter-derived Loop Current metrics. In: Sturges W, Lugo-Fernandez A (eds) Circulation in the Gulf of Mexico: observations and models. American Geophysical Union, Washington DC, p 181-201

Leipper DF, Volgenau D (1972) Hurricane heat potential of the Gulf of Mexico. J Phys Oceanogr 2:218-224

Lewis JK, Kirwan AD (1985) Some observations of ring topography and ring-ring interactions in the Gulf of Mexico. J Geophys Res 90:9017-9028

Lewis JK, Kirwan AD, Forristall GZ (1989) Evolution of a warm-core ring in the Gulf of Mexico, Lagrangian observations. J Geophys Res 94:8163-8178

Li Y, Nowlin Jr WD, Reid RO (1996) Spatial-scale analysis of hydrographic data over the Texas-Louisiana continental shelf. J Geophys Res 101:20595-20605

Lin I, Liu WT, Wu C, Wong GTF, Hu C, Chen Z, Liang W, Yang Y, Liu K (2003) New evidence for enhanced ocean primary production triggered by tropical cyclone. Geophys

Res Lett 30:1718, doi:10.1029/2003GL017141

Liddell WD (2007) Origin and Geology. In: Tunnell Jr JW, Chavez EA, Withers K (eds) Coral Reefs of the Southern Gulf of Mexico. Texas A&M University Press, College Station, p 23-33

Lohrenz SE, Fahnenstiel GL, Redalje DG, Lang GA, Chen X, Dagg MJ (1997) Variations in primary production of northern Gulf of Mexico continental shelf waters linked to nutrient inputs from the Mississippi River. Mar Ecol Prog Ser 155:45-54

Maul GA, Williams F, Roffer M, Sousa FM (1984) Remotely sensed oceanographic patterns and variability of bluefin tuna catch in the Gulf of Mexico. Oceanol Acta 7:469-479

Milliman JD, Meade RH (1983) World-wide delivery of river sediment to the oceans. J Geol 91:1-21

Mizuta G, Hogg NG (2004) Structure of the circulation induced by a shoaling topographic wave. J Phys Oceangr 34:1793-1810

Mooers CNK, Maul GA (1998) Intra-Americas Sea Circulation. In: Brink KH, Robinson AR (eds) The Sea. John Wiley, New York, 183-208

Morey SL, Zavala-Hidalgo J, O'Brien JJ (2005) The seasonal variability of continental shelf circulation in the northern and western Gulf of Mexico from a high-resolution numerical model. In: Sturges W, Lugo-Fernandez A (eds) Circulation in the Gulf of Mexico: observations and models. American Geophysical Union, Washington, DC, p 203-218

Müller-Karger FE, Walsh JJ, Evans RH, Meyers MB (1991) On the seasonal phytoplankton concentration and sea surface temperature cycles of the Gulf of Mexico as determined by satellites. J Geophys Res 96:12,645-12,665

Nowlin WD (1971) Water masses and general circulation of the Gulf of Mexico. Oceanology

5:28-33

Oey L (1995) Eddy and wind-forced shelf circulation. J Geophys Res 100:8621-8637

Oey L (1996) Simulation of mesoscale variability in the Gulf of Mexico: sensitivity studies, comparison with observations, and trapped wave propagation. J Phys Oceanogr 26:145-175

Oey L, Lee H-C, Schmitz Jr WJ (2003) Effects of winds and Caribbean Eddies on the frequency of the Loop Current eddy shedding: A numerical study. J Geophys Res 108:C103324, doi:10.1029/2002JC001698

Ohlmann JC, Niiler PP (2005) Circulation over the continental shelf in the northern Gulf of Mexico. Prog Oceanogr 64:45-81

O'Reilly JE, Maritorena S, Mitchell BG, Siegel DA, Carder KL, Garver SA, Kahru M, McClain C (1998) Ocean color chlorophyll algorithms for SeaWiFS. J Geophys Res 103:24937-24953

Pickett MH, Paduan JD (2003) Ekman transport and pumping in the California Current based on the U.S. Navy's high-resolution atmospheric model (COAMPS). J Geophys Res 108(C10), 3327, doi:10.1029/2003JC001902

Platt T, Denman K (1980) Patchiness in phytoplankton distribution. In: Morris, I (ed) The Physiological Ecology of Phytoplankton. University of California Press, Berkley CA, p 413-431

Platt T, Sathyendranath S (1993) Estimators of primary production for interpretation of remotely sensed data on ocean color. J Geophys Res 98:14561-14576

Rabalais NN, Turner RE, Justic D, Dortch Q, Wiseman WJ Jr, Sen Gupta BK (1999) Characterization of hypoxia: Topic 1 Report for the integrated assessment of hypoxia in

the Gulf of Mexico. Silver Spring, MD, NOAA Coastal Ocean Office. Decision Analysis Series no. 15

Riley GA (1937) The significance of the Mississippi River drainage for the biological conditions in the northern Gulf of Mexico. J Mar Res 1:60-74

Salvador A (1991) Introduction. In: Salvador A (ed) The Gulf of Mexico Basin. Geological Society of America, The Geology of North America, Boulder, CO, p 1-12

Schink DR, Santschi PH, Corapcioglu O, Sharma P, Fehn U (1995) $^{129}$I in Gulf of Mexico waters. Earth Planet Sci Lett 135:131-138

Schmitz Jr WJ, Biggs DC, Lugo-Fernandez A, Oey L-Y, Sturges W (2005) A synopsis of the circulation in the Gulf of Mexico and on its continental margins. In: Sturges W, Lugo-Fernandez A (eds) Circulation in the Gulf of Mexico: observations and models. American Geophysical Union, Washington, DC, p 11-29

Shay LK, Goni GJ, Black PG (2000) Effects of a warm oceanic feature on Hurricane Opal. Mon Wea Rev 128:1366-1383

Sheridan RE, Drake CL, Nafe JE, Hennion J (1966) Seismic refraction study of continental margin east of Florida. Am Assoc Petroleum Geologists Bull 50:1972-1991

Smith RL (1968) Upwelling. Oceanogr Mar Biol Annu Rev 6:11-46

Smith RC, Baker KS (1978) The bio-optical state of ocean waters and remote sensing. Limnol Oceangr 23:247-259

Strub PT, Kosro PM, Huyer A (1991) The nature of the cold filaments in the California Current System. J Geophys Res 96:14743-14768

Sturges W (1994) The frequency of ring separations from the Loop Current. J Phys Oceangr 24:1647-1651

Sturges W, Kenyon KE (2008) Mean flow in the Gulf of Mexico. J Phys Oceangr 38:1501-1514

Sturges W, Leben R (2000) Frequency of ring separations from the Loop Current in the Gulf of Mexico, a revised estimate. J Phys Oceangr 30:1814-1819

Thomas AC, Brickley P, Weatherbee R (2009) Interannual variability in chlorophyll concentrations in the Humboldt and California Current Systems. Prog Oceanogr 83:386-392

Thomas AC, Carr ME, Strub PT (2001) Chlorophyll variability in eastern boudary currents. Geophys Res Lett 28:3421-3424

Thomas AC, Strub PT, Brickley P (2003) Anomalous satellite-measured chlorophyll concentrations in the northern California Current in 2001-2002. Geophys Res Lett 30:8022, doi:10.1029/2003GL017409

Turner RE (1999) Inputs and outputs of the Gulf of Mexico. In: Kumpf K, Steidinger K, Sherman K (eds) The Gulf of Mexico Large Marine Ecosystem. Blackwell Science, Oxford, UK, p 64-73

Valiela I (1984) Marine ecological processes. New York, Springer-Verlag 546 p.

Vazquez de la Cerda AM, Reid RO, DiMarco SF, Jochens AE (2005) Bay of Campeche circulation: an update. In: Sturges W, Lugo-Fernandez A (eds) Circulation in the Gulf of Mexico: observations and models. American Geophysical Union, Washington, DC, p 279-293

Venegas RM, Strub PT, Beier E, Letelier R, Thomas AC, Cowles T, James C, Soto-Mardones L, Cabrera C (2008) Satellite-derived variability in chlorophyll, wind stress, sea surface height, and temperature in the northern California Current System. J Geophys Res 113:C03015, doi:10.1029/2007JC004481

Vidal VMV, Vidal FV, Pérez-Molero JM (1992) Collision of a Loop Current anticyclonic ring against the continental shelf slope of the western Gulf of Mexico. J Geophys Res 97:2155-2172

Vukovich FM, Maul GA (1985) Cyclonic eddies in the eastern Gulf of Mexico. J Phys Oceangr 15:105-117

Walker ND (2005) Wind and eddy-related shelf/slope circulation processes and coastal upwelling in the northwestern Gulf of Mexico. In: Sturges W, Lugo-Fernandez A (eds) Circulation in the Gulf of Mexico: observations and models. American Geophysical Union, Washington, DC, p 295-313

Walker ND (1996) Satellite assessment of Mississippi River plume variability: causes and predictability. Rem Sens Env 58:21-35

Walsh JJ, Dieterle DA, Meyers MB, Müller-Karger FE (1989) Nitrogen exchange at the continental margin: A numerical study of the Gulf of Mexico. Prog Oceanogr 23:248-301

Weisberg RH, Black BD, Yang H (1996) Seasonal modulation of the West Florida Continental Shelf Circulation. Geo Res Lett 23:2247-2250

Weisberg RH, He R, Liu Y, Virmani JI (2005) West Florida Shelf Circulation on synoptic, seasonal, and interannual time scales. In: Sturges W, Lugo-Fernandez A (eds) Circulation in the Gulf of Mexico: observations and models. American Geophysical Union, Washington, DC, p 325-347

Worzel JL, Leyden R, Ewing M (1968) Newly discovered diapirs in Gulf of Mexico. Am Assoc Petroleum Geologists Bull 52:1194-1203

Yentsch CS (1960) The influence of phytoplankton pigments on the colour of seawater. Deep Sea Res 7:1-9

Zavala-Hidalgo J, Gallegos-García A, Martínez-López B, Morey SL, O'Brien JJ (2006) Seasonal upwelling on the western and southern shelves of the Gulf of Mexico. Ocean Dynamics 56:333-338

Zavala-Hidalgo J, Morey SL, O'Brien JJ (2003a) Cyclonic eddies northeast of the Campeche Bank from altimetry data. J Phys Oceangr 33:623-629

Zavala-Hidalgo J, Morey SL, O'Brien JJ (2003b) Seasonal circulation on the western shelf of the Gulf of Mexico using a high-resolution numerical model. J Geophys Res 108:C12, doi:10.1029/2003JC001879

# CHAPTER III: The seasonal variability and dominant coupled patterns of satellite-estimated chlorophyll and winds in the Gulf of Mexico

Abstract

Seasonal associations between chlorophyll and wind forcing were examined in the Gulf of Mexico using the ESA's GlobColour and NASA's QuickSCAT Level 3 monthly products for 2000-2008. In general, chlorophyll has a stronger annual mean and seasonal variability over the Gulf shelves. The mean location of waters with high chlorophyll concentrations are to the west of the Mississippi mouth over the Louisiana-Texas Shelf and are driven by the annual mean easterly winds over the region. In the Gulf interior, the seasonal variability of chlorophyll and wind speed vary with annual periodicity and in phase with each other, increasing during the winter and decreasing during the summer. Stronger winds during the winter are likely to increase the upward turbulent transport of nutrients at the bottom of the mixed layer. In the Bay of Campeche and Florida shelves, the seasonal cycle is similar than that to the interior but the winter increase occurs earlier because of the development of northerly meridional winds during the fall. In the northern Gulf, the main feature of the seasonal chlorophyll variability is a "seesaw" (or dipole) pattern which indicates increased chlorophyll anomalies over the Western Shelf and decreased (out-of-phase) chlorophyll anomalies just east of the Mississippi River mouth during winter. This pattern of chlorophyll is associated with an intensification of the easterly winds over the northern Gulf during these months. A reversed seesaw pattern of chlorophyll coupled with a weakening of the easterly winds over the northern Gulf occurs during the summer.

## Introduction

The Gulf of Mexico is a semi-enclosed basin bounded on the north, northeast and northwest by the United States, on the southeast by Cuba, and on the south and southwest by

Mexico. It is approximately 1500 km wide and is connected to the Atlantic Ocean via the Florida Straits between the U.S. and Cuba, and to the Caribbean Sea via the Yucatan Channel between Mexico and Cuba (Liddell 2007). Based on the main coastal and topographic features, the Gulf of Mexico can be divided into six major regional areas: (a) Interior basin, located in the deep central region; (b) West Florida continental shelf, including the Alabama-Mississippi Shelf to east and northeast; (c) Louisiana-Texas Shelf, to the north and northwest; (d) Tamaulipas-Veracruz Shelf, to the west; (e) Bay of Campeche, to the southwest; and (f) Campeche Bank, to the south (Fig. 3.1).

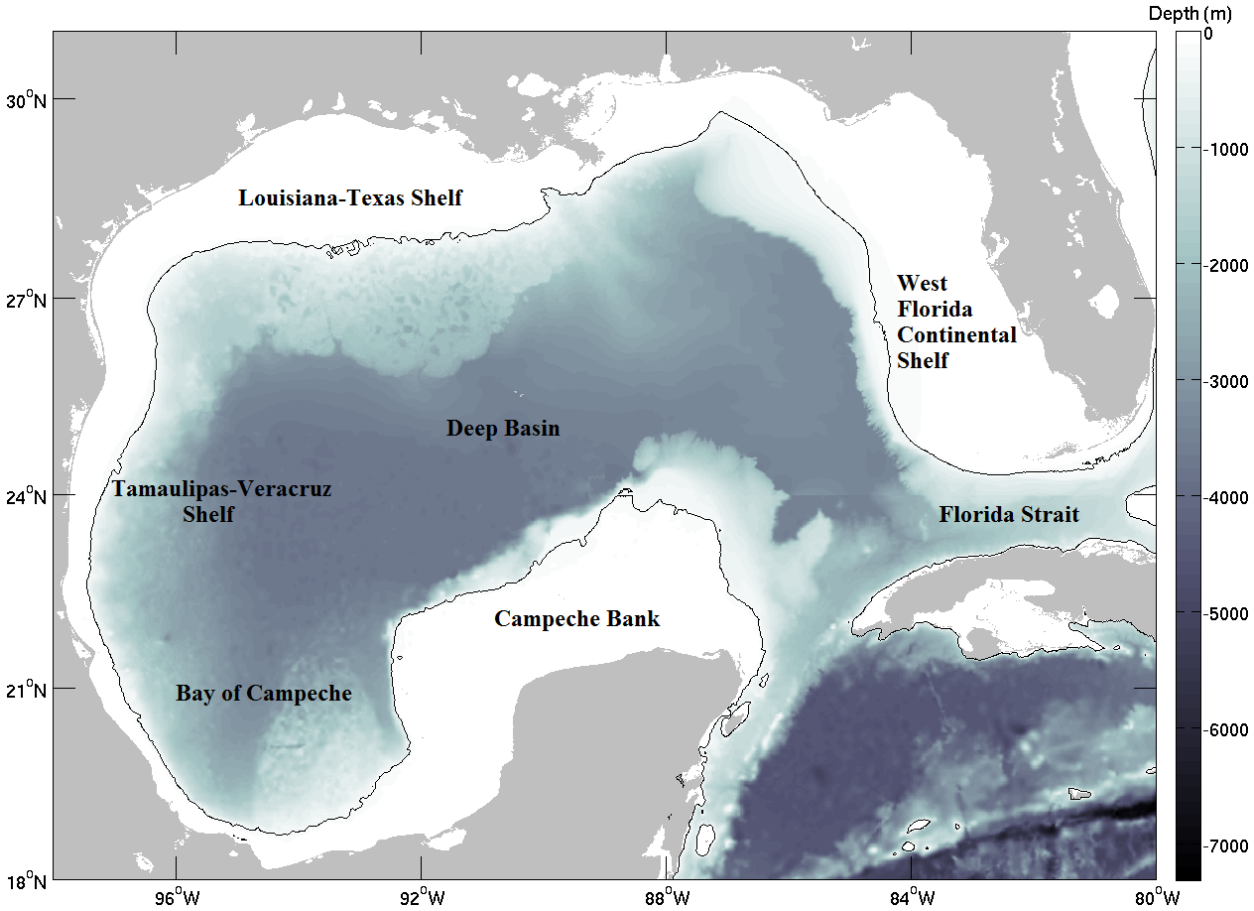


Fig. 3.1 Topography of the Gulf of Mexico with the 200 m isobath defining the continental shelf break (solid black line).

The general circulation in the interior Gulf is dominated by three semi-permanent large-scale features: (1) the energetic Loop Current in the eastern half, which is a component of the

Gulf Stream current system, (2) a large, weak anticyclonic gyre in the western half, with its characteristic western boundary current intensification (Behringer et al. 1977), and (3) a smaller weak cyclonic gyre also with western intensification in the Bay of Campeche (Vázquez de la Cerda et al. 2005). The Loop Current flows clockwise connecting the Yucatan Current which flows into the Gulf through the Yucatan Channel, and the Florida Current which flows out of the Gulf through the Florida Straits (Hofmann and Worley 1986). The Loop Current forms large meanders that can penetrate deep into the northern Gulf and separate forming large anticyclonic eddies (Behringer et al. 1977). The large anticyclonic eddies created by the Loop Current propagate westward through the interior basin and affect almost every aspect of the circulation of the entire Gulf (Sturges and Leben 2000). The eddies have a vertical scale of several hundred meters (Mooers and Maul 1998) and because of the conservation of potential vorticity are constrained to the interior of the Gulf but can induce cross-shelf transport when colliding with the shelf slope (e.g., Oey, 1995). No seasonality exists for the energetic Loop Current variability and its eddy shedding processes (e.g., Leben 2005, Morey et al. 2005). Over the inner shelves, however, the circulation has a strong seasonality in response to the surface winds with counterclockwise flow during the warm months and clockwise flow during the cold months (e.g., Morey et al. 2005). The shelf circulation is also influenced by riverine fresh water discharge with the main contribution being that of the Mississippi River in the northern Gulf.

The long-term annual mean satellite chlorophyll over the Gulf has a strong relation to areas where nutrients are present with low values over the interior Gulf and higher values over the shelves (Fig. 3.2A). Over the shelves the largest annual mean values are found in the northern inner shelves. Relative to the Mississippi River mouth, the larger annual mean chlorophyll values are towards the west over the Louisiana-Texas shelf following the mean

location of the plume (Fig. 3.2A) which is driven westward by the annual mean easterly winds (Fig. 3.2B; see also Cochrane and Kelly 1986, Nowlin et al. 2000). Both in the interior and over the shelves, chlorophyll has seasonality (e.g., Zavala-Hidalgo et al. 2014). In the interior, the chlorophyll follows the annual fluctuations of mixed layer depth with higher (lower) pigment concentrations during the deeper (shallower) mixed layer depths of the winter (summer) season (Müller-Karger et al. 1991). Over the shelf the dominant seasonal signal is the higher values of chlorophyll in the northern Gulf just east of the Mississippi River mouth during June-August (e.g., Martínez-López and Zavala Hidalgo 2009; Zavala-Hidalgo et al. 2014). Martínez-López and Zavala Hidalgo (2009) related this chlorophyll maximum to the reversal of the prevailing (easterly) winds favoring wind-driven coastal upwelling and eastward advection of Mississippi River waters. Zavala-Hidalgo et al. (2014), however, attributed this June-August chlorophyll maxima to southerly winds in this region favoring eastward Ekman transport during these months.

The studies of chlorophyll seasonal variability mentioned earlier (Martínez-López and Zavala-Hidalgo 2009, Zavala-Hidalgo et al. 2014) were derived using multiyear monthly satellite data from the Sea-Viewing Wide-Field-of-View Sensor (SeaWiFS). Here, the seasonal cycle of chlorophyll in the Gulf of Mexico is estimated from a satellite chlorophyll dataset that combines SeaWiFS with additional satellite chlorophyll datasets and then compared to the seasonal cycle of wind forcing from QuikSCAT. A description of the data and methods is included in section 3. The results are presented in section 4 and conclusions are in section 5.

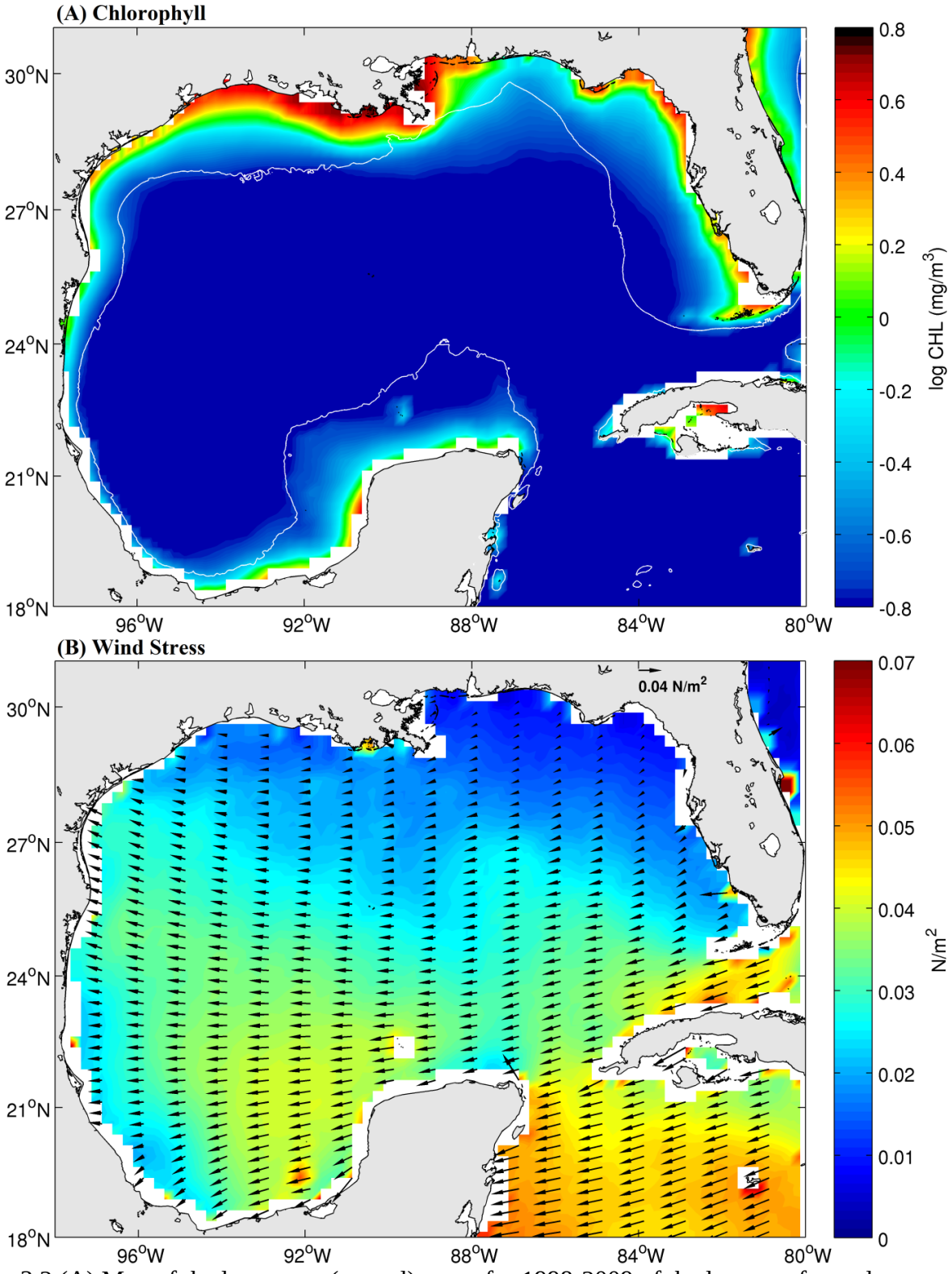


Fig. 3.2 (A) Map of the long-term (annual) mean for 1998-2009 of the log-transformed chlorophyll-*a* ($mg/m^3$) with the 200 m isobath (white line). (B) Long-term (annual) mean values for 2000-2008 of vector wind stress (arrows) and wind stress magnitude (color contours).

Data and Methods

3.1 Chlorophyll data

Several satellite sensors sample ocean color (e.g., NASA's SeaWiFS, NASA's MODIS on the TERRA and AQUA platforms, and ESA's MERIS on Envisat). The dataset used in this study is known as GlobColour (http://www.globcolour.info/) and comes from an European Space Agency (ESA) project that provides a long time series (12 years) of ocean color data merged from these various sources to create products generated from weighted averaging and the Garver-Siegel-Maritorena (GSM) model (Maritorena and Siegel 2005).

The GSM01 model is a bio-optical model which combines the normalized radiances of collected datasets from multiple sensors. Over each pixel of a geographical grid common to SeaWiFS, MODIS-AQUA, and MERIS, spectra from the sensors are selected and combined in a single, multi-source product which is then used in the inversion of the GSM01 semi-analytical ocean color model (Maritorena et al. 2002). The model inversion results in sub-surface (0-50 m) chlorophyll-*a* concentrations along with other products. The GlobColour global level-3 binned products used in this study have a resolution of 0.25° at the equator on a monthly data period. The chlorophyll data provided is on a 0.25° x 0.25° global grid. The chlorophyll-*a* data used in this project will be $CHL_1$ ($mg/m^3$) for case 1 water and will be used as a proxy for overall standing stock of phytoplankton biomass. Case 1 waters are those waters whose properties are determined primarily by phytoplankton and not color dissolved inorganic matter (CDOM) and inorganic mineral particles (Matsushita et al. 2012). This is the category used for the Gulf of Mexico.

3.2 Wind data

The surface winds were obtained from the QuikSCAT Level 3 products available from the NASA- Jet Propulsion Laboratory (http://podaac-www.jpl.nasa.gov/). The dataset consists of gridded values of scalar surface wind speed, meridional and zonal components of surface wind velocity, and time. The Level 3 data were obtained from the Direction Interval Retrieval with Threshold Nudging (DIRTH) wind vector solutions contained in the QuikSCAT data and are provided on global grid of 1440 pixels in longitude by 720 pixels in latitude (0.25° x 0.25°). In-situ studies (Ebuchi et al. 2002, Bourassa et al. 2003, Pickett et al. 2003) have found that QuikSCAT wind retrievals are accurate to better than the mission-stated accuracy of 2 m/s or 10% in speed and 20° in direction. Data are available from July 1999 to November 2009, however data used for this study were monthly values from January 2000 – December 2008.

The vector wind stress $\vec{\tau}$ is computed from QuikSCAT observations of the equivalent neutral stability vector winds at 10 m based on the following bulk aerodynamic formula:

$$\vec{\tau} = \rho\, C_D\, w\, \vec{u}$$

where $\rho$ is air density (taken here to be 1.2 kg/m$^3$) (Goldenberg and O'Brien 1981, Risien and Chelton 2008), $C_D$ is the drag coefficient, $w$ is wind speed, and $\vec{u}$ is the wind velocity vector in the eastward, $u$, and northward, $v$, components. The drag coefficient was computed using the modified equation (from Large and Pond 1981, 1982) found in the appendix of Large et al. (1994), which is the formulation most commonly used for scatterometer applications:

$$10^3 C_D = \frac{2.70}{w} + 0.142 + 0.0764w$$

## 3.3 Data Analysis

Oceanic bio-optical data including chlorophyll concentration are distributed approximately lognormally (e.g., Campbell 1995). Surface chlorophyll generally has larger values near the coast and much smaller values in the open ocean. For this reason, all analyses in this study are performed with log-transformed (base 10) chlorophyll concentrations ($mg/m^3$). Chlorophyll analysis was performed for the period of 1998-2009 and combined chlorophyll-wind analysis was performed for the overlapping period of 2000-2008. The climatological seasonal cycle of all fields is estimated by computing the averages for each calendar month over the entire time period, also known as the long-term monthly-mean seasonal cycle.

An empirical orthogonal function (EOF) analysis is a technique that uses fundamental matrix operations. The process reduces a multidimensional problem in vector space into a small set of orthogonal functions or statistical "modes" which provide a representation of the dominant spatial and temporal variability of a given field. The analysis is applied to a space- and time-dependent field that has a zero temporal mean. The auto-covariance matrix is created and diagonalized; resulting in a set of eigenvalues and eigenvectors. Each eigenvector (EOFs) can be displayed as a spatial pattern (map). To see how the spatial pattern changes in time, the eigenvector is projected onto the original field to obtain a time series (expansion coefficients). The EOFs are orthogonal (square) in space and the time series are orthogonal in time. The fraction of the total field variance explained by an EOF is proportional to its associated eigenvalue. An eigenvalue with its corresponding EOF and expansion coefficient define each mode of variability. The leading mode (the largest eigenvalue) explains the largest percentage of the total variance (e.g., Björnsson and Venegas 1997).

Singular Value Decomposition (SVD) analysis can be thought of as a generalization to rectangular matrices of the diagonalization of a square symmetric matrix (as in EOF analysis). Coupled SVD analysis can be applied to two fields simultaneously to identify coupled spatial patterns that explain the covariance between these variables. The two matrices do not need to be defined on the same number of grid points, however the variables must contain the same number of temporal data points. The SVD of the cross-covariance matrix produces two spatially uncorrelated sets of singular vectors (analogous to the eigenvectors, but one for each variable) and a set of singular values associated with each pair of vectors (analogous to the eigenvalues). Each pair of singular vectors describe a fraction of the square covariance. The first pair describes the largest fraction of the square covariance and each subsequent pair describes the fraction of the square covariance that is unexplained prior. The square covariance fraction accounted for by the *k*th pair of singular vectors is proportional to the square of the *k*th pair of singular value. The *k*th expansion coefficient for each variable is computed by projecting the respective *k*th singular vector onto the original data field. The correlation value (*r*) between the *k*th expansion coefficients indicates how strongly related the coupled patterns are for the two variables (Björnsson and Venegas 1997). Both EOF and SVD analysis assume the data to be complete. Gaps in the data result in matrices that are not orthogonal. This problem is overcome by filling gaps prior to analysis through interpolation. Linear interpolation was used for interior matrix points that had less than 7 empty values in time (< 5%). Extra data points available beyond the time period for the project were used to fill empty values at the beginning or end of the time series. Any remaining empty data points were filled through spatial interpolation of neighboring values.

## Results

### 3.4 Chlorophyll

To describe the seasonal cycle of chlorophyll in the Gulf of Mexico, maps of monthly mean deviations from the long-term annual mean (Fig. 3.2A) are in Fig. 3.3. This method of displaying the seasonal variability as "seasonal anomalies" relative to the annual mean follows Martínez-López and Zavala-Hidalgo (2009) and is helpful in interpreting the seasonal successional patterns of chlorophyll. The maps (Fig. 3.3) based in the merged GlobColour product agree well with those of Martínez-López and Zavala-Hidalgo (2009; their Fig. 5) which were derived from SeaWiFS and those of Zavala-Hidalgo et al. (2014; their Fig. 8) which were derived from SeaWiFS and MODIS, even though the base periods for these studies (1997-2007 and 1997-2012, respectively) are slightly different that the one used here (1998-2009).

In the deep Gulf, moderate positive seasonal anomalies are observed during December-January-February with a shift towards moderate negative seasonal anomalies during June-July-August. The largest seasonal anomalies are found over the shelf (defined by the 200 m isobaths, see e.g., Fig. 3.2A) and near the shelf break. Strong positive anomalies occur just east of the Mississippi River mouth during June-August and these anomalies swiftly reverse to negative anomalies in September, becoming strongly negative in October. The eastern shelf of the Bay of Campeche displays strong positive anomalies in October-December and moderately negative anomalies in February-April. The Florida Shelf has moderate to large positive (negative) seasonal anomalies over the outer (inner) shelf during January-March. This pattern reverses in June displaying moderately to large negative (positive) anomalies in the outer (inner) shelf through October. The Tamaulipas-Veracruz shelf and the waters surrounding Cuba, which

include the Yucatan and Florida straits, have seasonal anomalies in phase with that of the deep Gulf.

The evolution of the seasonal cycle of chlorophyll variability can be described well by the first two EOFs in Figure 3.4. The leading EOF accounts for 68% of the overall seasonal-cycle variance and has annual periodicity with maximum (minimum) in summer (winter). The space pattern of EOF1 has two localized regions of strong out-of-phase loadings namely the western Gulf shelf and just east of the Mississippi River mouth. Because individual EOFs represent standing oscillations, EOF1 can be interpreted as an annual dipole or "seesaw" pattern of variability at both extremes of the annual mean location of the Mississippi River plume (see Fig. 3.2A) and captures the dominant seasonality over the entire basin. The second EOF mode accounts for 15% of the seasonal variance and its amplitude time series is also annual but nearly in quadrature with the amplitude time series of EOF1, i.e., its maximum (minimum) is in the fall (spring). The EOF2 space pattern has more widespread structure around the Gulf coastal areas. In particular, it has strong positive loadings over the Florida Shelf and the Bay of Campeche eastern shelf, and strong negative anomalies just east of the Mississippi River mouth and Campeche Bank.

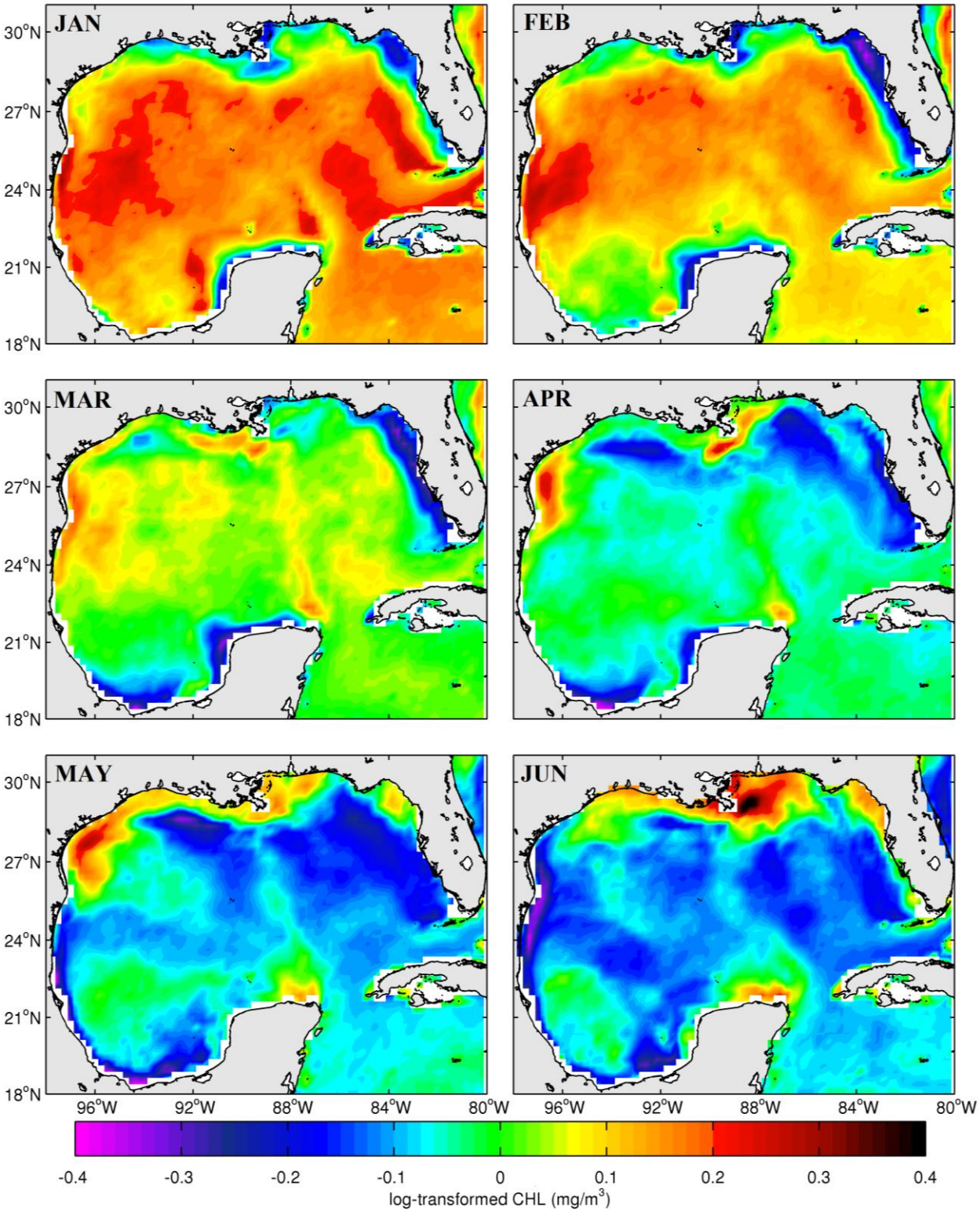


Fig. 3.3 Difference (color contour) maps between the 1998-2009 monthly means and the 1998-2009 annual mean (Figure 3.2A) of log-transformed chlorophyll-a concentration (mg/m3).

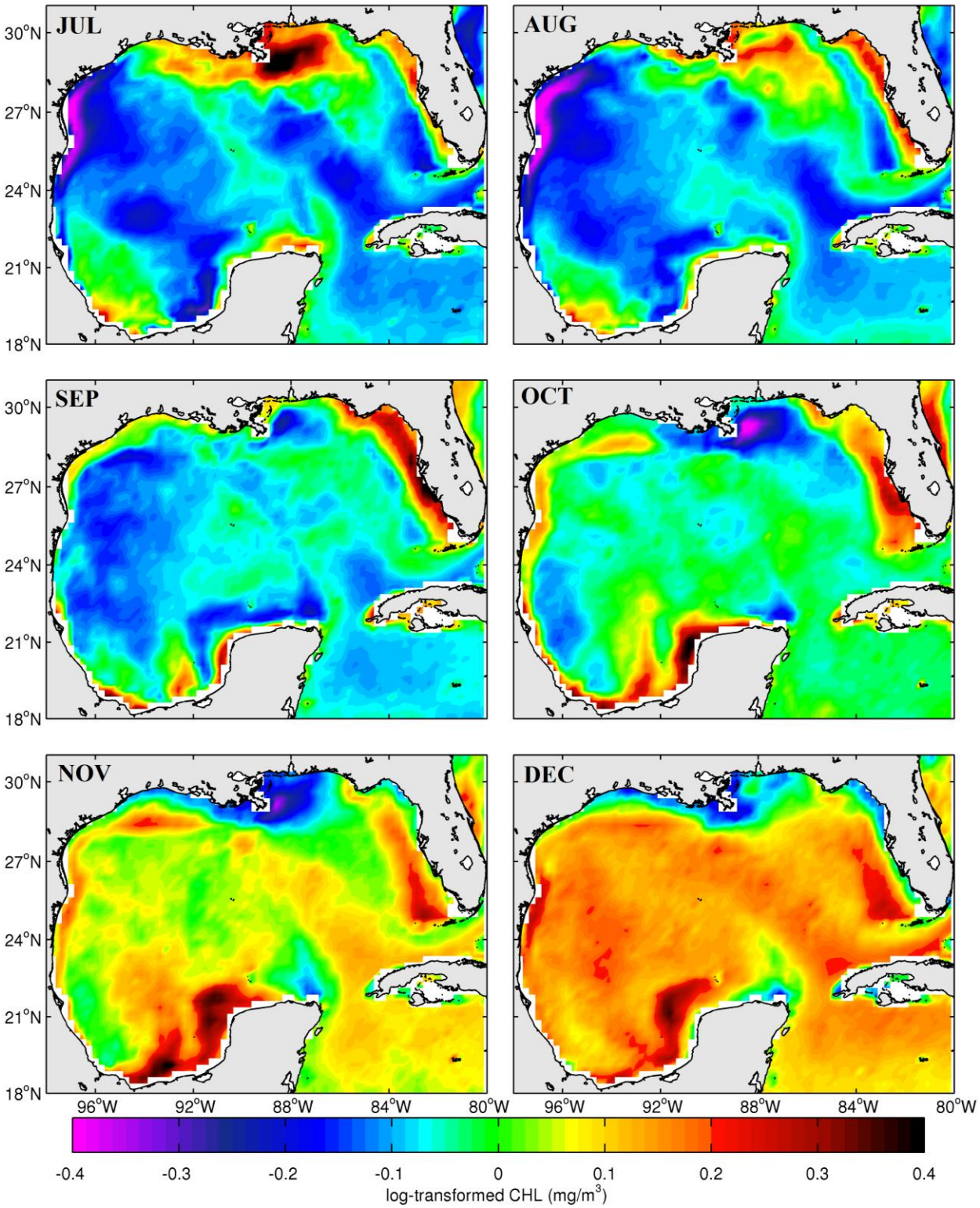


Fig. 3.3 (continued) Difference (color contour) maps between the 1998-2009 monthly means and the 1998-2009 annual mean (Figure 3.2A) of log-transformed chlorophyll-*a* concentration ($mg/m^3$).

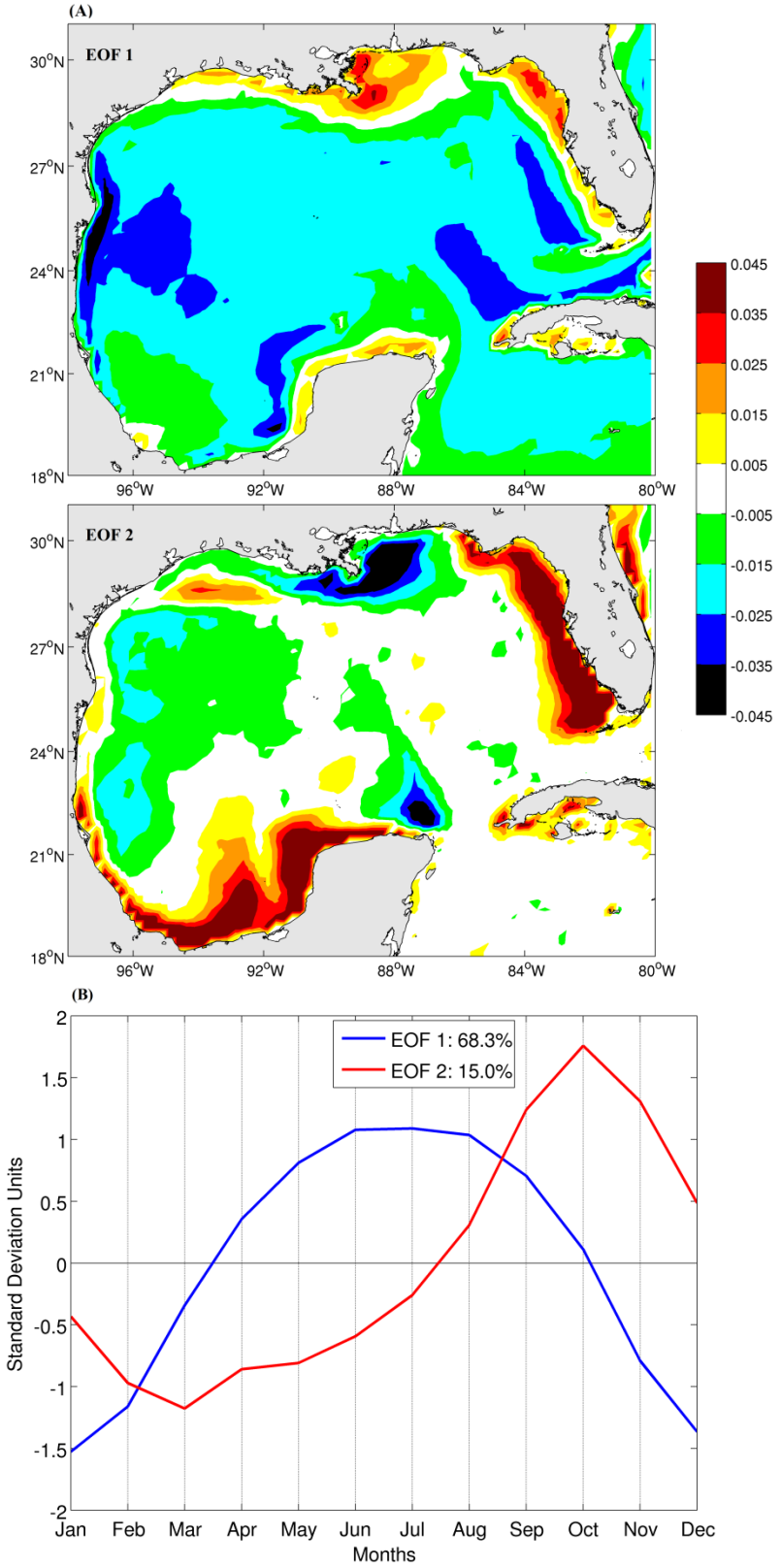


Fig. 3.4 (A) First two EOFs of the climatological seasonal cycle of log-transformed chlorophyll-*a* (mg/m$^3$) in Figure 3.3. (B) Standardized amplitude time series (expansion coefficients) of EOF1 (blue) and EOF2 (red).

## 3.5 Wind forcing

The 2000-2008 monthly means (also referred to as climatology) of surface vector wind stress over the Gulf of Mexico are in Figure 3.5. Overall, the spatial structure of this vector wind stress climatology looks similar to the spatial structure of the 1999-2006 vector wind climatology of Zavala-Hidalgo et al. (2014, their Fig. 2). The Zavala-Hidalgo et al. vector wind climatology was also derived from QuikSCAT scatterometer observations, but from an unspecified version of the dataset.

From October to February, winds are predominantly northeasterly with strong amplitudes over the entire Gulf. During March-April the winds are mostly easterlies with weaker magnitudes in the northeast. From May to August southeasterly winds dominate the Gulf with weaker magnitudes in the northeast region and strong magnitudes in the southwest region. During September the winds return to mostly easterlies but with uniform high magnitudes over the entire Gulf.

The monthly climatology of wind speed is presented in Figure 3.6. The monthly climatology of wind speeds has wind speeds that are higher during the winter and weaker during the summer. The stronger climatological wind speeds are seen in the period November-December-January and they correspond to the northeasterly climatological winds observed during these months (see Fig. 3.5). The months with the weaker wind speeds are June, July and August and they correspond to the southeasterly winds of Figure 3.5.

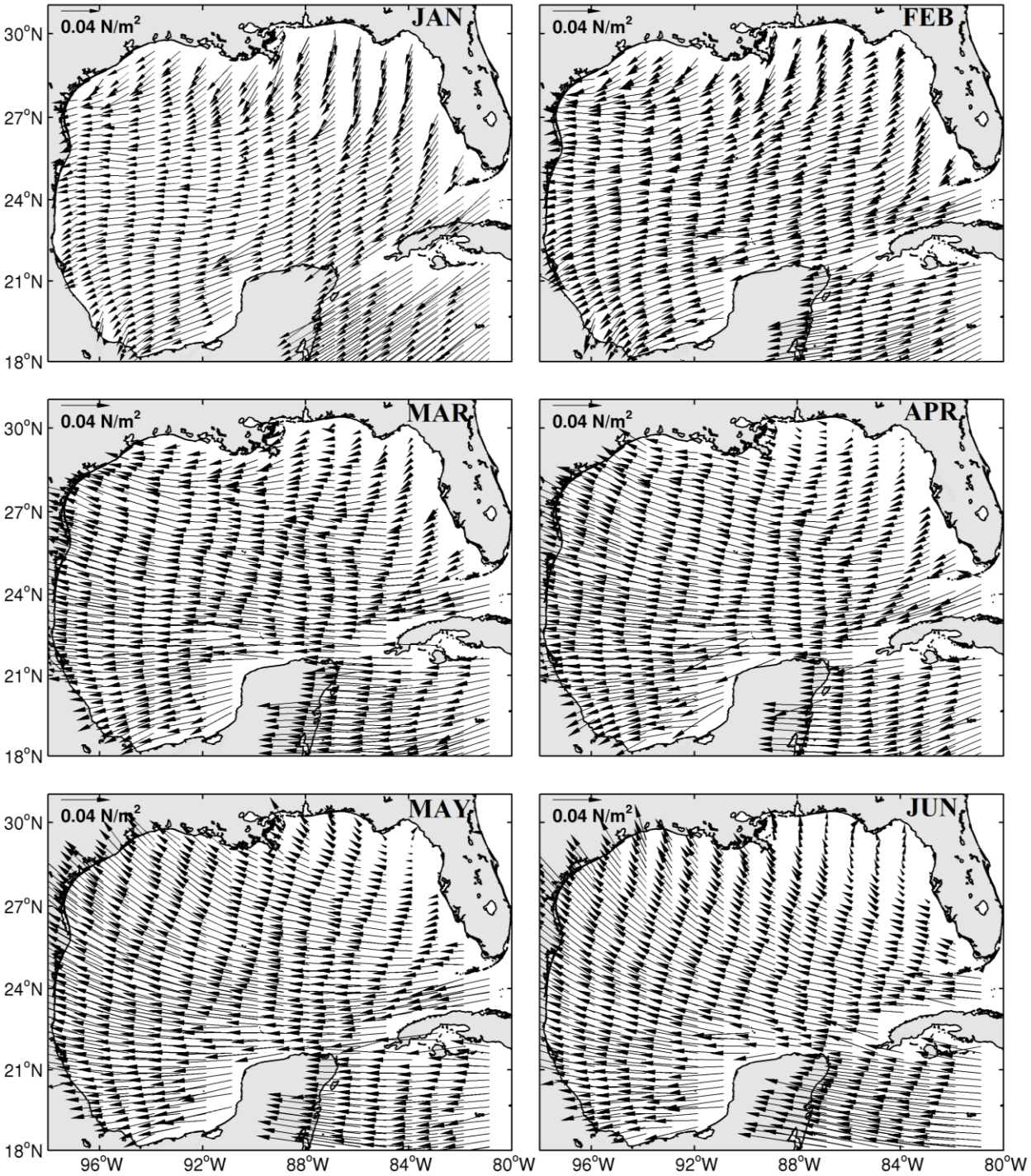


Fig. 3.5 Long-term monthly means (2000-2008) of surface vector wind stress ($N/m^2$) with the combined contributions of the monthly mean zonal and meridional wind components. A reference arrow of 0.04 $N/m^2$ is provided in the upper left corner of every map.

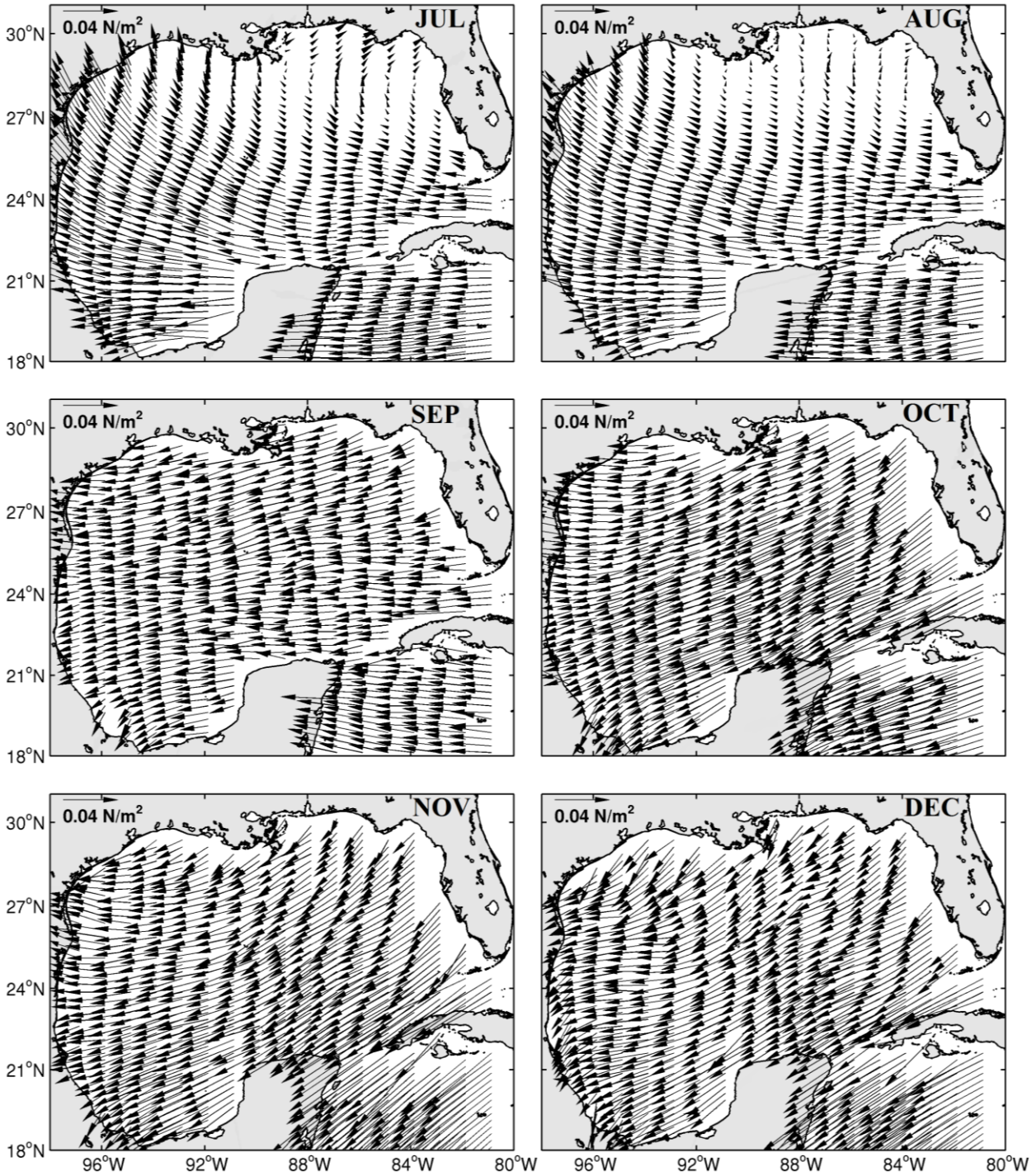


Fig. 3.5 (continued) Long-term monthly means (2000-2008) of surface vector wind stress ($N/m^2$) with the combined contributions of the monthly mean zonal and meridional wind components. A reference arrow of 0.04 $N/m^2$ is provided in the upper left corner of every map.

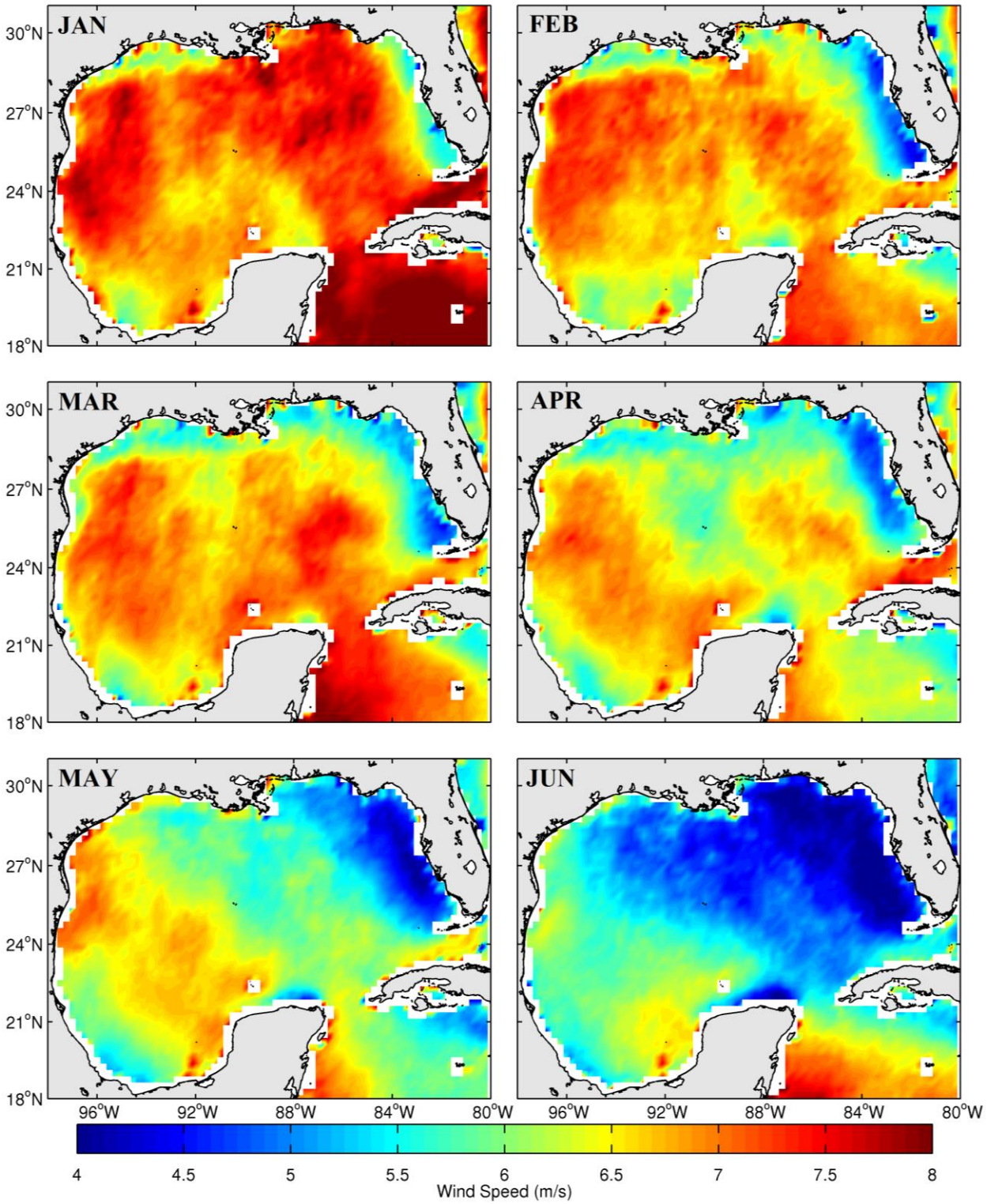


Fig. 3.6 Color contour maps of the long-term monthly means (2000-2008) of the surface wind speed (m/s).

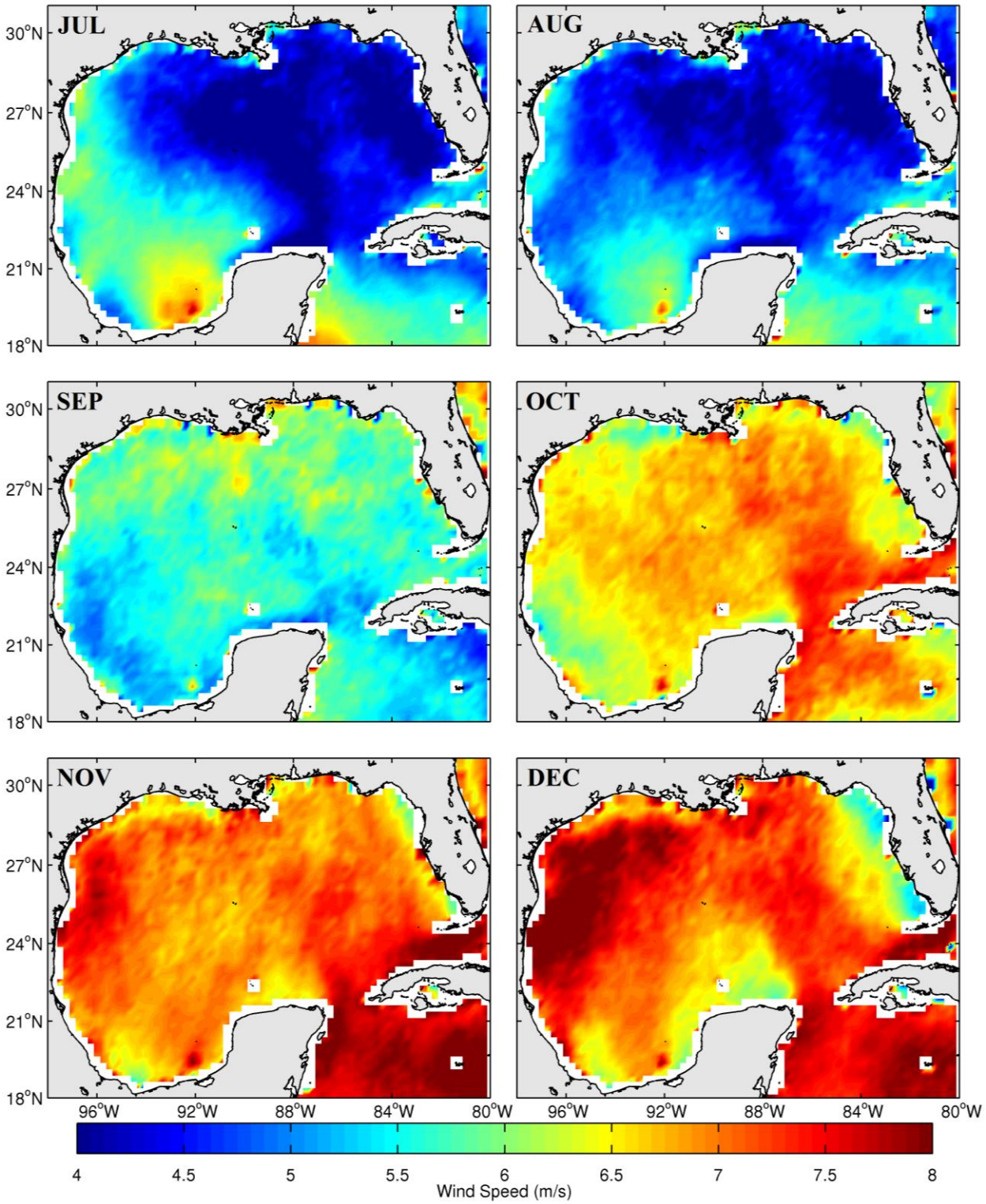


Fig. 3.6 (continued) Color contour maps of the long-term monthly means (2000-2008) of the surface wind speed (m/s).

3.6 Comparison of chlorophyll and wind forcing

To compare the seasonal variability of chlorophyll with that of wind forcing, an index approach is used based on (a) identifying regions where the seasonal chlorophyll variability is relatively stronger and (b) comparing the seasonal cycle of chlorophyll and winds spatially averaged over these areas. Seven regions of relatively large seasonal chlorophyll variability were identified from the standard deviation map of the chlorophyll seasonal cycle in Figure 3.7 and defined by the polygonal boundaries in Figure 3.8. These regions are as follows: Florida Shelf, Mississippi River mouth, Louisiana-Texas Shelf, Western Shelf, Western Interior, Bay of Campeche Shelf, and Eastern Interior.

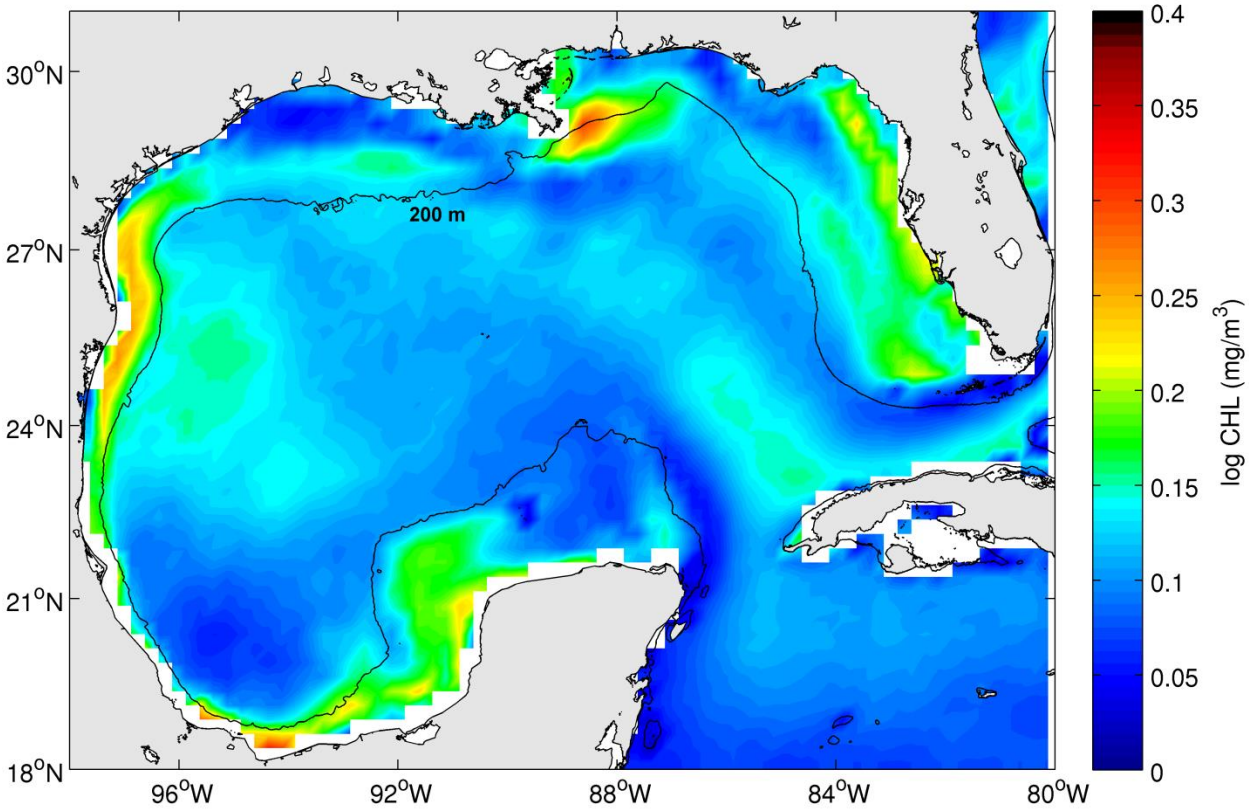


Fig. 3.7 Color contour map of the standard deviation calculated from the twelve monthly mean (1998-2009) values at every grid point of the log-transformed chlorophyll-*a* ($mg/m^3$) fields in Figure 3.3. The 200 m isobaths defining the continental shelf break are a solid black line.

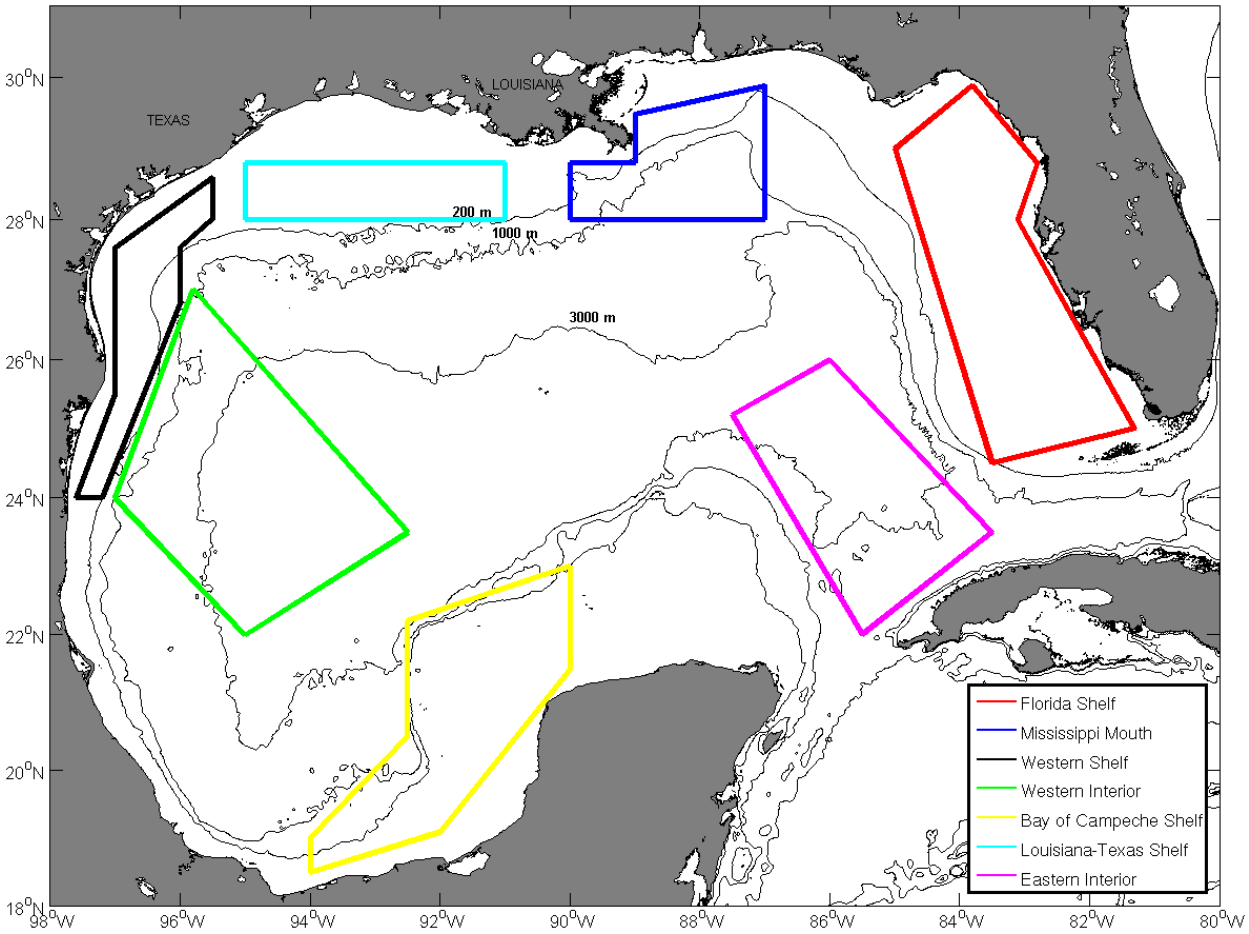


Fig. 3.8 Locations of polygonal boundaries defining regional indices of area-averaged chlorophyll-*a* based on regions of high seasonal variability as indicated in Figure 3.7. Black solid lines are the 200, 1000, and 3000 m isobaths.

The seasonal cycle of chlorophyll averaged in the index regions of Figure 3.8 are in Figure 3.9. Overall the Eastern Interior (pink) and Western Interior (green) have lower values of chlorophyll than the other regions. In these interior regions there are higher chlorophyll concentrations in the winter (December-January-February) and lower chlorophyll concentrations in the summer (June-July-August). The Bay of Campeche Shelf (yellow) and Florida Shelf (red) follow a similar cycle (although with slightly different phase) as the interior indices. The Louisiana-Texas Shelf (light blue) has two peaks, a larger one in December and a smaller one in July with minima in April and August. The Mississippi mouth (blue) has a strong chlorophyll peak in July and smaller values the rest of the year. The Western Shelf (black) chlorophyll is

approximately out of phase with the Mississippi mouth with a strong minimum in July and large values the rest of the year consistent the EOF1 of the seasonal cycle of chlorophyll in Figure 3.4.

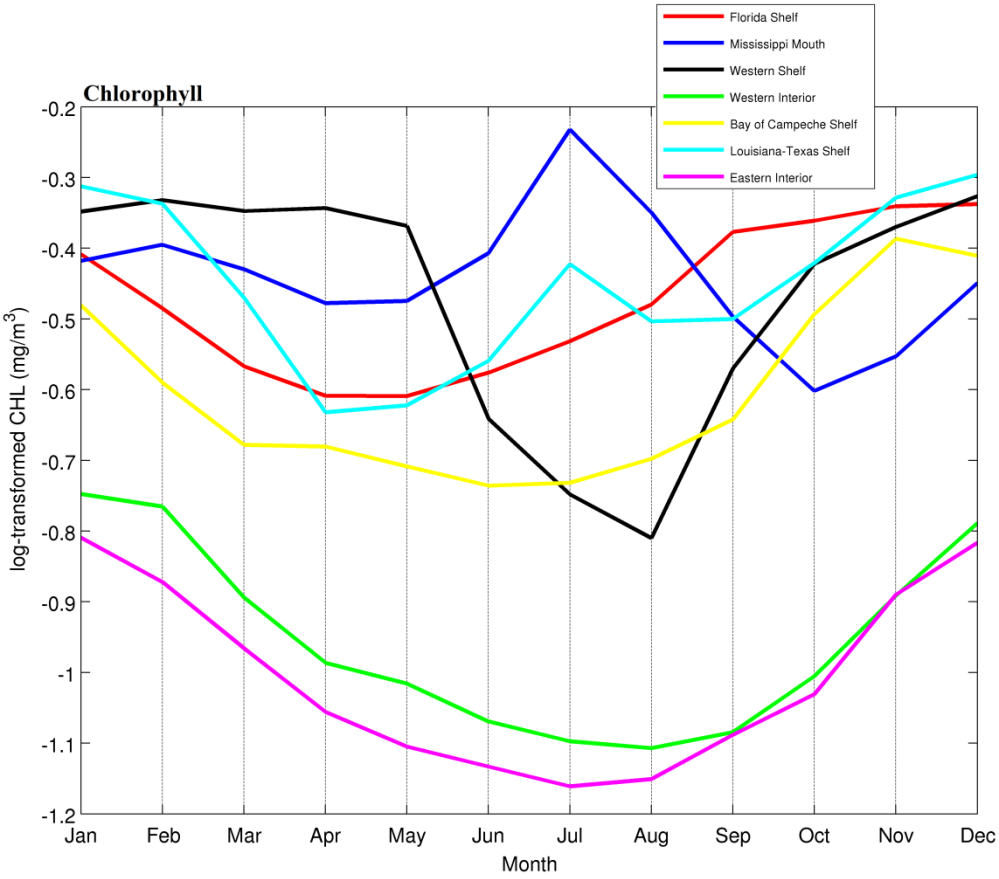


Fig. 3.9 Regional index time series of seasonal chlorophyll-*a* variability constructed by averaging the chlorophyll-*a* climatology in Figure 3.3 in the areas enclosed by the polygonal boundaries in Figure 3.8.

To compare the seasonal cycle of chlorophyll with that of wind forcing, average values for the seasonal cycle of zonal wind stress (Fig. 3.11A), meridional wind stress (Fig. 3.10B), and wind speed (Fig. 3.11) were calculated in the index regions of Figure 3.8.

The zonal wind stress in all index regions and throughout the year is dominated by easterly winds indicated by the predominantly negative values of the indices in Figure 3.10A. The temporal evolution in general has weakening easterlies through the spring and summer (February-July) with a sharp intensification in the fall from August to October which sets up stronger easterly winds throughout the winter. The region with the stronger zonal easterly winds

throughout the year is the Bay of Campeche Shelf (yellow). Westerly winds only occur in July for the Mississippi mouth index (blue).

The meridional wind stress (Fig. 3.10B) in most of the index regions generally experience southerly (positive) winds in the spring and summer and northerly (negative) winds in the fall and winter. The stronger southerly winds are in May, June, and July while the stronger northerly winds are in October and November. The region with the most dominant southerly winds is the Western Shelf (black). The Bay of Campeche Shelf (yellow) is the area more dominated by northerly winds. The stronger northerly winds are seen in the Eastern Interior (pink) during October-November. The meridional wind indices experience a sharp transition from southerly to northerly winds from August to October which coincides with the timing of the easterly wind intensification in Figure 3.10A.

The regional wind speed indices (Fig. 3.11) have an annual cycle of low wind speeds during winter spring and fall (January to August) and a sharp increase in the fall to winter transition (August to December). The exact timing of minimum and maximum between two indices, however, may differ by one month. The minimum wind speed in the Florida Shelf (red), Mississippi mouth (blue), and Eastern Interior (pink) occurs in July. The minimum wind speed in the Louisiana-Texas Shelf (light blue), Western Interior (green), and Western Shelf (black) occurs in August. The Bay of Campeche Shelf (yellow) is the only index with a minimum wind speed in September. The maximum wind speed in the Florida Shelf (red), Bay of Campeche (yellow), and Eastern Interior (pink) occurs in November and the maximum wind speed in the other indices occurs in December.

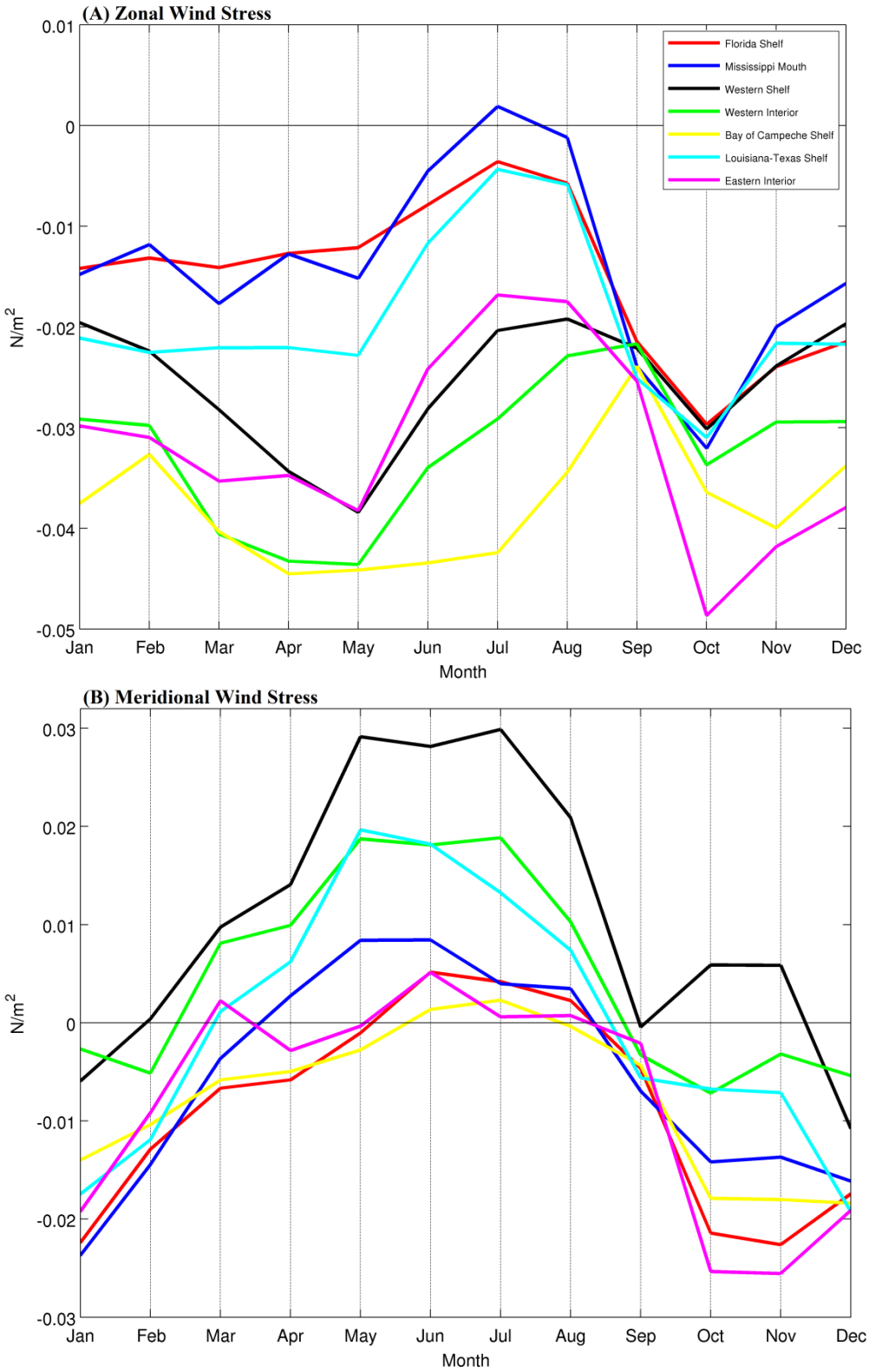


Fig. 3.10 Regional index time series for (A) zonal wind stress and (B) meridional wind stress ($N/m^2$) in the areas enclosed by the polygonal boundaries in Figure 3.8. Negative zonal values are wind towards the west. Negative meridional values are wind towards the south.

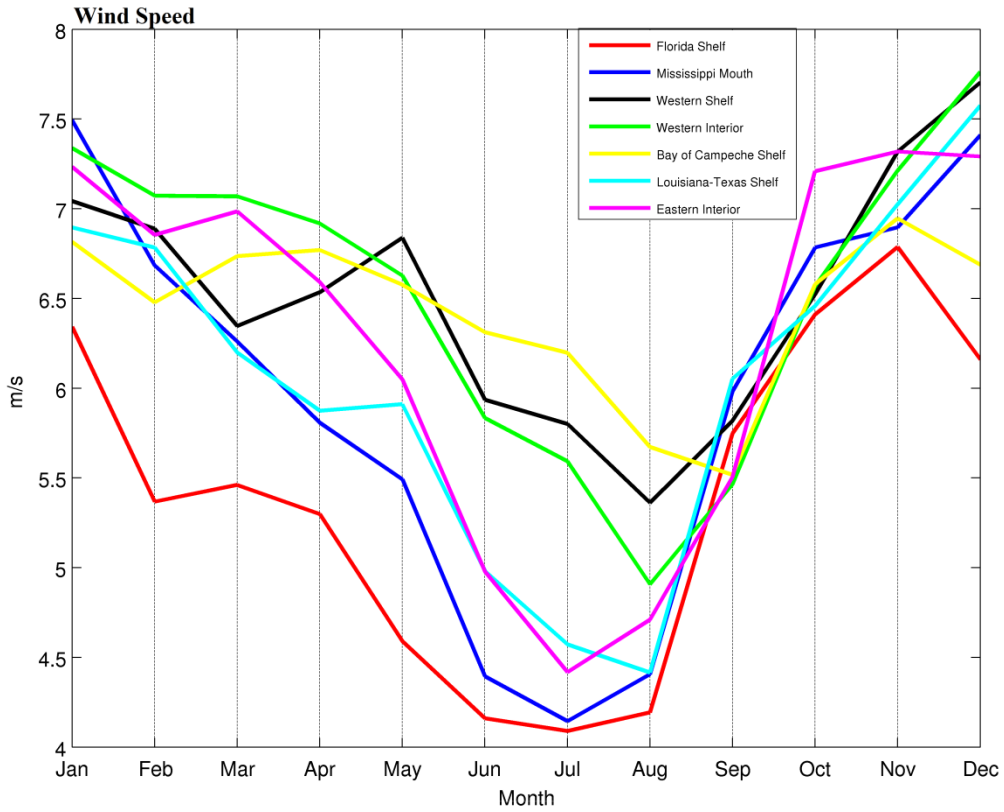


Fig. 3.11 Regional index time series for wind speed (m/s) in the areas enclosed by the polygonal boundaries in Figure 3.8.

The time evolution of the chlorophyll indices in Figure 3.9 are compared with those of the wind indices in Figures 3.10 and 3.11. Some associations involving wind speed and zonal winds are apparent from this comparison. Over the interior regions the lower (higher) values chlorophyll during the summer (winter) correspond well with the simultaneous weaker (stronger) wind speeds. Over the Bay of Campeche and Florida shelves the seasonal cycle is similar to the interior but chlorophyll increases more rapidly after the summer months because of the development of northerly winds during the fall. The increase (decrease) of chlorophyll in the Mississippi mouth (Western Shelf) from May to July corresponds well with the simultaneous weakening of the easterlies over most of the Gulf.

Table 3.1 Standard deviations for each time series in Figures 3.9-3.11 within in each regional box (Fig. 3.8).

| | Chlorophyll (log-mg/$m^3$) | Zonal Wind Stress ($N/m^2$) | Meridional Wind Stress ($N/m^2$) | Wind Speed (m/s) |
|---|---|---|---|---|
| Florida Shelf | 0.1052 | 0.0078 | 0.0105 | 0.9491 |
| Mississippi Mouth | 0.0954 | 0.0095 | 0.0109 | 1.1687 |
| Western Shelf | 0.1759 | 0.0063 | 0.0140 | 0.6921 |
| Western Interior | 0.1331 | 0.0072 | 0.0103 | 0.8799 |
| Bay of Campeche Shelf | 0.1274 | 0.0060 | 0.0077 | 0.4484 |
| Louisiana-Texas Shelf | 0.1176 | 0.0079 | 0.0132 | 0.9890 |
| Eastern Interior | 0.1309 | 0.0096 | 0.0113 | 1.0904 |

Table 3.2 Standard deviation for each regional box (Fig. 3.8) in a given month for chlorophyll (log-mg/$m^3$) (Fig. 3.9).

| | Florida Shelf | Mississippi Mouth | Western Shelf | Western Interior | Bay of Campeche Shelf | Louisiana-Texas Shelf | Eastern Interior |
|---|---|---|---|---|---|---|---|
| January | 0.2413 | 0.2572 | 0.2065 | 0.0474 | 0.1811 | 0.1915 | 0.0402 |
| February | 0.2249 | 0.2308 | 0.1974 | 0.0846 | 0.1654 | 0.1848 | 0.0462 |
| March | 0.2762 | 0.3112 | 0.2169 | 0.0757 | 0.1651 | 0.2378 | 0.0352 |
| April | 0.3253 | 0.3919 | 0.2044 | 0.0769 | 0.1824 | 0.2363 | 0.0325 |
| May | 0.3929 | 0.3845 | 0.2384 | 0.0975 | 0.2004 | 0.2297 | 0.0378 |
| June | 0.4331 | 0.4149 | 0.2034 | 0.0727 | 0.2253 | 0.2032 | 0.0391 |
| July | 0.4381 | 0.4031 | 0.1705 | 0.0622 | 0.2507 | 0.2487 | 0.0615 |
| August | 0.4520 | 0.3387 | 0.1402 | 0.0443 | 0.2726 | 0.2105 | 0.0688 |
| September | 0.4726 | 0.2791 | 0.2384 | 0.0540 | 0.2803 | 0.2394 | 0.0564 |
| October | 0.4093 | 0.2551 | 0.2237 | 0.0719 | 0.3101 | 0.2204 | 0.0414 |
| November | 0.3058 | 0.2394 | 0.2109 | 0.0545 | 0.2738 | 0.2036 | 0.0256 |
| December | 0.2667 | 0.2423 | 0.2098 | 0.0531 | 0.2160 | 0.1828 | 0.0326 |

Table 3.3 Standard deviation for each regional box (Fig. 3.8) in a given month for zonal wind stress ($N/m^2$) (Fig 3.10A).

| | Florida Shelf | Mississippi Mouth | Western Shelf | Western Interior | Bay of Campeche Shelf | Louisiana-Texas Shelf | Eastern Interior |
|---|---|---|---|---|---|---|---|
| January | 0.0067 | 0.0033 | 0.0033 | 0.0035 | 0.0031 | 0.0025 | 0.0047 |
| February | 0.0055 | 0.0036 | 0.0039 | 0.0024 | 0.0048 | 0.0032 | 0.0028 |
| March | 0.0069 | 0.0047 | 0.0039 | 0.0031 | 0.0058 | 0.0032 | 0.0023 |
| April | 0.0082 | 0.0044 | 0.0045 | 0.0027 | 0.0064 | 0.0026 | 0.0033 |
| May | 0.0080 | 0.0046 | 0.0048 | 0.0027 | 0.0059 | 0.0025 | 0.0033 |
| June | 0.0061 | 0.0026 | 0.0042 | 0.0031 | 0.0043 | 0.0024 | 0.0030 |
| July | 0.0061 | 0.0027 | 0.0040 | 0.0048 | 0.0072 | 0.0031 | 0.0035 |
| August | 0.0060 | 0.0017 | 0.0035 | 0.0035 | 0.0053 | 0.0019 | 0.0032 |
| September | 0.0048 | 0.0032 | 0.0022 | 0.0026 | 0.0034 | 0.0026 | 0.0024 |
| October | 0.0057 | 0.0036 | 0.0019 | 0.0033 | 0.0045 | 0.0028 | 0.0039 |
| November | 0.0081 | 0.0028 | 0.0026 | 0.0029 | 0.0040 | 0.0023 | 0.0052 |
| December | 0.0082 | 0.0024 | 0.0032 | 0.0040 | 0.0048 | 0.0033 | 0.0043 |

Table 3.4 Standard deviation for each regional box (Fig. 3.8) in a given month for meridional wind stress ($N/m^2$) (Fig 3.10B).

| | Florida Shelf | Mississippi Mouth | Western Shelf | Western Interior | Bay of Campeche Shelf | Louisiana-Texas Shelf | Eastern Interior |
|---|---|---|---|---|---|---|---|
| January | 0.0042 | 0.0058 | 0.0037 | 0.0030 | 0.0040 | 0.0044 | 0.0032 |
| February | 0.0033 | 0.0034 | 0.0041 | 0.0041 | 0.0046 | 0.0035 | 0.0025 |
| March | 0.0039 | 0.0031 | 0.0029 | 0.0036 | 0.0043 | 0.0032 | 0.0022 |
| April | 0.0038 | 0.0021 | 0.0026 | 0.0038 | 0.0042 | 0.0040 | 0.0034 |
| May | 0.0043 | 0.0014 | 0.0020 | 0.0057 | 0.0043 | 0.0041 | 0.0031 |
| June | 0.0016 | 0.0016 | 0.0029 | 0.0052 | 0.0046 | 0.0035 | 0.0016 |
| July | 0.0014 | 0.0012 | 0.0032 | 0.0053 | 0.0067 | 0.0039 | 0.0019 |
| August | 0.0014 | 0.0016 | 0.0025 | 0.0035 | 0.0057 | 0.0032 | 0.0020 |
| September | 0.0042 | 0.0019 | 0.0021 | 0.0013 | 0.0033 | 0.0028 | 0.0018 |
| October | 0.0042 | 0.0025 | 0.0023 | 0.0060 | 0.0028 | 0.0058 | 0.0033 |
| November | 0.0055 | 0.0017 | 0.0036 | 0.0053 | 0.0032 | 0.0029 | 0.0039 |
| December | 0.0050 | 0.0022 | 0.0041 | 0.0030 | 0.0027 | 0.0035 | 0.0027 |

Table 3.5 Standard deviation for each regional box (Fig. 3.8) in a given month for wind speed (m/s) (Fig 3.11).

| | Florida Shelf | Mississippi Mouth | Western Shelf | Western Interior | Bay of Campeche Shelf | Louisiana-Texas Shelf | Eastern Interior |
|---|---|---|---|---|---|---|---|
| January | 0.6170 | 0.2558 | 0.3458 | 0.3099 | 0.2139 | 0.3340 | 0.1291 |
| February | 0.5321 | 0.3497 | 0.4040 | 0.2467 | 0.2827 | 0.3330 | 0.1921 |
| March | 0.4650 | 0.3877 | 0.3381 | 0.1386 | 0.3537 | 0.3042 | 0.2685 |
| April | 0.4609 | 0.2469 | 0.2720 | 0.1442 | 0.3365 | 0.2380 | 0.2058 |
| May | 0.4340 | 0.2683 | 0.1705 | 0.1947 | 0.3627 | 0.2226 | 0.1464 |
| June | 0.2991 | 0.2697 | 0.2038 | 0.1613 | 0.3059 | 0.2081 | 0.1575 |
| July | 0.2943 | 0.2558 | 0.2462 | 0.2490 | 0.5187 | 0.2301 | 0.1737 |
| August | 0.3070 | 0.2435 | 0.2552 | 0.2240 | 0.4371 | 0.1898 | 0.1751 |
| September | 0.3029 | 0.1774 | 0.1803 | 0.2071 | 0.2614 | 0.1794 | 0.2185 |
| October | 0.3070 | 0.2011 | 0.1533 | 0.1842 | 0.2309 | 0.2098 | 0.1731 |
| November | 0.3981 | 0.1612 | 0.2760 | 0.3047 | 0.2322 | 0.2174 | 0.1723 |
| December | 0.4609 | 0.2133 | 0.3749 | 0.4292 | 0.2619 | 0.3291 | 0.1209 |

The standard deviation for the mean values of each time series (Figs. 3.9-3.11) within each regional box (Fig. 3.8) is in Table 3.1. The highest variability for chlorophyll is on the Western Shelf and the lowest variability is at the Mississippi mouth. Zonal wind stress has high variabilities at the Mississippi mouth and Eastern Interior while the meridional wind stress has the highest variability on the Western Shelf. The wind speed has the highest variability within each regional box among the four variables listed. The regional area with the highest variability for wind speed is the Mississippi mouth.

Tables 3.2, 3.3, 3.4, and 3.5 have standard deviation budgets within each month for chlorophyll, zonal wind stress, meridional wind stress, and wind speed, respectively. Within each table, seasonal cycles are apparent within each region. For example, in Table 3.2, chlorophyll at the Mississippi mouth has the highest variability over the summer months (June, July, August) when chlorophyll values are at their peak (Fig. 3.9).

The relationship between the seasonal variability of chlorophyll and wind speed suggested by the index analysis can be extracted by an SVD analysis applied to the seasonal anomalies of these two variables. The leading SVD of chlorophyll and wind speed explaining 98% of the total square covariance is in Figure 3.12. Except near the Mississippi mouth and the northeast Florida Shelf, the seasonal anomalies of chlorophyll and wind speed are in phase with a simultaneous increase of wind speed and chlorophyll during the winter and the opposite holding true during the summer.

The leading SVD modes of the seasonal anomalies of chlorophyll with both zonal and meridional wind stress explain 78% and 98% of the total square covariance, respectively (Figs. 3.13 and 3.14). The chlorophyll-zonal stress SVD coupled mode (Fig. 3.13) describes well the annual “seesaw” pattern of chlorophyll between the Western Shelf and just east of the

Mississippi mouth, as suggested by the index analysis. A decrease (increase) of chlorophyll in the Western Shelf and an increase (decrease) of chlorophyll in the Mississippi mouth are associated with a weakening (strengthening) of the easterlies over the northern Gulf. The chlorophyll-meridional stress coupled SVD mode (Fig. 3.14) captures the development of upwelling (downwelling) favorable northerly (southerly) winds over the Campeche and Florida shelves during the fall (spring).

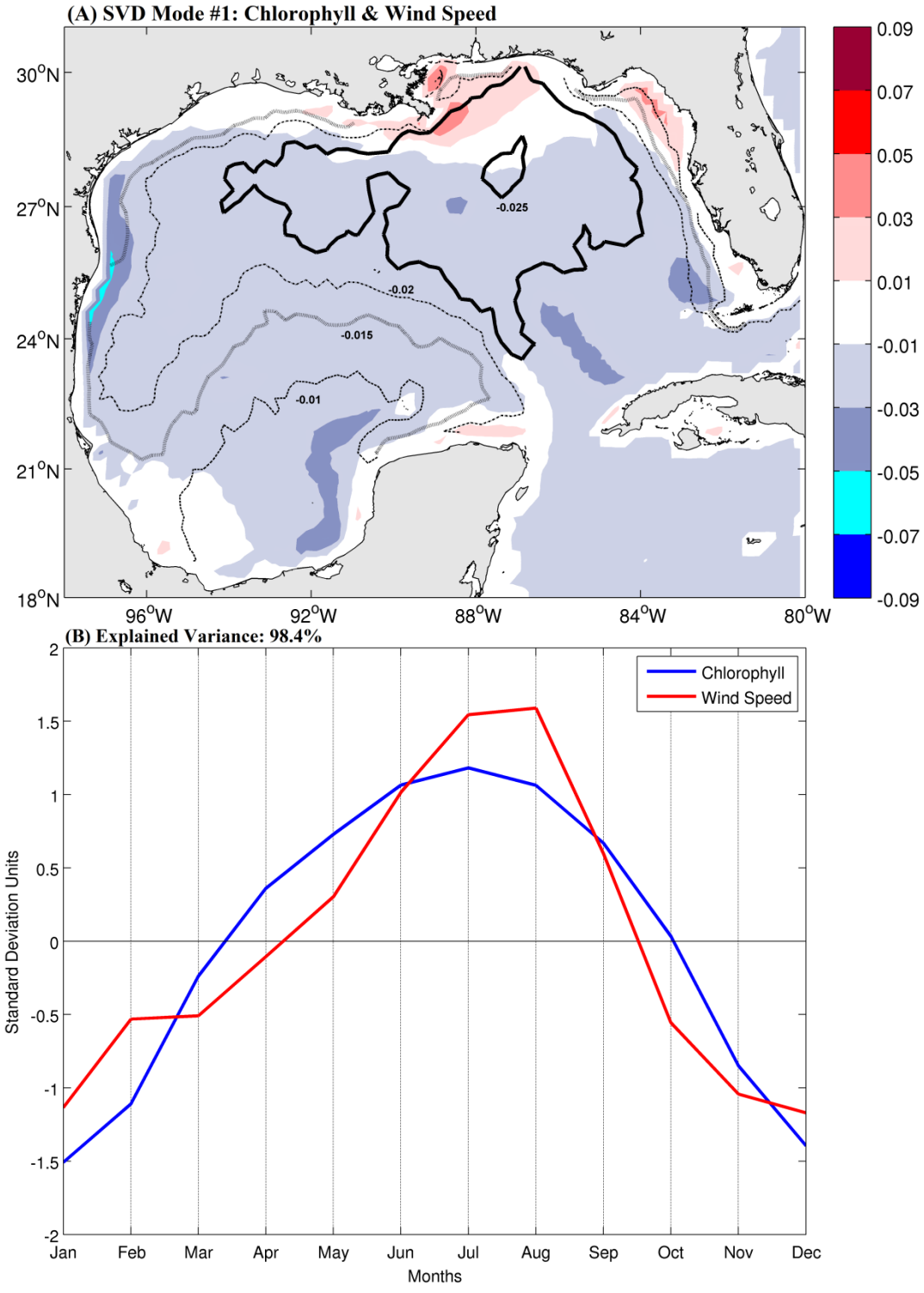


Fig. 3.12 (A) Mode 1 of a combined SVD analysis of chlorophyll-*a* (color contours) and wind speed (line contours) of the seasonal cycle. (B) Each month of the 9-year (2000-2008) time series of chlorophyll (blue) and wind speed (red) is used with the percent of total variance as indicated.

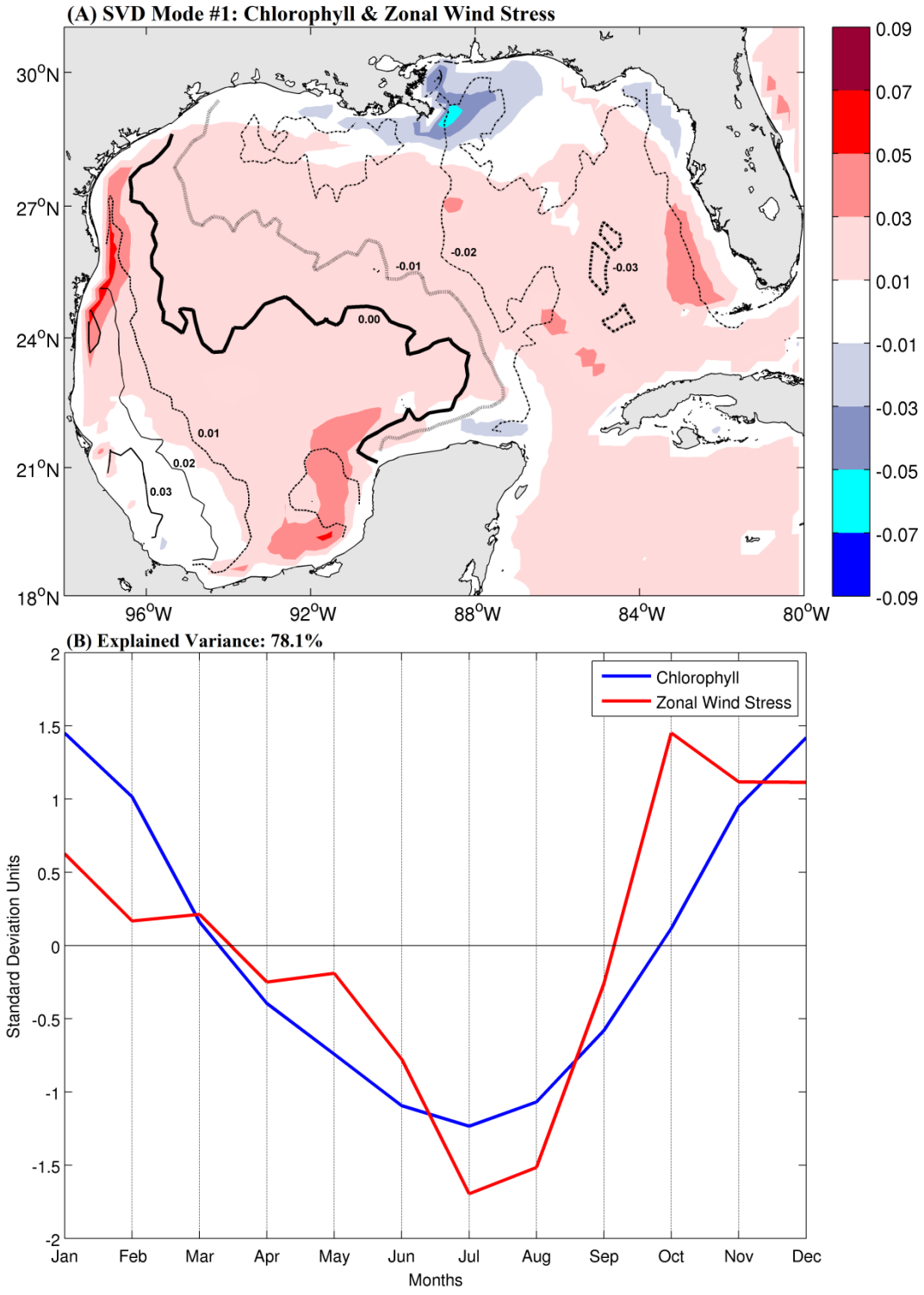


Fig. 3.13 (A) Mode 1 of a combined SVD analysis of chlorophyll-*a* (color contours) and zonal wind stress (line contours) of the seasonal cycle. (B) Each month of the 9-year (2000-2008) time series of chlorophyll (blue) and zonal wind stress (red) is used with the percent of total variance as indicated.

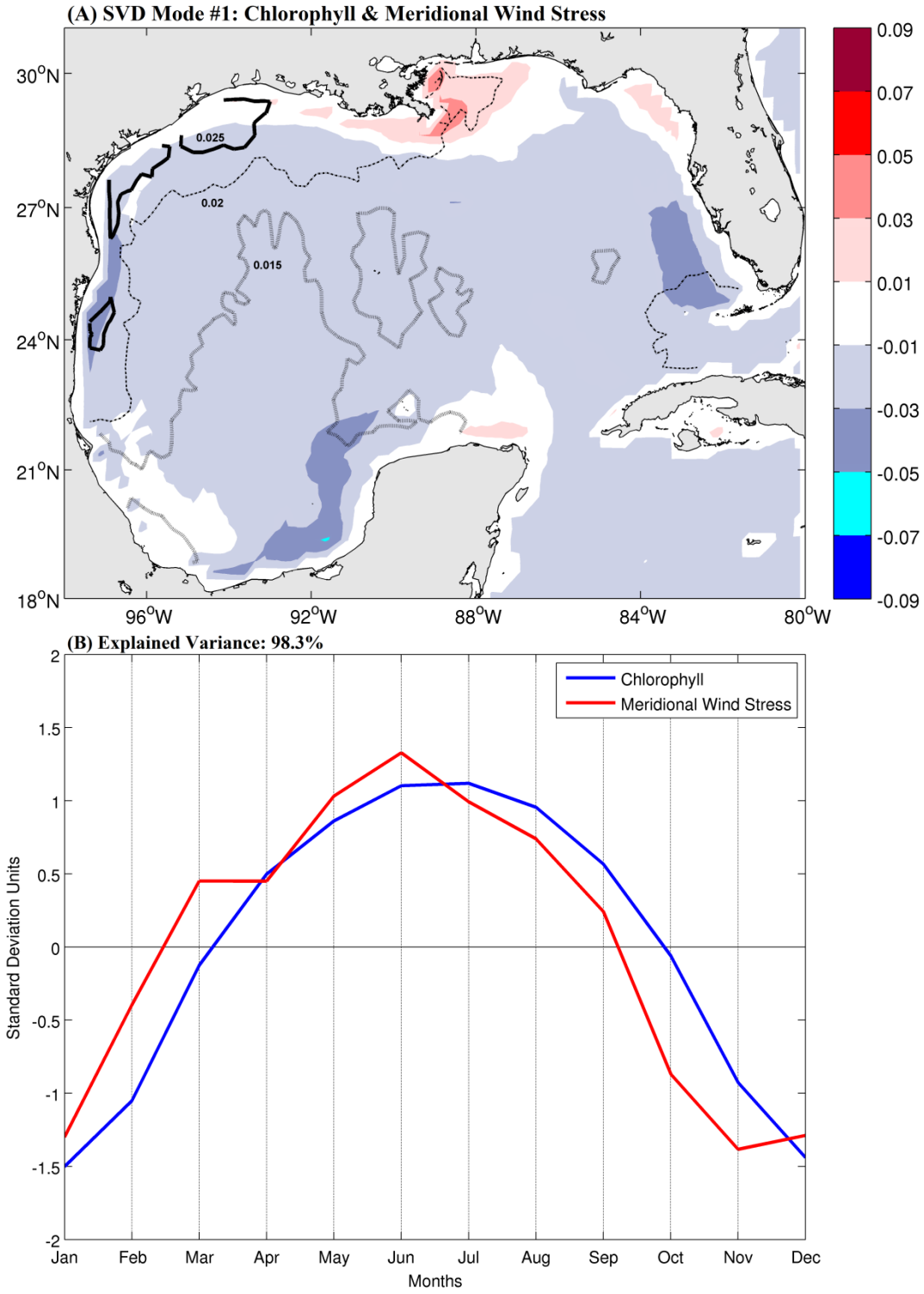


Fig. 3.14 (A) Mode 1 of a combined SVD analysis of chlorophyll-*a* (color contours) and meridional wind stress (line contours) of the seasonal cycle. (B) Each month of the 9-year (2000-2008) time series of chlorophyll (blue) and zonal wind stress (red) is used with the percent of total variance as indicated.

Discussion

The regional distribution of chlorophyll in the Gulf of Mexico is dependent upon many variables such as nutrient inputs, physical forcing, circulation patterns, and areas of upwelling. One of the most prominent features of the Gulf of Mexico system is the massive influx of nutrients from the Mississippi River off the coast of Louisiana. As a result of this input, the primary productivity and chlorophyll concentration in the northern coastal areas of the Gulf are high; this nutrient-enhanced high-productivity region has been the focus of many research studies (e.g., Lohrenz et al. 1990, 1997, 1999, Rabalais et al. 1999, 2002). The maximum climatological discharge for the Mississippi-Atchafalaya River system occurs in the winter and spring (peak flow in March, April, and May) and low discharge in the summer and early fall (June-September) (e.g., Lohrenz et al. 1997, Martínez-López and Zavala-Hidalgo 2009). Although the flow is reduced in the summer, Rabalais et al. (1999) asserted that large-scale circulation patterns facilitate the retention of fresh water on the shelf. Therefore, the summer peaks of chlorophyll near the Mississippi mouth could result from accumulation of river inputs leading up to that time period.

The direct correlation between river borne nutrient fluxes and primary production in the areas of the northern Gulf was demonstrated by Lohrenz et al. (1997). The Lohrenz et al. study used in situ data from cruises during the period of 1988-1994 to evaluate primary production measurements in three geographical regions around the delta of the Mississippi River. Elevated levels of primary production (~10 gC $m^{-2}$ $d^{-1}$) were found at the mouth of the Mississippi in July, while drastically lower values occurred in September (~0.5 gC $m^{-2}$ $d^{-1}$). The month of August had intermediate levels (~3 gC $m^{-2}$ $d^{-1}$) west of the delta region (their Fig. 2). Monthly climatology of phytoplankton pigment concentrations were measured by the Coastal Zone Color

Scanner from November 1978-November 1985 by Müller-Karger et al. 1991. Phytoplankton pigment concentrations were highest (>0.18 mg/$m^3$) in December-February and lowest (~0.06 mg/$m^3$) May-July. They attributed that the most important factor impacting pigment concentrations was the depth of the mixed layer.

Hypoxia, or low oxygen, is an environmental phenomenon where the concentration of dissolved oxygen in the water column decreases to a level that can no longer support living aquatic organisms. Hypoxic areas, or "Dead Zones," have increased in duration and frequency since first being noted in the 1970s. The largest hypoxic zone currently affecting the United States, and the second largest hypoxic zone worldwide, is the northern Gulf of Mexico adjacent to the Mississippi River (Fig. 3.15). Hypoxia in the northern Gulf of Mexico is defined as a concentration of dissolved oxygen less than 2 mg/L (2 ppm). The first concerted, continuous, and consistent documentation of the temporal and spatial extent of hypoxia on the Louisiana and Texas continental shelf began in 1985 and continues with active research groups. How the knowledge about the hypoxic zone in the northern Gulf relate to findings from this current study create additional research questions to be pursued.

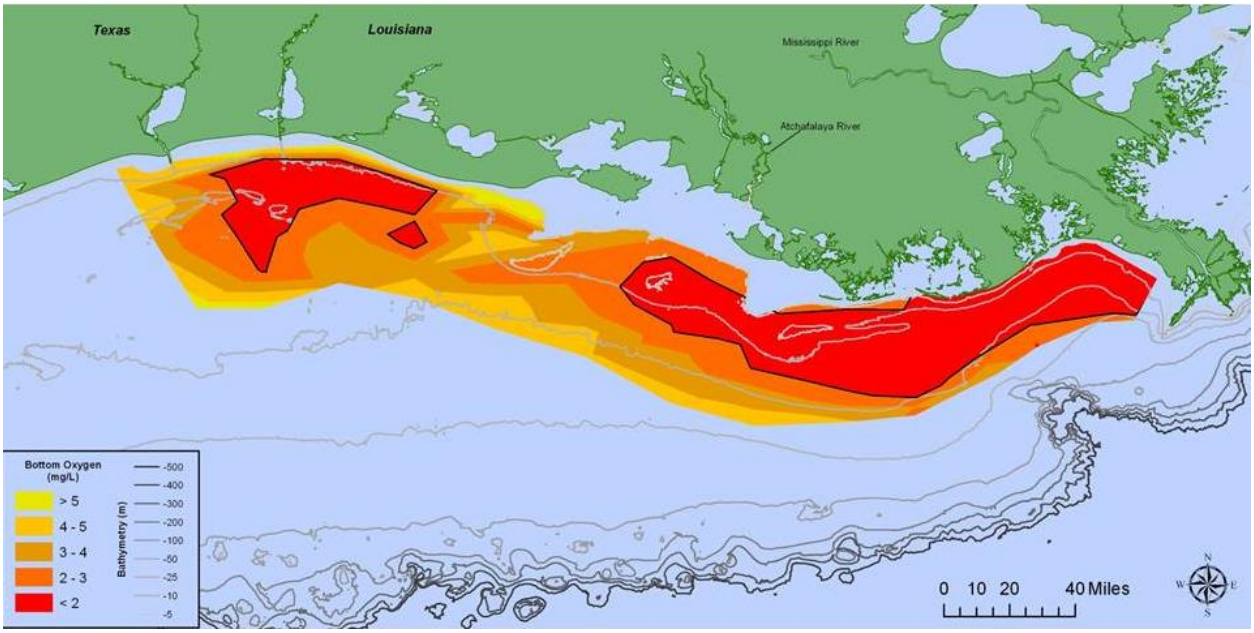


Fig. 3.15 Distribution of bottom-water dissolved oxygen July 27-August 1, 2014. Black line indicates dissolved oxygen level of 2 mg/L. Data source of figure is Nancy N. Rabalais, LUMCON, and R. Eugene Turner, LSU via the NOAA Center for Sponsored Coastal Ocean Research and the U.S. EPA Gulf of Mexico Program.

In this study, I used a multiyear, monthly dataset of merged satellite chlorophyll (GlobColour) to explore association with QuikSCAT satellite scatterometer wind speed and vector wind stress over the Gulf of Mexico. I confirm that the influence of the Mississippi River is important not only for the annual mean chlorophyll but also for its seasonal variability, which in turn can be associated with seasonal changes in the winds as suggested by previous studies (e.g., Martínez-López and Zavala-Hidalgo 2009). The main conclusions of this study follow:

1) Analysis of annual mean chlorophyll confirms that larger values of chlorophyll are observed over the shelf or near the shelf break (Fig. 3.2A). The larger overall values of chlorophyll are found near the mouth of the Mississippi River extending westward over the Louisiana-Texas inner shelf. The annual mean vector winds indicate that this may be because of westward advection of nutrient-rich Mississippi River waters by the mean easterly winds over the northern Gulf (Fig. 3.2B).

2) The seasonal cycle of chlorophyll has larger amplitude variations over the Gulf shelves than over the interior (Fig. 3.7). Near and to the east of the Mississippi River mouth larger amplitudes in the seasonal cycle extend beyond the shelf break.
3) In the interior, the seasonal variability of chlorophyll has lower values during the summer and higher values during the winter. These annual fluctuations of chlorophyll are in phase with the seasonal cycle of wind speed (i.e., summer weakening and winter strengthening) over the Gulf (Fig. 3.12). Wind speed can be considered as a proxy directly related to turbulent mixing, mixed layer depth, and entrainment of nutrients at the bottom of the mixed layer. Thus, this direct seasonal association between chlorophyll and wind speed may be interpreted as increased (decreased) turbulent mixing/mixed layer depth during winter (summer) as suggested by Müller-Karger et al. (1991).
4) Over the Bay of Campeche and Florida shelves the seasonal cycle of chlorophyll is similar than that of the interior except the increase of chlorophyll from summer to winter occurs earlier because of the development of upwelling favorably (northerly) meridional winds during the fall.
5) The most remarkable feature of the climatological seasonal chlorophyll variability is an annual "seesaw" (dipole) pattern between the two extremes of the annual mean Mississippi River plume that is associated with simultaneous annual changes in the zonal wind stress (Fig. 3.13). Strengthening of the zonal easterly winds during the winter is associated with increases in chlorophyll over the Western Shelf and decreases of chlorophyll near the Mississippi mouth. The opposite seasonal changes of chlorophyll and zonal winds occur during the summer. This out of phase

relationship between the Western Shelf and the Mississippi mouth was also evident in the seasonal cycle results of Martínez-López and Zavala-Hidalgo (2009; see their Fig. 4) although their non-logged chlorophyll representations did not facilitate the interpretation. For example, the range of variation in the Western Shelf is about 0.15-0.3 $mg/m^3$ while in the Mississippi mouth is about 0.4-1.2 $mg/m^3$.

References

Behringer DW, Molinari RL, Festa JF (1977) The variability of anticyclonic flow patterns in the Gulf of Mexico. J Geophys Res 82:5469-5476

Björnsson H, Venegas SA (1997) A manual for EOF and SVD analyses of climate data. McGill University, CCGCR Report No. 97-1, Montreal, Quebec, 52 pp

Bourassa MA, Legler DM, O'Brien JJ, Smith SR (2003) SeaWinds validation with research vessels. J Geophys Res 108(C2):3019, doi:10.1029/2001JC001028

Campbell JW (1995) The lognormal distribution as a model for bio-optical variability in the sea. J Geophys Res 100:13237-13254

Cochrane JD, Kelly FJ (1986) Low-frequency circulation on the Texas-Louisiana continental shelf. J Geophys Res 91:10645-10659

Ebuchi N, Graber HC, Caruso MJ (2002) Evaluation of wind vectors observed by QuikSCAT/SeaWinds using ocean buoy data. J Atom Oceanic Technol 19:2049-2062

Goldenberg SB, O'Brien JJ (1981) Time and space variability of tropical Pacific wind stress. Mon Wea Rev 109:1190-1207

Hofmann EE, Worley SJ (1986) An investigation of the circulation of the Gulf of Mexico. J Geophys Res 91:14221-14236

Large WG, McWilliams JC, Doney SC (1994) Oceanic vertical mixing: A review and a model with a nonlocal boundary layer parameterization. Rev Geophys 32:363-403

Large WG, Pond S (1981) Open ocean momentum flux measurements in moderate to strong winds. J Phys Oceangr 11:324-336

Large WG, Pond S (1982) Sensible and latent heat flux measurements over the ocean. J Phys Oceangr 12:464-482

Leben RR (2005) Altimeter-derived Loop Current metrics. In: Sturges W, Lugo-Fernandez A (eds) Circulation in the Gulf of Mexico: observations and models. American Geophysical Union, Washington DC, p 181-201

Liddell WD (2007) Origin and Geology. In: Tunnell Jr JW, Chavez EA, Withers K (eds) Coral Reefs of the Southern Gulf of Mexico. Texas A&M University Press, College Station, p 23-33

Lohrenz SE, Dagg MJ, Whitledge TE (1990) Enhanced primary production at the plume/oceanic interface of the Mississippi River. Cont Shelf Res 10:639-664

Lohrenz SE, Fahnenstiel GL, Redalje DG, Lang GA, Chen X, Dagg MJ (1997) Variations in primary production of northern Gulf of Mexico continental shelf waters linked to nutrient inputs from the Mississippi River. Mar Ecol Prog Ser 155:45-54

Lohrenz SE, Fahnenstiel GL, Redalje DG, Lang GA, Dagg MJ, Whitledge TE, Dortch Q (1999) Nutrients, irradiance, and mixing as factors regulating primary production in coastal waters impacted by the Mississippi River plume. Cont Shelf Res 19:1113-1141

Maritorena S, Siegel DA, Peterson A (2002) Optimization of a semi-analytical ocean color model for global scale applications. Appl Opt 41:2705-2714

Maritorena S, Siegel DA (2005) Consistent merging of satellite ocean color data sets using a bio-optical model. Remote Sensing Env 94:429-440

Martínez-López B, Zavala-Hidalgo J (2009) Seasonal and interannual variability of cross-shelf transports of chlorophyll in the Gulf of Mexico. J Mar Sys 77:1-20

Matsushita B, Yang W, Chang P, Yang F, Fukushima T (2012) A simple method for distinguishing global Case-1 and Case-2 waters using SeaWiFS measurements. ISPRS J Photo Rem Sen 69:74-87

Mooers CNK, Maul GA (1998) Intra-Americas Sea Circulation. In: Brink KH, Robinson AR (eds) The Sea. John Wiley, New York, 183-208

Morey SL, Zavala-Hidalgo J, O'Brien JJ (2005) The seasonal variability of continental shelf circulation in the northern and western Gulf of Mexico from a high-resolution numerical model. In: Sturges W, Lugo-Fernandez A (eds) Circulation in the Gulf of Mexico: observations and models. American Geophysical Union, Washington, DC, p 203-218

Müller-Karger FE, Walsh JJ, Evans RH, Meyers MB (1991) On the seasonal phytoplankton concentration and sea surface temperature cycles of the Gulf of Mexico as determined by satellites. J Geophys Res 96:12,645-12,665

Nowlin WD, Jochens AE, Howard MK, DiMarco SF, Schroeder WW (2000) Hydrographic properties and inferred circulation over the northeastern shelves of the Gulf of Mexico during spring to midsummer of 1998. Gulf Mex Sci 18:40-54

Oey L (1995) Eddy and wind-forced shelf circulation. J Geophys Res 100:8621-8637

Pickett MH, Tang W, Rosenfeld LK, Walsh CH (2003) QuikSCAT satellite comparisons with nearshore buoy data off the U.S. west coast. J Atom Oceanic Technol 20:1869-1879

Rabalais NN, Turner RE, Dortch Q, Justic D, Bierman Jr VJ, Wiseman Jr WJ (2002) Nutrient-enhanced productivity in the northern Gulf of Mexico: past, present and future. Hydrobiologia 475/476:39-63

Rabalais NN, Turner RE, Justic D, Dortch Q, Wiseman Jr WJ, Sen Gupta BK (1999) Characterization of hypoxia: Topic 1 Report for the integrated assessment of hypoxia in the Gulf of Mexico. Silver Spring, MD, NOAA Coastal Ocean Office. Decision Analysis Series no. 15

Risien CM, Chelton DB (2008) A global climatology of surface wind and wind stress fields from 8 years of QuikSCAT scatterometer data. J Phys Oceangr 38:2379-2413

Sturges W, Leben R (2000) Frequency of ring separations from the Loop Current in the Gulf of Mexico, a revised estimate. J Phys Oceangr 30:1814-1819

Vázquez de la Cerda AM, Reid RO, DiMarco SF, Jochens AE (2005) Bay of Campeche circulation: an update. In: Sturges W, Lugo-Fernandez A (eds) Circulation in the Gulf of Mexico: observations and models. American Geophysical Union, Washington, DC, p 279-293

Zavala-Hidalgo J, Romero-Centeno R, Mateos-Jasso A (2014) The response of the Gulf of Mexico to wind and heat flux forcing: What has been learned in recent years? Atmósfera 27:317-334

# CHAPTER IV: The non-seasonal variability and dominant coupled patterns of satellite-measured chlorophyll and wind in the Gulf of Mexico

Abstract

Associations between non-seasonal monthly anomalies of chlorophyll and wind forcing were examined in the Gulf of Mexico using the ESA's GlobColour and NASA's QuickSCAT Level 3 data for 2000-2008. In general, the non-seasonal variability of chlorophyll can be associated statistically with non-seasonal fluctuations of wind speed and zonal and meridional fluctuations of the wind, depending on the region. The suggested mechanisms behind these associations are turbulent vertical mixing, horizontal advection, and coastal upwelling. The temporal variability related to the non-seasonal associations between chlorophyll and winds are mostly intraseasonal but interannual modulations are also apparent.

## Introduction

Chapter 3 of this dissertation investigated the seasonal associations between wind forcing and surface chlorophyll over the Gulf of Mexico using satellite observations. That study highlighted the linkage between the wind driven seasonal fluctuations of the Mississippi River plume and the seasonal log-transformed chlorophyll variability over the northern and western coastal areas of the Gulf. This association was attributed to the downcoast and upcoast advection of nutrient rich Mississippi River waters driven by the respective intensification and weakening of the zonal surface easterly wind stress over the northern Gulf. In the interior Gulf and consistent with previous studies (e.g., Müller-Karger et al. 1991), chlorophyll increased (decreased) in winter (summer) following increases (decreases) of surface wind speed, a proxy for turbulent vertical mixing and upward entrainment of nutrients.

In this study, the seasonal analysis of Chapter 3 is extended to examine the relationship between the non-seasonal variability in surface log-transformed chlorophyll and wind forcing.

Chlorophyll and wind forcing datasets come from remotely sensed monthly averaged data for 2000-2008 and the associations are extracted using correlation analysis and coupled singular value decomposition (SVD). The SVD is a technique that has been used by other authors to investigate associations between different geophysical variables (e.g., Lanzante 1984 for seas surface temperature and atmospheric geopotential heights; Fang and Wallace 1994 for sea ice and atmospheric geopotential heights; Peng and Fyfe 1996, Venegas et al. 1997, Sterl and Hazeleger 2003 for sea surface temperature and sea level pressure).

## Data and Methods

### 4.1 Chlorophyll data

The chlorophyll data used in this study are from the GlobColour dataset (http://www.globcolour.info/) from the European Space Agency (ESA) which provides global fields of ocean color merged from various sources through weighted averaging and the Garver-Siegel-Maritorena (GSM) model (Maritorena and Siegel 2005). The GSM model is a bio-optical model which combines the normalized radiances from datasets from different sensors. Over each pixel of a geographical grid common to SeaWiFS, MODIS-AQUA, and MERIS, spectra from the available sensors at the pixel are selected and combined in a single, multi-source spectrum which is then used in the inversion of the GSM01 semi-analytical ocean color model (Maritorena et al. 2002). The model inversion results in the retrieval of the sub-surface chlorophyll-*a* concentration. These GlobColour products have a spatial resolution of 0.25° at the equator and temporal resolutions of 1 day, 8 days, and 1 (calendar) month. The chlorophyll data are provided on a 0.25° x 0.25° global grid. This project uses the monthly version of this dataset over the Gulf of Mexico for the 1998-2009 twelve-year period.

## 4.2 Wind data

The surface winds used here come from the QuikSCAT Level 3 products available from the NASA- Jet Propulsion Laboratory (http://podaac-www.jpl.nasa.gov/). The Level 3 data were obtained from the Direction Interval Retrieval with Threshold Nudging (DIRTH) wind vector solutions and are provided on a global 0.25° × 0.25° latitude-longitude grid. Data is available from July 1999 through November 2009, however data used for this study were from January 2000 – December 2008. The vector wind stress is computed from QuikSCAT observations of the equivalent neutral stability vector winds at 10 m based on the bulk aerodynamic formula where air density is 1.2 kg/m$^3$ (Goldenberg and O'Brien 1981, Risien and Chelton 2008). The drag coefficient was computed using the modified equation (from Large and Pond 1981, 1982) found in the appendix of Large et al. (1994), which is the formulation most commonly used for scatterometer applications.

## 4.3 Data Analysis

The chlorophyll analysis was performed for the period 1998-2009 and the coupled chlorophyll-wind analysis for the overlapping period January 2000-December 2008. Ample evidence exists that oceanic bio-optical data including chlorophyll concentration are distributed approximately log normally (e.g., Campbell 1995). In the Gulf of Mexico for example, the values of chlorophyll in surface shelf waters are very large and they decrease very rapidly offshore towards the deep ocean. This makes the analysis of surface chlorophyll fields over combined coastal and deep waters difficult. For this reason, the chlorophyll dataset used in this study was first log-transformed (base 10). The monthly non-seasonal time series at every grid point were created by subtracting out the seasonal cycle from each year of data so that the

resulting time series represent monthly anomalies or deviations from the seasonal cycle for each year of data (12 data points per year).

In this study, the associations between chlorophyll and wind anomalies were first investigated using simple correlation analysis of area averaged fields around the Gulf. To calculate significance levels for these temporal correlations, the large-lag standard error between two time series was calculated following the method of Davis (1976; see also Björnsson and Venegas 1997). The 95% significance level was approximated as twice the large-lag standard error.

For examining the variability of a single geophysical field Empirical Orthogonal Function (EOF) analysis, which is an eigenvalue decomposition of the autocovariance matrix, is commonly used (e.g., Davis 1976, Wallace et al. 1990, Deser and Blackmoon 1993, Enfield and Mayer 1997). An extension of EOF analysis to two fields to extract coupled or co-variability patterns is the Singular Value Decomposition (SVD; e.g., Lanzante 1984, Fang and Wallace 1994, Peng and Fyfe 1996, Venegas et al. 1997, Sterl and Hazeleger 2003). The SVD technique is based on an eigenvalue decomposition of the cross-covariance matrix constructed from the two fields. In this study, the SVD technique was used to extract the dominant coupled patterns of anomalous chlorophyll and wind forcing co-variability.

## Results

### 4.4 Non-seasonal variability of chlorophyll and winds

The Gulf of Mexico shelf and deep water regions were separated based on bottom topography for this study of the non-seasonal chlorophyll variability in the Gulf, as in a standard deviation map of the non-seasonal chlorophyll anomalies (Fig. 4.1). Figure 4.1 has the larger

amplitudes of the non-seasonal chlorophyll variability occur over the shelf (within the 200 m contour) or near and beyond the shelf break. Of these areas with strong non seasonal variability, the largest values are found around the mouth of the Mississippi River extending beyond the shelf break. Smaller amplitudes of the non-seasonal chlorophyll variability are seen beyond the continental shelf break in other regions and in the deep interior Gulf.

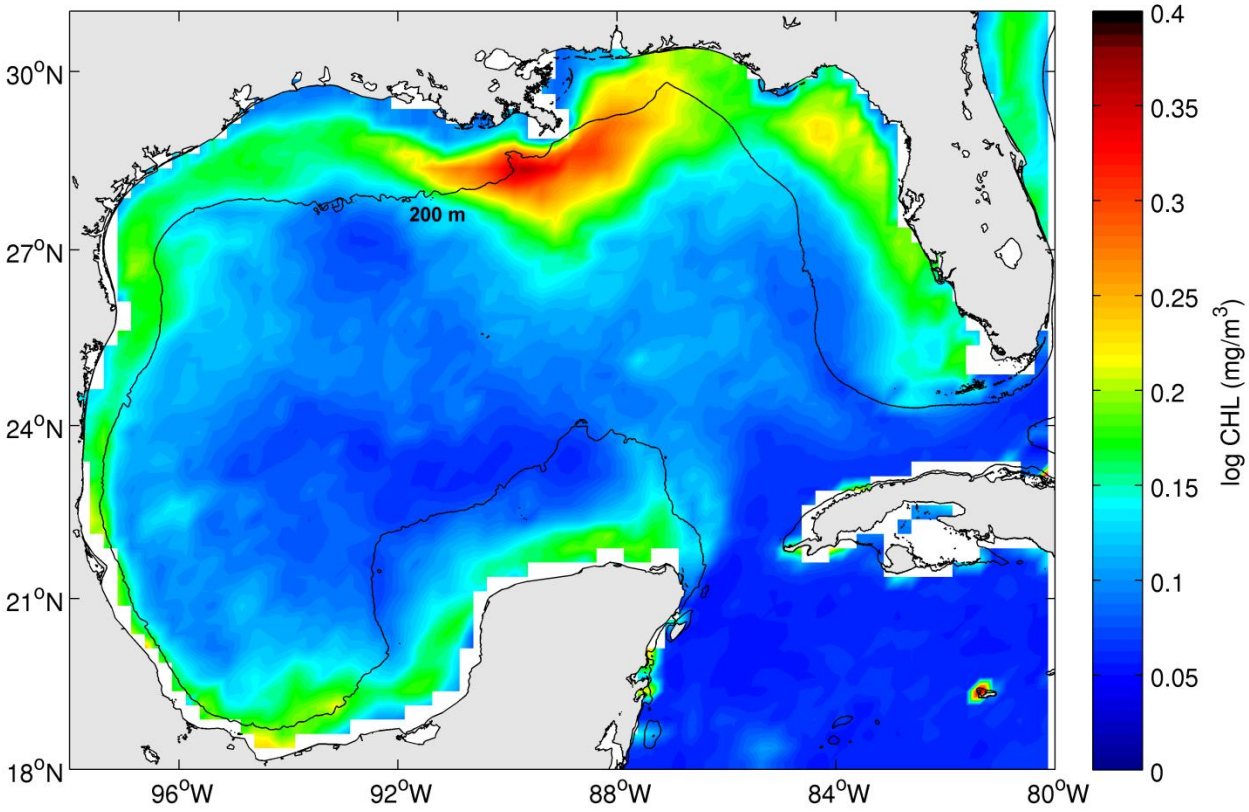


Fig. 4.1 Standard deviation of the monthly non-seasonal anomaly time series at every grid point for the log-transformed chlorophyll-*a* (mg/m$^3$) for 1998-2009. The 200 m isobath defining the continental shelf break is a solid black line.

To characterize the non-seasonal variability of the wind forcing over the Gulf of Mexico, standard deviation maps of non-seasonal anomalies for wind speed, zonal wind stress, and meridional wind stress were developed (Fig. 4.2A, 4.2B, and 4.2C, respectively). Large non-seasonal wind speed variability is found in the eastern half of the Gulf, intermediate non-seasonal wind speed variability in the western half, and low non-seasonal wind variability in the

Bay of Campeche (Fig. 4.2A). The zonal wind stress has larger non-seasonal variability over the eastern Gulf (Fig. 4.2B) and the meridional wind stress has larger non-seasonal variability over the central and western Gulf (Fig. 4.2C). The Bay of Campeche has intermediate non-seasonal variability for both components of the vector wind stress.

The non-seasonal variability of chlorophyll and winds were quantified using regional indexes in ten different latitude-longitude boxes around the Gulf (Fig. 4.3). The boxes have equal areas ($200 \times 200$ km$^2$); nine were non-overlapping in the more variable coastal areas and one was located in the ocean interior. Three boxes are in the northern Gulf: east of the Mississippi River Mouth (blue), at the Mississippi River Mouth (red), and west of the Mississippi River Mouth (light green); one in the northeast Gulf over the Louisiana-Texas shelf (light blue); two in the western Gulf: Tamaulipas (orange) and Veracruz (purple); two in the southern Gulf: Bay of Campeche (pink) and Campeche Bank (yellow); one in the eastern Gulf over the West Florida continental shelf (dark green); and one in the deep central Gulf (black). Area-averaged indices (2000-2008) for non-seasonal anomalies of chlorophyll, wind speed, zonal wind stress, meridional wind stress, wind stress curl, and vector wind stress magnitude were then generated for each of the boxes and displayed in Figures 4.4, 4.6, 4.8, 4.10, 4.12, and 4.14, respectively. High frequency intraseasonal as well as low frequency interannual variability is evident in the non-seasonal anomaly time series. For chlorophyll (Fig. 4.4), the Mississippi mouth (red) and east of the Mississippi mouth (blue) indices have the largest intraseasonal anomalies consistent with the larger values of the standard deviation in those regions (Fig. 4.1). The interannual non-seasonal variability in chlorophyll is evidenced by the predominantly positive anomalies from mid-2000 through 2005 and beyond 2008, and predominantly negative anomalies from 2005-2008.

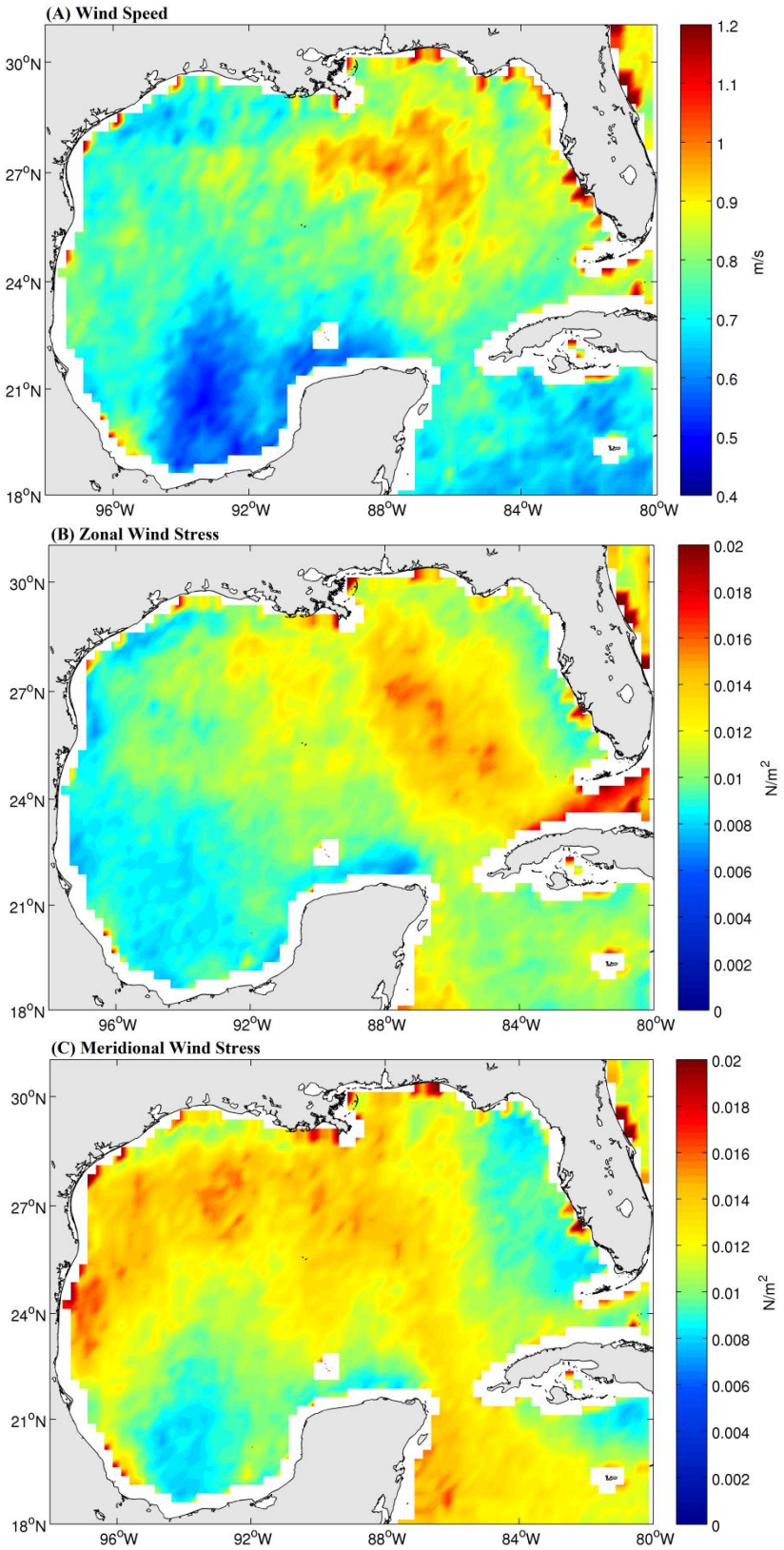


Fig. 4.2 Standard deviation of the non-seasonal anomaly time series at every grid point for (A) wind speed, (B) zonal wind stress, and (C) meridional wind stress for 2000-2008.

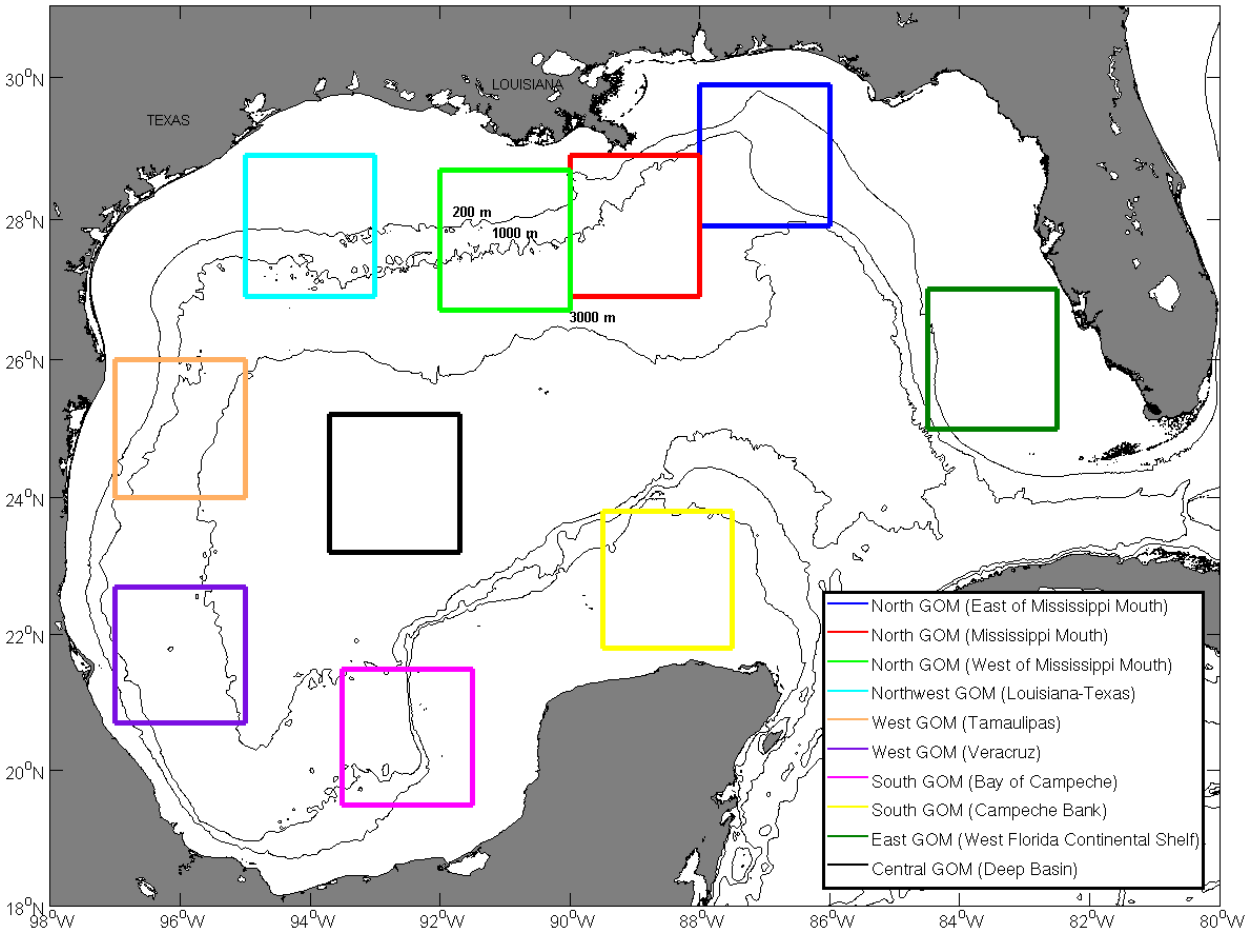


Fig. 4.3 Map of the Gulf of Mexico with regional areas of interest. Each box covers an area of 200 x 200-km$^2$. Boxes are centered at 28.9°N, 87.4°W (dark blue), 27.9°N, 89.2°W (red), 27.7°N, 91°W (light green), 27.9°N, 94°W (light blue), 25°N, 96°W (orange), 21.7°N, 96°W (purple), 20.5°N, 92.5°W (pink), 22.8°N, 88.5°W (yellow), 26°N, 83.5°W (dark green), and 24.2°N, 92.7°W (black). Depth contours are at 200, 1000, and 3000 m.

For the non-seasonal wind speed anomaly time series (Fig. 4.6), spatial coherency among several index areas is apparent for both positive and negative intraseasonal wind events. An interannual modulation in wind speed anomalies may be present. For example, predominantly negative non-seasonal wind speed anomalies are seen in early 2000, 2003, late 2004 to early 2005, and during most of 2006, and predominantly positive anomalies occur over other periods. The character of the non-seasonal variability in the zonal and meridional wind stress (Figs. 4.8 and 4.10, respectively) is similar to that of the wind speed (Fig. 4.6) but with the spatial coherence in the intraseasonal fluctuations even more apparent than for wind speed. The non-

seasonal anomaly time series of wind stress curl (Fig. 4.12) has no apparent spatial coherence in the intraseasonal fluctuations or evidence of interannual modulations. The non-seasonal anomaly variability in the time series of wind stress magnitude (Fig. 4.14) is similar in character to that of wind speed (Fig. 4.6). To get a better grasp of the relative amplitudes of the variability in the non-seasonal anomaly time series of Figures 4.4-4.14, their standard deviations are in Table 4.7. The standard deviation of chlorophyll ranges from 0.05 log-($mg/m^3$) to 0.14 log-($mg/m^3$). The highest variability is in the areas of the Mississippi River and Louisiana-Texas shelf. Wind speed variability ranges from 0.51 m/s to 0.75 m/s with the highest variability in the northern Gulf and lower values in the southern Gulf. Zonal wind stress varies from 0.008 $N/m^2$ to 0.011 $N/m^2$ with the highest variability surrounding the Mississippi River and low values on the Western Shelf. Meridional wind stress ranges from 0.008 $N/m^2$ to 0.013 $N/m^2$ with the lowest values in the southern Gulf and West Florida continental shelf. Wind curl varies from $0.45 \times 10^{-7}$ $N/m^3$ to $0.68 \times 10^{-7}$ $N/m^3$ and wind stress magnitude from 0.007 $N/m^2$ to 0.011 $N/m^2$. The variability of wind curl is similar to that of the meridional wind stress with the lowest values in the southern and eastern Gulf. The wind stress magnitude values and regional patterns are similar to those for the zonal wind stress. For wind speed, and zonal and meridional wind stress the distribution of standard deviations in Table 4.7 are consistent with those in Fig. 4.2.

To visualize each variable on a regional basis, the time series from Figures 4.4, 4.6, 4.8, 4.10, 4.12, 4.14 were displayed for the northern, western/central, and southern/eastern boxes in Figures 4.5, 4.7, 4.9, 4.11, 4.13, and 4.15. Correlation coefficients were calculated between each regional area for chlorophyll (Table 4.1, Fig. 4.5), wind speed (Table 4.2, Fig. 4.7), zonal wind stress (Table 4.3, Fig. 4.9), meridional wind stress (Table 4.4, Fig. 4.11), wind curl (Table 4.5, Fig. 4.13), and wind stress magnitude (Table 4.6, Fig. 4.15). Meridional wind stress was found to

be the only variable with significant correlations among each regional area (Table 4.4). The variable with the fewest correlations regionally was wind curl (Table 4.5).

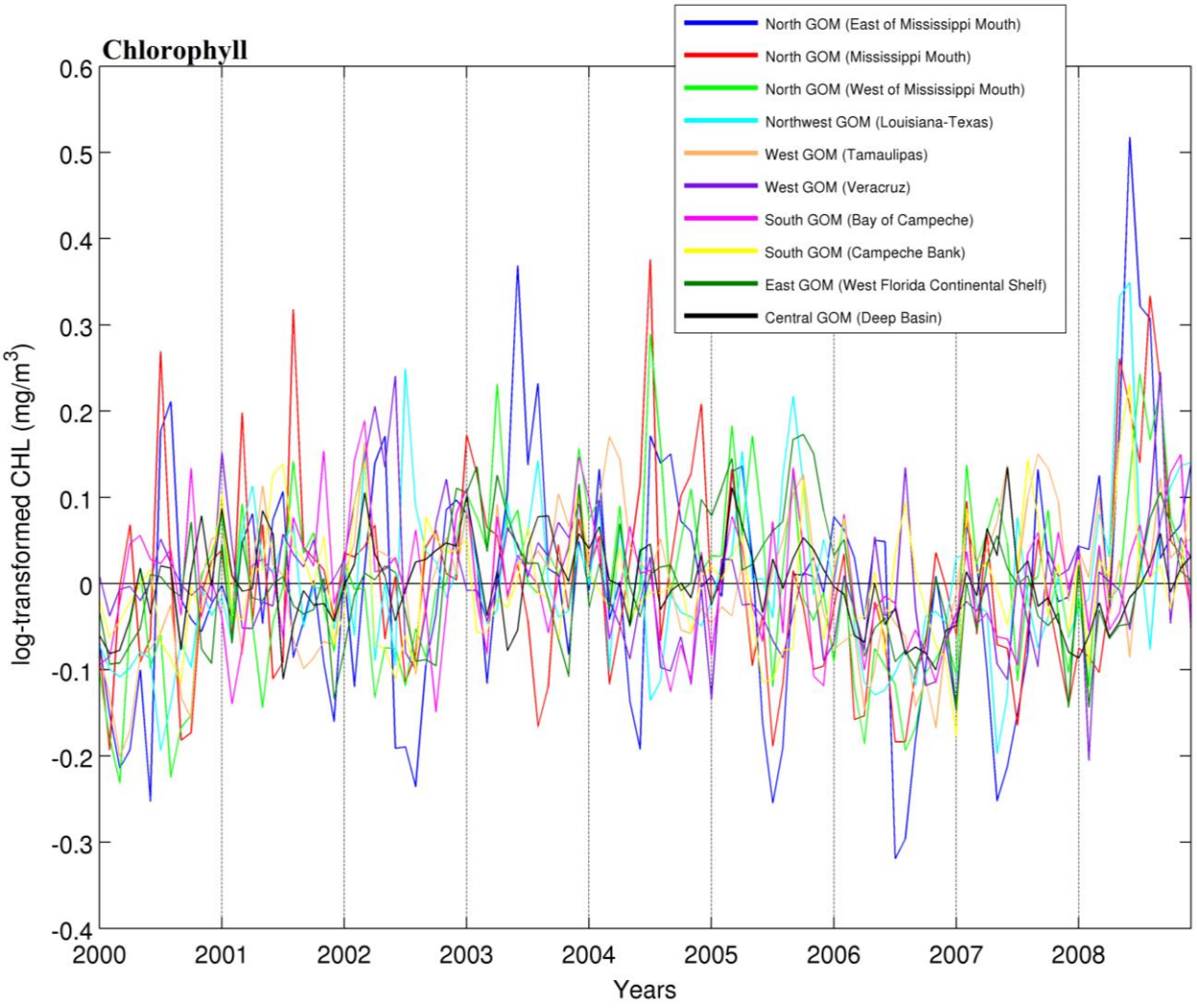


Fig. 4.4 Time series of box-averaged monthly log-transformed chlorophyll-*a* anomalies for the period of 2000-2008. Each colored line corresponds to a regional box (Fig. 4.3).

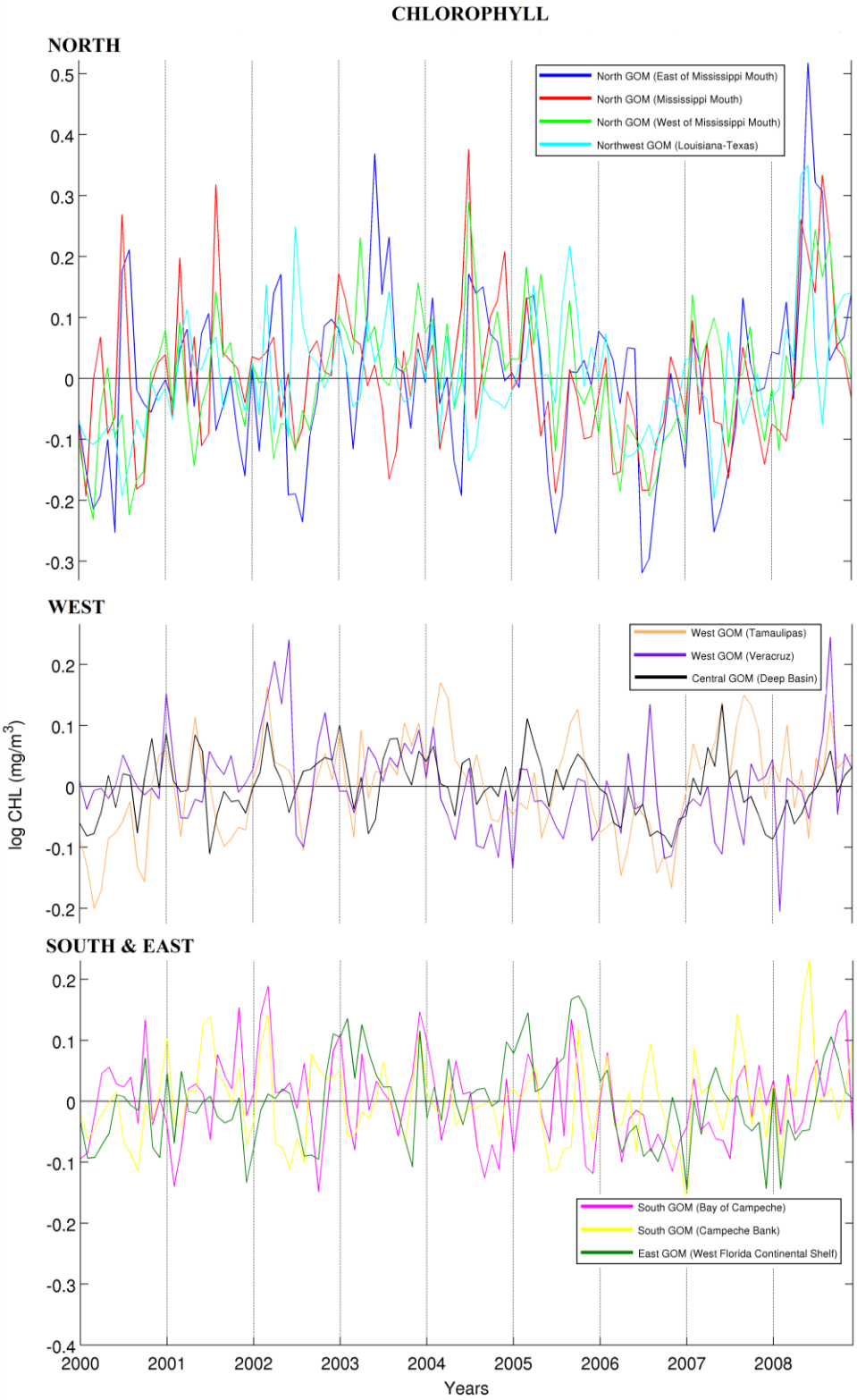


Fig. 4.5 Time series of box-averaged monthly log-transformed chlorophyll-*a* anomalies displayed based on regional location.

Table 4.1 Correlation coefficients among the regional areas listed for the chlorophyll time series plot (Fig. 4.4). In parenthesis are the 95% significance levels for the correlations. Significant correlations are indicated with bold numbers.

| | East of Mississippi Mouth | Mississippi Mouth | West of Mississippi Mouth | Louisiana-Texas | Tamaulipas | Veracruz | Bay of Campeche | Campeche Bank | West Florida Cont. Shelf | Deep Basin |
|---|---|---|---|---|---|---|---|---|---|---|
| East of Mississippi Mouth | - | **0.4249** (0.2549) | **0.4161** (0.2925) | **0.3324** (0.2925) | 0.2055 (0.2794) | 0.1619 (0.2518) | 0.1425 (0.2220) | **0.3006** (0.2617) | 0.2703 (0.2714) | 0.1527 (0.2340) |
| Mississippi Mouth | | - | **0.5787** (0.2857) | 0.1685 (0.2413) | 0.1050 (0.2565) | 0.2213 (0.2261) | **0.2638** (0.2196) | **0.2229** (0.1972) | 0.2409 (0.2721) | **0.2484** (0.2259) |
| West of Mississippi Mouth | | | - | 0.2718 (0.2925) | **0.4117** (0.3319) | 0.1211 (0.2761) | **0.2535** (0.2366) | **0.2509** (0.2301) | **0.4771** (0.3060) | **0.3954** (0.2577) |
| Louisiana-Texas | | | | - | 0.2514 (0.2963) | 0.0086 (0.2390) | 0.2401 (0.2601) | **0.3845** (0.2418) | 0.2193 (0.2795) | 0.1851 (0.2450) |
| Tamaulipas | | | | | - | 0.2451 (0.2723) | **0.2642** (0.2506) | **0.2629** (0.2184) | 0.2912 (0.3050) | **0.5085** (0.3257) |
| Veracruz | | | | | | - | **0.3006** (0.2327) | 0.2035 (0.2245) | 0.1317 (0.2696) | 0.2277 (0.2671) |
| Bay of Campeche | | | | | | | - | **0.2603** (0.2233) | **0.2751** (0.2341) | **0.2998** (0.2596) |
| Campeche Bank | | | | | | | | - | 0.1392 (0.2152) | **0.2292** (0.2156) |
| West Florida Cont. Shelf | | | | | | | | | - | **0.4197** (0.2777) |
| Deep Basin | | | | | | | | | | - |

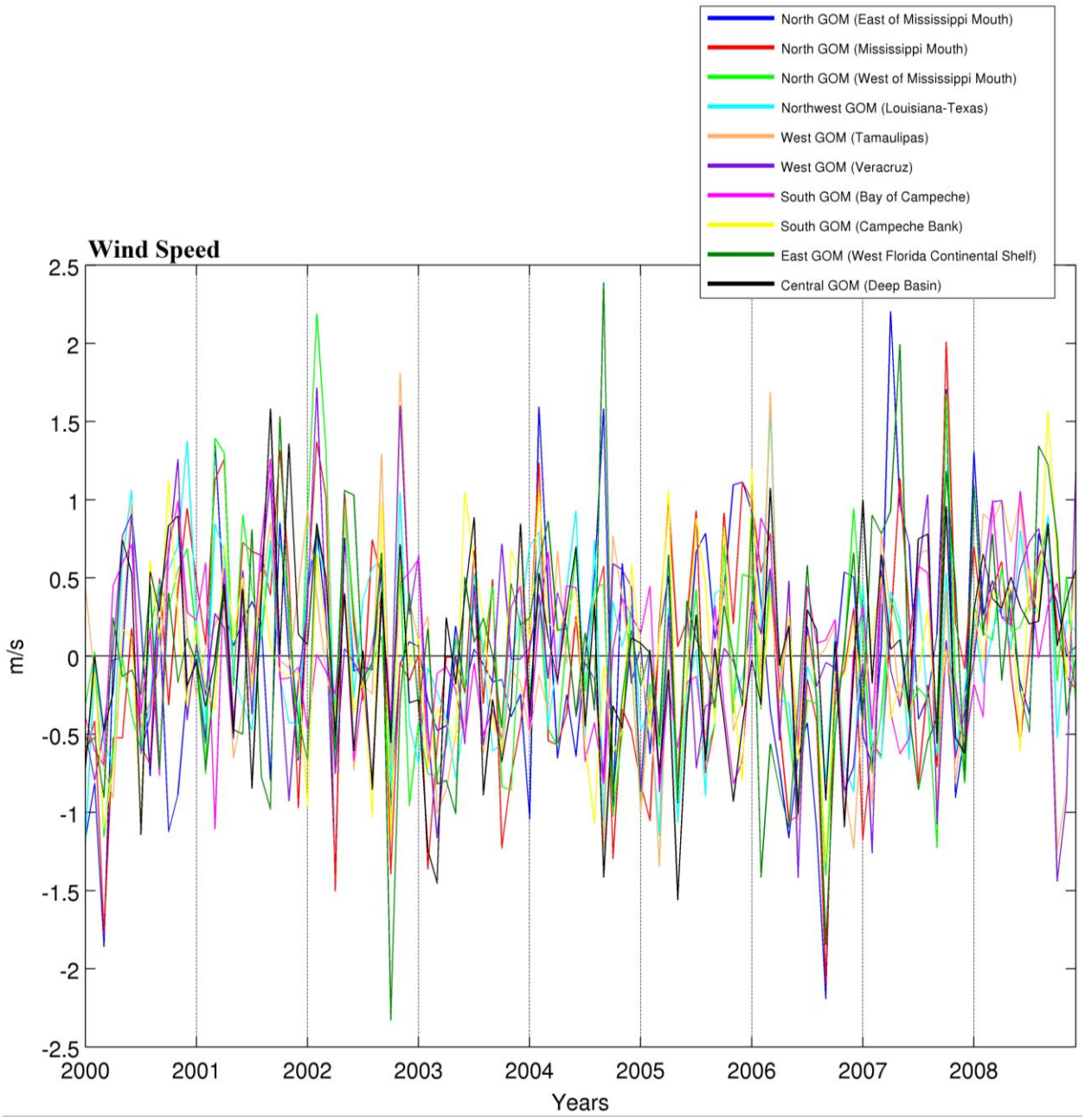


Fig. 4.6 Time series of box-averaged monthly wind speed anomalies for the period of 2000-2008. Each colored line corresponds to a regional box (Fig. 4.3).

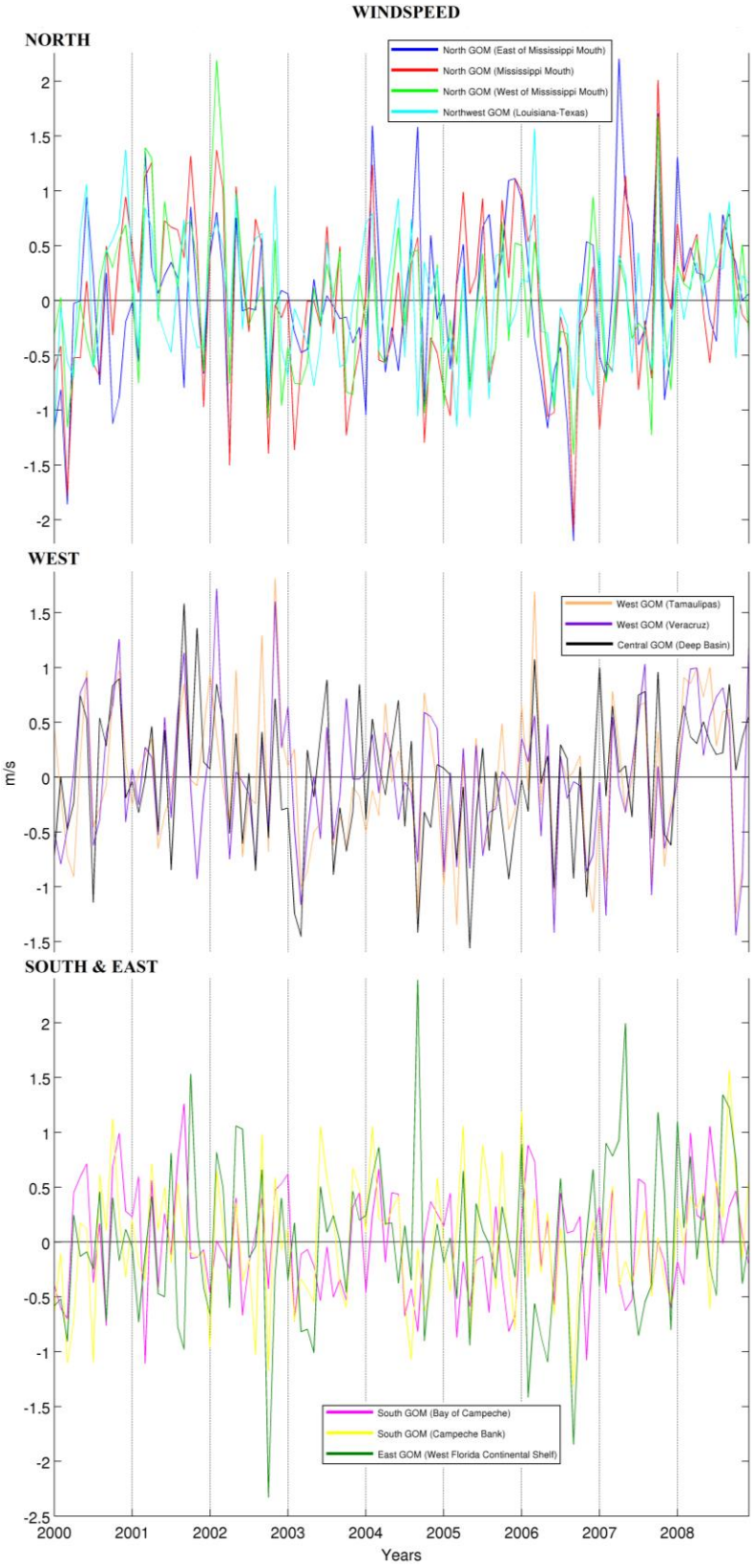


Fig. 4.7 Time series of box-averaged monthly wind speed anomalies displayed based on regional location.

Table 4.2 Correlation coefficients between the regional areas listed for the wind speed time series plot (Fig. 4.6). In parenthesis are the 95% significance levels for the correlations. Significant correlations are indicated with bold numbers.

| | East of Mississippi Mouth | Mississippi Mouth | West of Mississippi Mouth | Louisiana-Texas | Tamaulipas | Veracruz | Bay of Campeche | Campeche Bank | West Florida Cont. Shelf | Deep Basin |
|---|---|---|---|---|---|---|---|---|---|---|
| East of Mississippi Mouth | - | **0.6753** (0.2439) | **0.5024** (0.2287) | 0.2118 (0.2165) | 0.0508 (0.2030) | 0.1222 (0.2141) | -0.1290 (0.1907) | **0.2627** (0.2252) | **0.5651** (0.2394) | 0.0871 (0.1885) |
| Mississippi Mouth | | - | **0.7801** (0.2680) | **0.4359** (0.2216) | 0.2020 (0.2216) | **0.2082** (0.2079) | 0.0485 (0.1900) | **0.3969** (0.2271) | **0.4826** (0.2237) | **0.2936** (0.2006) |
| West of Mississippi Mouth | | | - | **0.5663** (0.2297) | **0.3176** (0.2001) | **0.3513** (0.2008) | 0.1274 (0.1882) | **0.4212** (0.2208) | **0.4301** (0.2294) | **0.5142** (0.2238) |
| Louisiana-Texas | | | | - | **0.6203** (0.2450) | **0.5147** (0.2245) | **0.4194** (0.2138) | **0.3559** (0.2106) | 0.1278 (0.2117) | **0.5900** (0.2249) |
| Tamaulipas | | | | | - | **0.7745** (0.2467) | **0.4908** (0.2202) | **0.3092** (0.1962) | 0.0207 (0.1818) | **0.5544** (0.2219) |
| Veracruz | | | | | | - | **0.4933** (0.2268) | **0.3500** (0.2012) | 0.0177 (0.1924) | **0.5441** (0.2146) |
| Bay of Campeche | | | | | | | - | **0.3534** (0.1975) | -0.0400 (0.1782) | **0.5807** (0.2390) |
| Campeche Bank | | | | | | | | - | **0.4589** (0.2367) | **0.5236** (0.2158) |
| West Florida Cont. Shelf | | | | | | | | | - | 0.1232 (0.1928) |
| Deep Basin | | | | | | | | | | - |

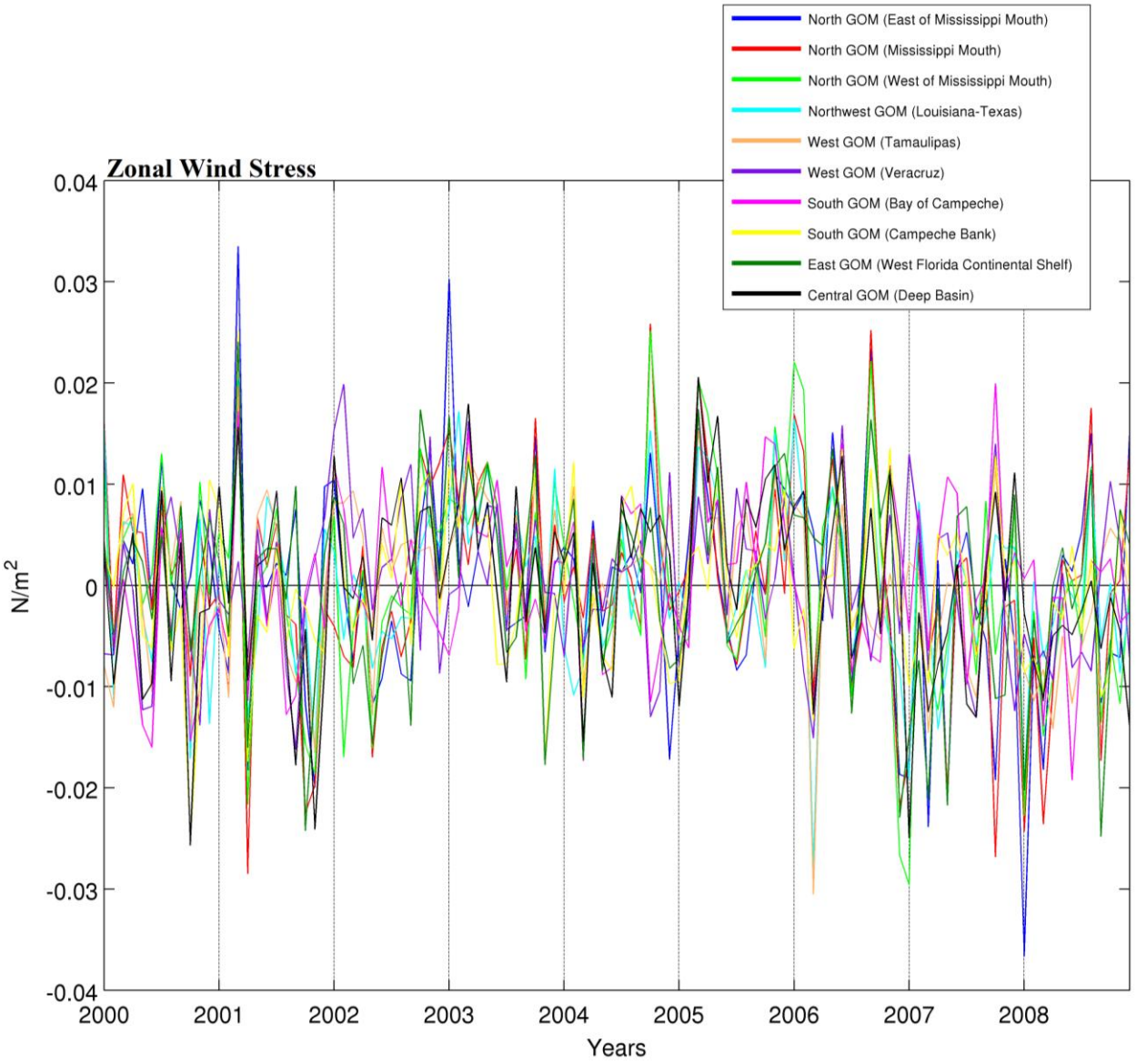


Fig. 4.8 Time series of box-averaged monthly zonal wind stress anomalies for the period of 2000-2008. Each colored line corresponds to a regional box (Fig. 4.3).

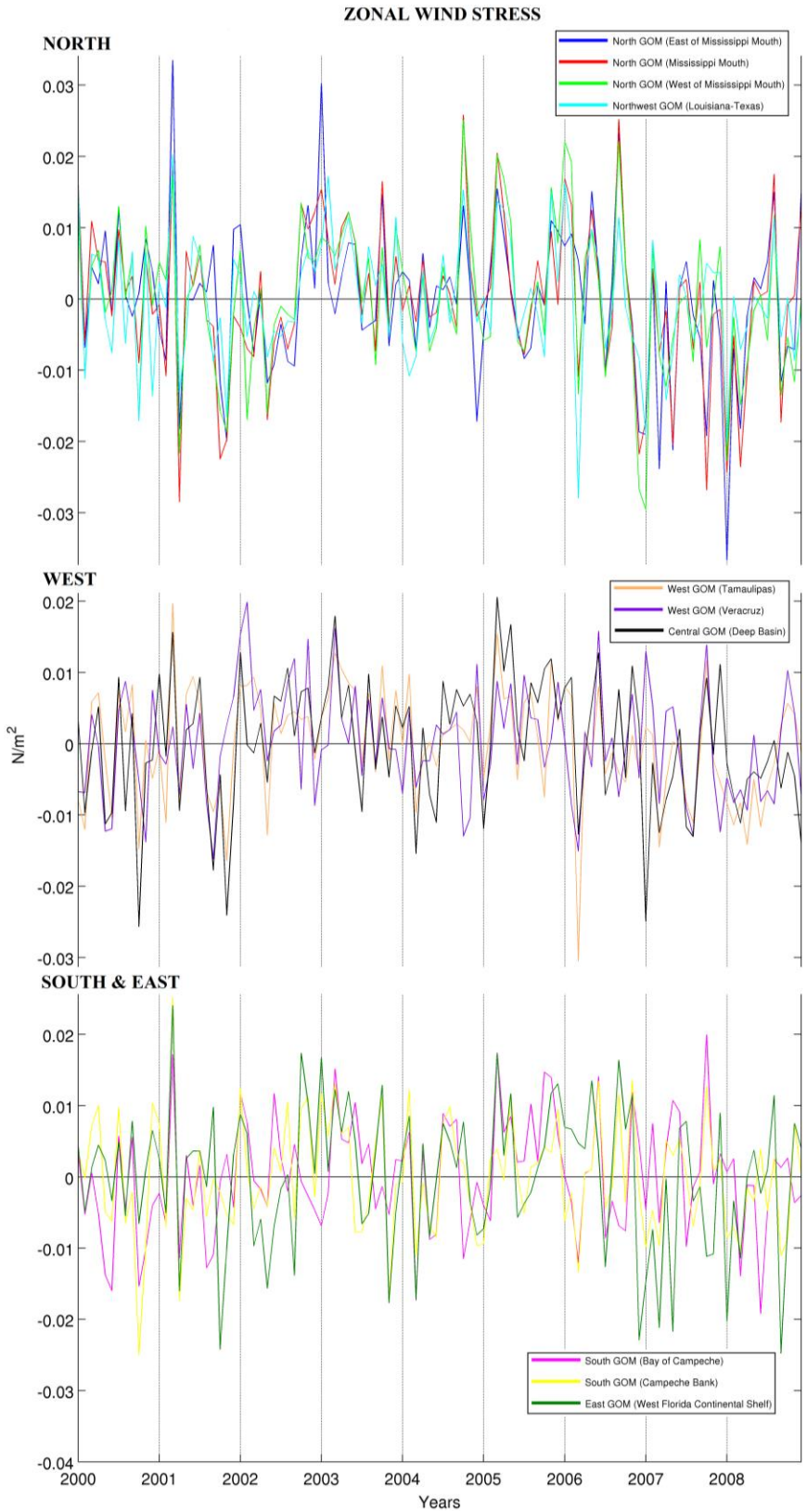


Fig. 4.9 Time series of box-averaged monthly zonal wind stress anomalies displayed based on regional location.

Table 4.3 Correlation coefficients between the regional areas listed for the zonal wind stress series plot (Fig. 4.8). In parenthesis are the 95% significance levels for the correlations. Significant correlations are indicated with bold numbers.

| | East of Mississippi Mouth | Mississippi Mouth | West of Mississippi Mouth | Louisiana-Texas | Tamaulipas | Veracruz | Bay of Campeche | Campeche Bank | West Florida Cont. Shelf | Deep Basin |
|---|---|---|---|---|---|---|---|---|---|---|
| East of Mississippi Mouth | - | **0.8338** (0.2456) | **0.7078** (0.2319) | **0.5895** (0.2252) | **0.2919** (0.1994) | -0.0663 (0.1905) | 0.0494 (0.1902) | **0.4458** (0.1953) | **0.8017** (0.2258) | **0.3384** (0.2047) |
| Mississippi Mouth | | - | **0.8608** (0.2613) | **0.7103** (0.2386) | **0.4257** (0.2180) | -0.0414 (0.1926) | 0.0894 (0.2004) | **0.4044** (0.1920) | **0.7423** (0.2309) | **0.4538** (0.2203) |
| West of Mississippi Mouth | | | - | **0.8328** (0.2454) | **0.4936** (0.2242) | 0.0018 (0.2013) | **0.2192** (0.2096) | **0.4426** (0.2025) | **0.6721** (0.2245) | **0.6436** (0.2337) |
| Louisiana-Texas | | | | - | **0.5958** (0.2121) | 0.0947 (0.1847) | **0.3242** (0.2005) | **0.4369** (0.2057) | **0.5110** (0.2228) | **0.6451** (0.2186) |
| Tamaulipas | | | | | - | **0.6354** (0.2244) | **0.5843** (0.2280) | **0.5072** (0.2053) | **0.3591** (0.1940) | **0.6778** (0.2335) |
| Veracruz | | | | | | - | **0.5873** (0.2226) | **0.3504** (0.1971) | 0.0661 (0.1821) | **0.3719** (0.2041) |
| Bay of Campeche | | | | | | | - | 0.5221 (0.2169) | **0.2354** (0.2002) | **0.6411** (0.2322) |
| Campeche Bank | | | | | | | | - | **0.6270** (0.2203) | **0.6782** (0.2418) |
| West Florida Cont. Shelf | | | | | | | | | - | **0.4985** (0.2251) |
| Deep Basin | | | | | | | | | | - |

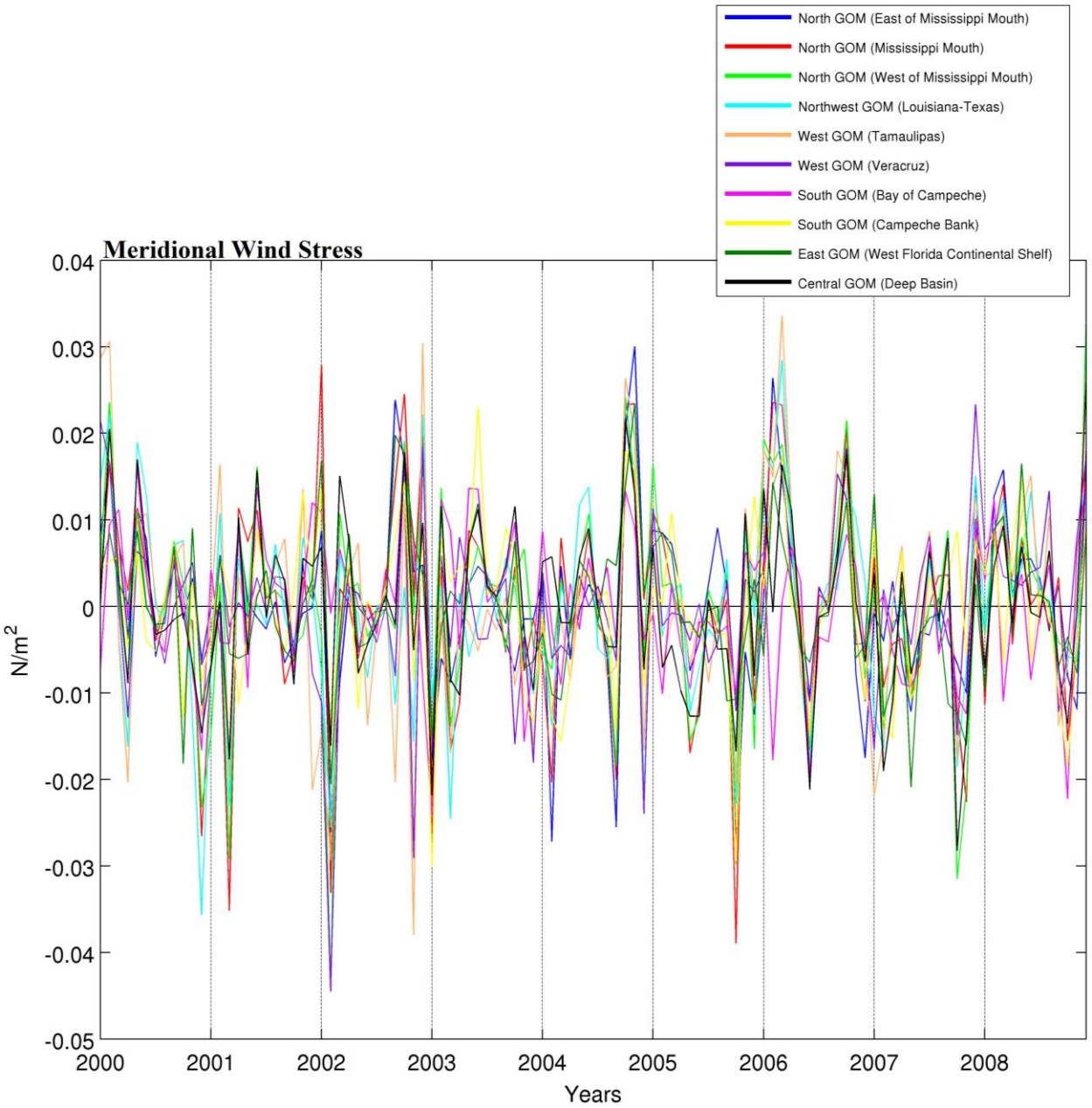


Fig. 4.10 Time series of box-averaged monthly meridional wind stress anomalies for the period of 2000-2008. Each colored line corresponds to a regional box (Fig. 4.3).

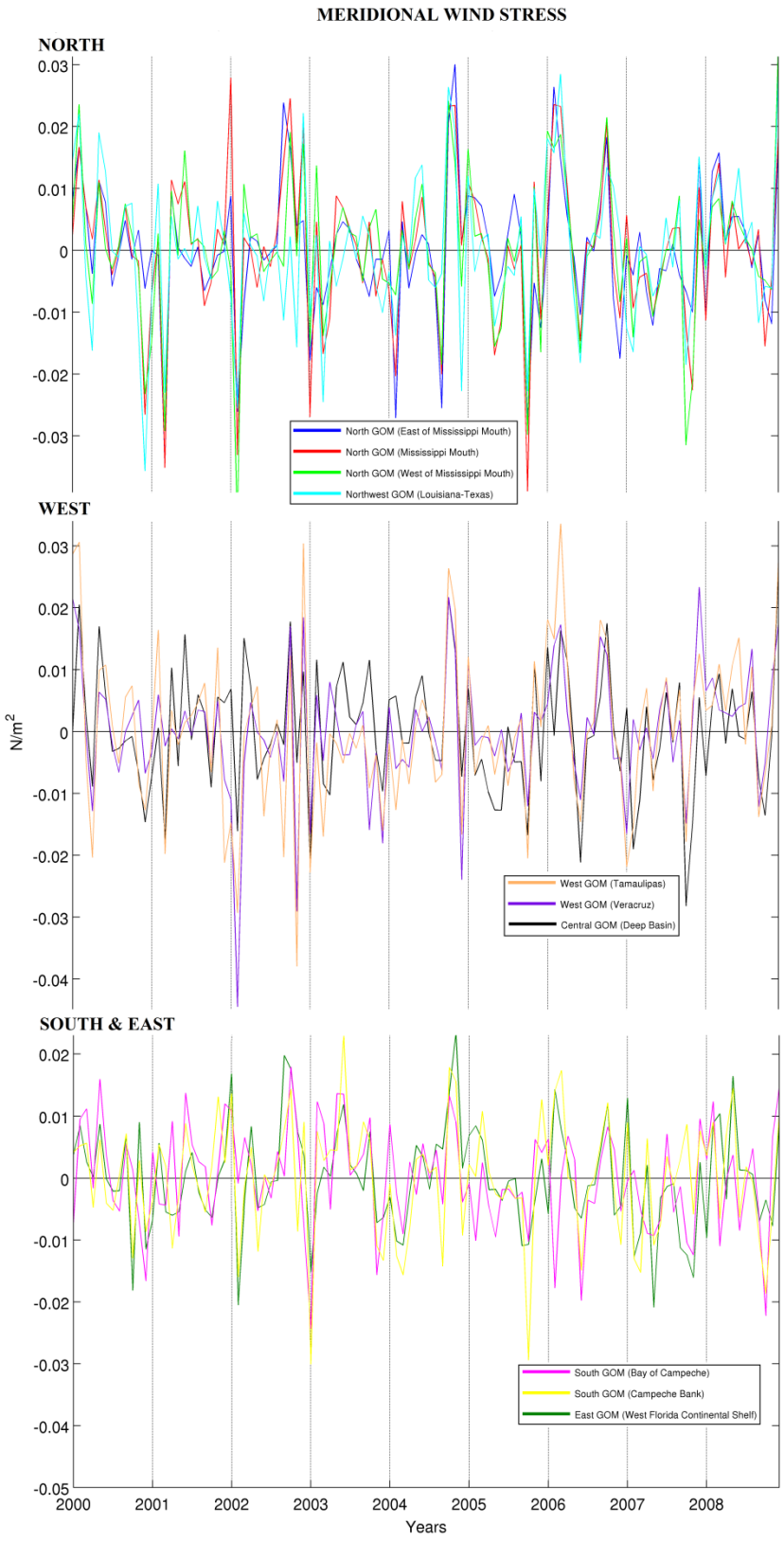


Fig. 4.11 Time series of box-averaged monthly meridional wind stress anomalies displayed based on regional location.

Table 4.4 Correlation coefficients between the regional areas listed for the meridonal wind stress plot (Fig. 4.10). In parenthesis are the 95% significance levels for the correlations. Significant correlations are indicated with bold numbers.

| | East of Mississippi Mouth | Mississippi Mouth | West of Mississippi Mouth | Louisiana-Texas | Tamaulipas | Veracruz | Bay of Campeche | Campeche Bank | West Florida Cont. Shelf | Deep Basin |
|---|---|---|---|---|---|---|---|---|---|---|
| East of Mississippi Mouth | - | **0.8585** (0.2426) | **0.7245** (0.2290) | **0.5898** (0.2039) | **0.5279** (0.2014) | **0.5046** (0.2059) | **0.3128** (0.2004) | **0.5413** (0.2193) | **0.6605** (0.2349) | **0.5459** (0.2203) |
| Mississippi Mouth | | - | **0.8546** (0.2490) | **0.6943** (0.2179) | **0.5592** (0.2090) | **0.4963** (0.2126) | **0.4813** (0.2120) | **0.6377** (0.2314) | **0.6872** (0.2460) | **0.7556** (0.2481) |
| West of Mississippi Mouth | | | - | **0.8139** (0.2342) | **0.6952** (0.2337) | **0.6311** (0.2224) | **0.4505** (0.2020) | **0.5198** (0.2107) | **0.5580** (0.2232) | **0.8482** (0.2447) |
| Louisiana-Texas | | | | - | **0.8610** (0.2497) | **0.7204** (0.2314) | **0.3492** (0.2070) | **0.4771** (0.2050) | **0.4053** (0.1995) | **0.7454** (0.2346) |
| Tamaulipas | | | | | - | **0.8605** (0.2556) | **0.2314** (0.1914) | **0.4628** (0.2006) | **0.3173** (0.1927) | **0.6423** (0.2260) |
| Veracruz | | | | | | - | **0.2791** (0.2009) | **0.5100** (0.2132) | **0.3584** (0.2102) | **0.5519** (0.2164) |
| Bay of Campeche | | | | | | | - | **0.5547** (0.2130) | **0.4229** (0.2047) | **0.6825** (0.2217) |
| Campeche Bank | | | | | | | | - | **0.6934** (0.2434) | **0.5772** (0.2178) |
| West Florida Cont. Shelf | | | | | | | | | - | **0.5623** (0.2208) |
| Deep Basin | | | | | | | | | | - |

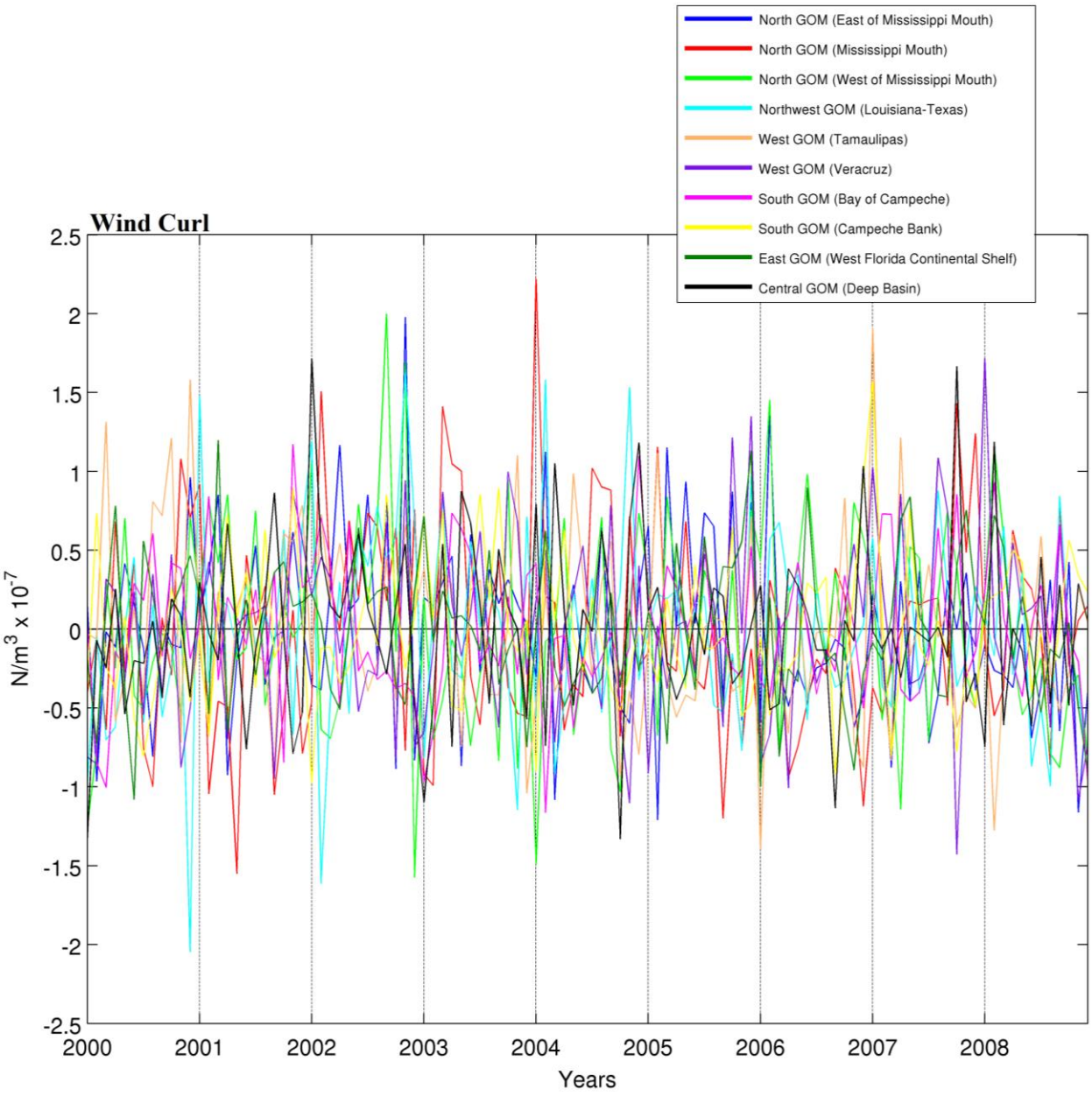


Fig. 4.12 Time series of box-averaged monthly wind curl anomalies for the period of 2000-2008. Each colored line corresponds to a regional box (Fig. 4.3).

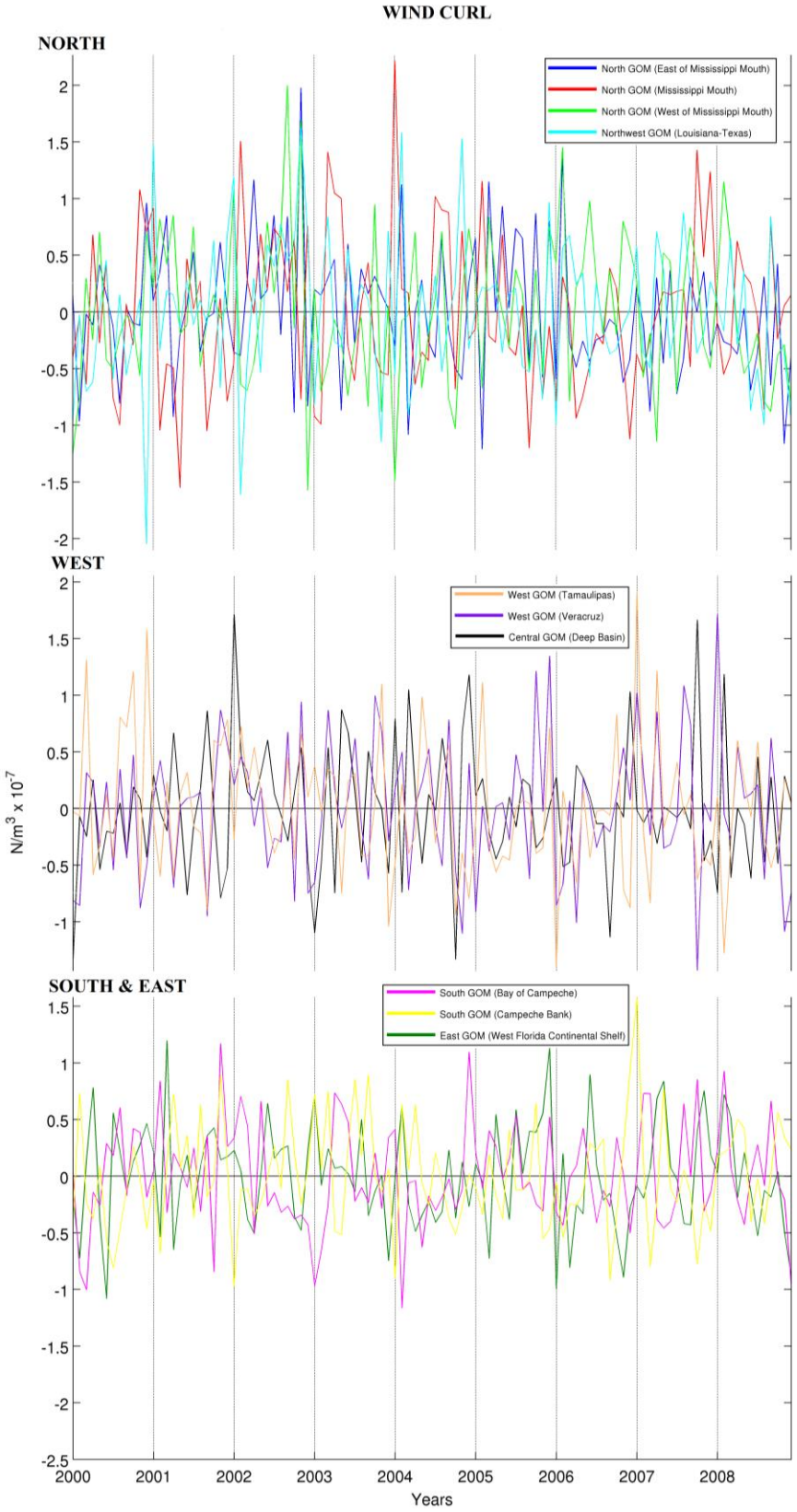


Fig. 4.13 Time series of box-averaged monthly wind curl anomalies displayed based on regional location.

Table 4.5 Correlation coefficients between the regional areas listed for the wind curl (Fig. 4.12). In parenthesis are the 95% significance levels for the correlations. Significant correlations are indicated with bold numbers.

| | East of Mississippi Mouth | Mississippi Mouth | West of Mississippi Mouth | Louisiana-Texas | Tamaulipas | Veracruz | Bay of Campeche | Campeche Bank | West Florida Cont. Shelf | Deep Basin |
|---|---|---|---|---|---|---|---|---|---|---|
| East of Mississippi Mouth | - | -0.0398 (0.2006) | **0.3653** (0.2240) | 0.1409 (0.2165) | **0.2328** (0.2238) | **0.2642** (0.2120) | -0.0563 (0.1827) | 0.0178 (0.1936) | 0.1794 (0.1948) | -0.2143 (0.2213) |
| Mississippi Mouth | | - | **-0.2215** (0.2089) | 0.0357 (0.1893) | 0.0469 (0.1882) | -0.0339 (0.1947) | 0.0777 (0.1949) | -0.1414 (0.2287) | 0.0734 (0.1835) | 0.1448 (0.1972) |
| West of Mississippi Mouth | | | - | 0.1724 (0.2107) | -0.0942 (0.1732) | 0.1151 (0.1957) | 0.0860 (0.1997) | 0.1030 (0.2018) | 0.0958 (0.1977) | 0.1889 (0.2223) |
| Louisiana-Texas | | | | - | -0.0328 (0.1967) | 0.1796 (0.2094) | -0.1056 (0.1807) | 0.1502 (0.1806) | 0.0737 (0.2099) | 0.0589 (0.2005) |
| Tamaulipas | | | | | - | **0.4050** (0.2295) | **-0.2088** (0.1867) | 0.1076 (0.1889) | 0.1119 (0.2141) | -0.2074 (0.2118) |
| Veracruz | | | | | | - | **0.1967** (0.1886) | 0.1370 (0.1979) | 0.0942 (0.2123) | -0.1006 (0.2179) |
| Bay of Campeche | | | | | | | - | **-0.2628** (0.2065) | -0.0413 (0.1847) | **0.3074** (0.1983) |
| Campeche Bank | | | | | | | | - | -0.0384 (0.2007) | -0.0339 (0.1895) |
| West Florida Cont. Shelf | | | | | | | | | - | -0.0405 (0.2071) |
| Deep Basin | | | | | | | | | | - |

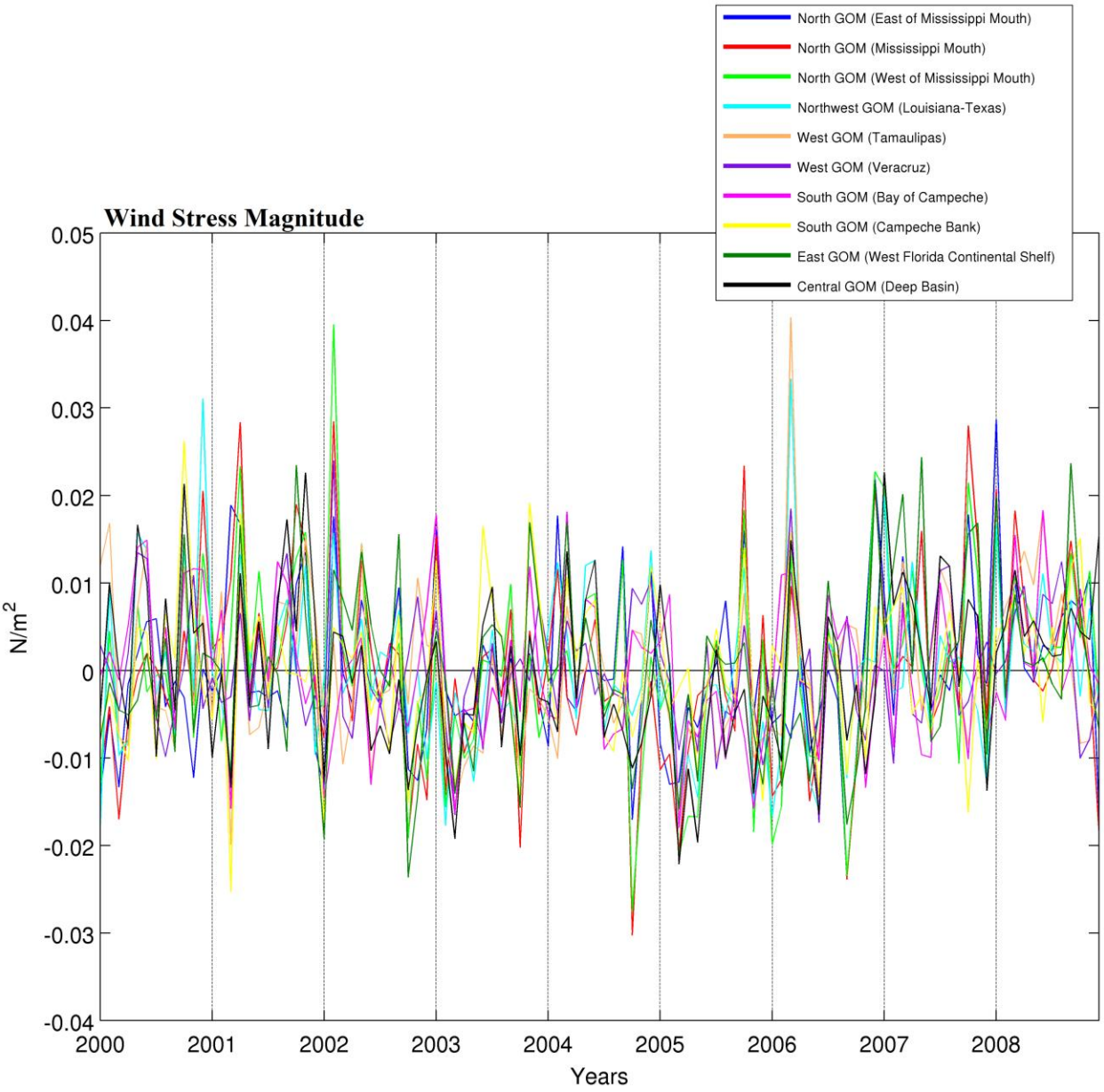


Fig. 4.14 Time series of box-averaged monthly wind stress magnitude anomalies for the period of 2000-2008. Each colored line corresponds to a regional box (Fig. 4.3).

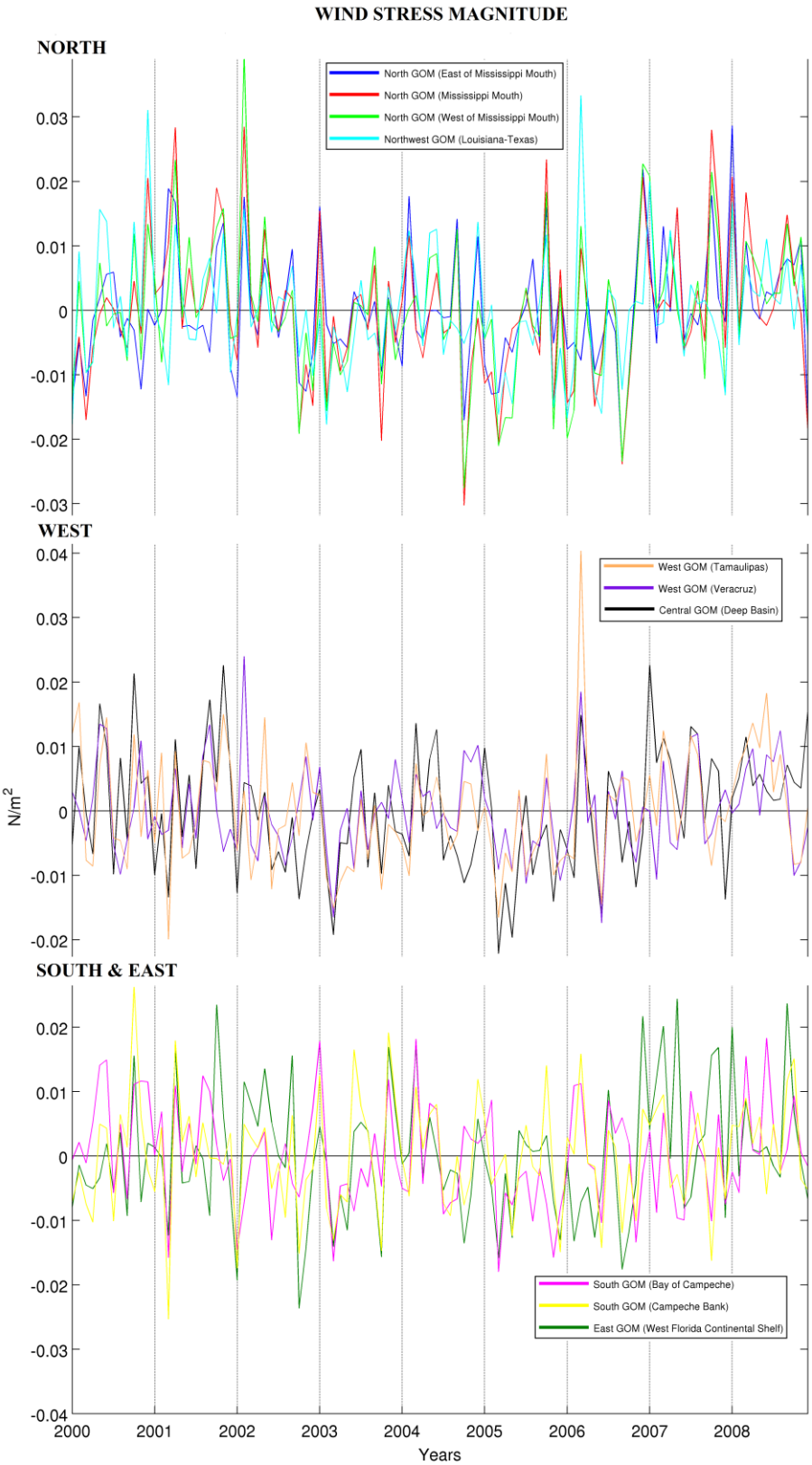


Fig. 4.15 Time series of box-averaged monthly wind stress magnitude anomalies displayed based on regional location.

Table 4.6 Correlation coefficients between the regional areas listed for the wind stress magnitude plot (Fig. 4.14). In parenthesis are the 95% significance levels for the correlations. Significant correlations are indicated with bold numbers.

| | East of Mississippi Mouth | Mississippi Mouth | West of Mississippi Mouth | Louisiana-Texas | Tamaulipas | Veracruz | Bay of Campeche | Campeche Bank | West Florida Cont. Shelf | Deep Basin |
|---|---|---|---|---|---|---|---|---|---|---|
| East of Mississippi Mouth | - | **0.8151** (0.2527) | **0.6917** (0.2418) | **0.4133** (0.2190) | 0.0336 (0.2028) | 0.0414 (0.1875) | -0.0260 (0.2015) | **0.2390** (0.2018) | **0.6376** (0.2276) | **0.2190** (0.1981) |
| Mississippi Mouth | | - | **0.8762** (0.2770) | **0.5805** (0.2413) | **0.2339** (0.2149) | 0.1441 (0.2012) | 0.1155 (0.2056) | **0.3495** (0.1988) | **0.6542** (0.2390) | **0.4149** (0.2330) |
| West of Mississippi Mouth | | | - | **0.6996** (0.2415) | **0.3339** (0.2148) | **0.2276** (0.1883) | 0.1884 (0.2077) | **0.4021** (0.2051) | **0.6161** (0.2329) | **0.5976** (0.2491) |
| Louisiana-Texas | | | | - | **0.5761** (0.2122) | **0.3599** (0.2009) | **0.4308** (0.2257) | **0.4605** (0.2272) | **0.4124** (0.2231) | **0.6250** (0.2262) |
| Tamaulipas | | | | | - | **0.6175** (0.2252) | **0.5628** (0.2265) | **0.4277** (0.2069) | **0.1989** (0.1935) | **0.6111** (0.2283) |
| Veracruz | | | | | | - | **0.5030** (0.2303) | **0.3171** (0.2035) | 0.0602 (0.1804) | **0.3750** (0.1986) |
| Bay of Campeche | | | | | | | - | **0.5180** (0.2217) | **0.2487** (0.2014) | **0.6019** (0.2337) |
| Campeche Bank | | | | | | | | - | **0.5841** (0.2209) | **0.6039** (0.2277) |
| West Florida Cont. Shelf | | | | | | | | | - | **0.4872** (0.2181) |
| Deep Basin | | | | | | | | | | - |

Table 4.7 Standard deviations for each long-term time series seen in Figures 4.4, 4.6, 4.8, 4.10, 4.12, and 4.14 within in each regional box (Fig. 4.3).

| | Chlorophyll (log-mg/$m^3$) | Wind Speed (m/s) | Zonal Wind Stress ($N/m^2$) | Meridional Wind Stress ($N/m^2$) | Wind Curl ($N/m^3$ x $10^{-7}$) | Wind Stress Magnitude ($N/m^2$) |
|---|---|---|---|---|---|---|
| East of Mississippi Mouth | 0.1408 | 0.7335 | 0.0106 | 0.0106 | 0.5766 | 0.0091 |
| Mississippi Mouth | 0.1152 | 0.7532 | 0.0107 | 0.0123 | 0.6800 | 0.0111 |
| West of Mississippi Mouth | 0.1033 | 0.6491 | 0.0104 | 0.0119 | 0.6525 | 0.0109 |
| Louisiana-Texas | 0.0949 | 0.6491 | 0.0085 | 0.0117 | 0.6327 | 0.0094 |
| Tamaulipas | 0.0797 | 0.6545 | 0.0079 | 0.0130 | 0.5955 | 0.0089 |
| Veracruz | 0.0741 | 0.6307 | 0.0076 | 0.0101 | 0.5849 | 0.0071 |
| Bay of Campeche | 0.0708 | 0.5054 | 0.0080 | 0.0084 | 0.4556 | 0.0080 |
| Campeche Bank | 0.0679 | 0.5698 | 0.0080 | 0.0094 | 0.4598 | 0.0086 |
| West Florida Continental Shelf | 0.0696 | 0.7361 | 0.0099 | 0.0084 | 0.4534 | 0.0099 |
| Deep Basin | 0.0505 | 0.6220 | 0.0090 | 0.0100 | 0.5430 | 0.0094 |

4.5 Associations between chlorophyll and winds

To investigate the associations between the non-seasonal variability of chlorophyll and wind forcing the temporal correlations between the regional chlorophyll indices of Figure 4.4 and those corresponding to the wind variables of Figures 4.6, 4.8, 4.10, 4.12, and 4.14 are presented in Table 4.8. Correlations that are significant for 95% confidence are in bold fonts. Non-seasonal anomalies of chlorophyll are significantly correlated with those of wind speed in the Campeche Bank (yellow), Bay of Campeche (pink), and the West Florida continental shelf (dark green). Chlorophyll is significantly correlated with zonal wind stress only in the Mississippi River mouth region (red). The larger number of index regions with significant correlations correspond to chlorophyll and meridional wind stress, namely the Bay of Campeche (pink), Tamaulipas (orange), westward of the Mississippi mouth (light green), and the West Florida continental shelf (dark green). Chlorophyll is not significantly correlated to wind stress curl in any of the Gulf index regions. The marginal significant correlation between chlorophyll and wind stress magnitude in the Campeche Bank is most likely resulting from the chlorophyll-wind speed correlation in that region, since there is no physical mechanism directly associated with the magnitude of the wind stress. Thus, associations between chlorophyll and wind stress curl or between chlorophyll and wind stress magnitude were not pursued further.

Following the correlation analysis, SVD analysis was applied to the combined fields of chlorophyll-wind speed, chlorophyll-zonal wind stress, and chlorophyll-meridional wind stress, with the purpose of extracting coupled patterns of non-seasonal co-variability. The leading chlorophyll-wind speed SVD of non-seasonal coupled variability accounted for 50% of the cross-covariance is in Figure 4.16. The chlorophyll space pattern (Fig. 4.16A, color contours) has large loadings in coastal and shelf areas around the Gulf. The wind speed space pattern

(Fig. 4.16A, line contours) has increasing loadings from nearly zero in the west to maximum values in the east. Consistent with the correlation analysis, both chlorophyll and wind speed patterns have moderate to large loadings in the Campeche Bank, Bay of Campeche, and West Florida continental shelf. The time series of the first chlorophyll-wind speed SVD in Figure 4.16B captures the close association between the temporal variability of these coupled patterns as well as their intraseasonal and interannual character. The interpretation is that non-seasonal wind fluctuations in those regions drive surface chlorophyll variability through upward turbulent mixing of nutrients.

The leading chlorophyll-zonal wind stress SVD of non-seasonal coupled variability accounting for 59% of the cross-covariance is in Figure 4.17. The chlorophyll space pattern (Fig. 4.17A, color contours) has a dipole between the area of the Mississippi mouth and Florida panhandle and that of the western Gulf shelf. The zonal wind stress pattern (Fig. 4.17A, line contours) has an increase in loadings from the southwest to the northeast gulf. The correspondence of positive loadings around the Mississippi mouth is consistent with the significant correlation between chlorophyll and zonal wind stress found in that region in the correlation analysis. Assessing the consistency between the SVD and correlation analysis in the western Gulf is not possible because the western lobe of the non-seasonal chlorophyll dipole does not coincide with any of the index regions in Figure 4.3. The temporal variability of these non-seasonal coupled patterns (Fig. 4.17B) includes intraseasonal as well as interannual periodicities. The interpretation of this chlorophyll-zonal wind stress non-seasonal SVD is similar to the corresponding SVD of the seasonal cycle analysis (Chapter 3, this dissertation). Namely, non-seasonal strengthening (weakening) of the easterly winds in the northern Gulf drive increases (decreases) of chlorophyll in the western Gulf shelf and decreases (increases) in the

northern/northeastern Gulf. The mechanism is the horizontal advection of Mississippi River nutrient-rich waters by the zonal winds.

The leading chlorophyll-meridional wind stress SVD of non-seasonal coupled variability accounting for 59% of the cross-covariance is in Figure 4.18. The chlorophyll space pattern (Fig. 4.18A, color contours) has larger loadings in the northern and western Gulf and in the Bay of Campeche. The meridional wind stress pattern (Fig. 4.18A, line contours) has northerly wind anomalies over the entire Gulf but with a strong meridional jet-like structure over the longitudes of the Mississippi mouth and a smaller regional maximum in the western Gulf. In the northern Gulf, the chlorophyll anomalies have a dipole structure with positive/negative loadings to the west/east of the Mississippi River mouth. The temporal expansion coefficients of the first chlorophyll-meridional wind stress SVD has intraseasonal and interannual fluctuations similarly to the chlorophyll-wind speed and chlorophyll-zonal wind stress coupled patterns. The chlorophyll dipole could be interpreted as westward Ekman transport, by the northerly anomaly wind jet centered on those longitudes, of Mississippi high chlorophyll waters from the east to the west flanks of the river mouth. The high positive chlorophyll loadings in the western Gulf may be related to advection of Mississippi River waters from the north by the northerly anomalous winds. The positive chlorophyll loadings in the Bay of Campeche may be related to coastal upwelling driven by the northerly winds. The chlorophyll-meridional wind stress SVD analysis is in general consistent with the correlation analysis with the four regions (Bay of Campeche, western Gulf, northern Gulf, and West Florida continental shelf) with significant correlations in that analysis (Table 4.8) corresponding to areas with moderate to large loadings in the leading SVD patterns of Figure 4.18A.

Table 4.8 Correlation coefficients between the variables listed (Figs. 4.6, 4.8, 4.10, 4.12, 4.14) when compared to the chlorophyll time series plot (Fig. 4.4). In parenthesis are the 95% significance levels for the correlations. Significant correlations are indicated with bold numbers.

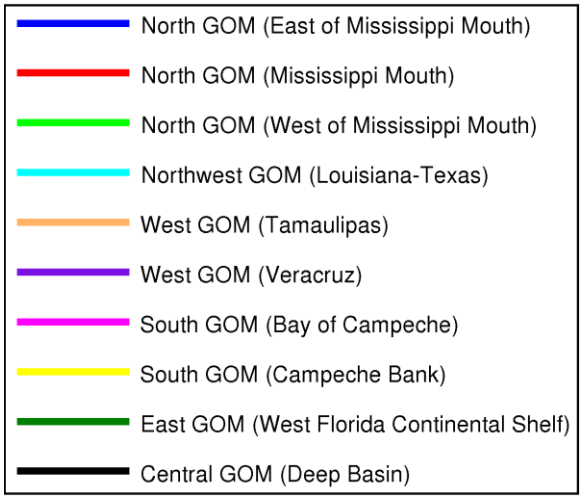


| | East of Mississippi Mouth | Mississippi Mouth | West of Mississippi Mouth | Louisiana-Texas | Tamaulipas | Veracruz | Bay of Campeche | Campeche Bank | West Florida Continental Shelf | Deep Basin |
|---|---|---|---|---|---|---|---|---|---|---|
| Wind Speed | 0.15 (0.20) | -0.01 (0.22) | 0.07 (0.24) | 0.22 (0.23) | 0.00 (0.21) | 0.19 (0.20) | **0.29** (0.22) | **0.25** (0.21) | **0.20** (0.19) | 0.03 (0.21) |
| Zonal Stress | 0.20 (0.21) | **0.26** (0.22) | 0.14 (0.23) | 0.02 (0.20) | 0.10 (0.21) | 0.10 (0.21) | -0.10 (0.21) | -0.11 (0.21) | 0.12 (0.20) | 0.13 (0.21) |
| Meridional Stress | -0.02 (0.20) | -0.11 (0.19) | **-0.23** (0.20) | 0.04 (0.19) | **-0.26** (0.23) | -0.21 (0.21) | **-0.25** (0.22) | -0.13 (0.19) | **-0.24** (0.21) | -0.11 (0.20) |
| Wind Curl | -0.01 (0.16) | -0.02 (0.21) | -0.10 (0.22) | 0.06 (0.17) | -0.03 (0.16) | 0.06 (0.18) | 0.18 (0.20) | 0.03 (0.23) | 0.05 (0.21) | -0.04 (0.17) |
| Wind Stress Magnitude | 0.06 (0.20) | -0.03 (0.22) | -0.04 (0.25) | 0.07 (0.22) | -0.11 (0.21) | 0.10 (0.20) | 0.21 (0.22) | **0.22** (0.21) | 0.04 (0.20) | -0.09 (0.21) |

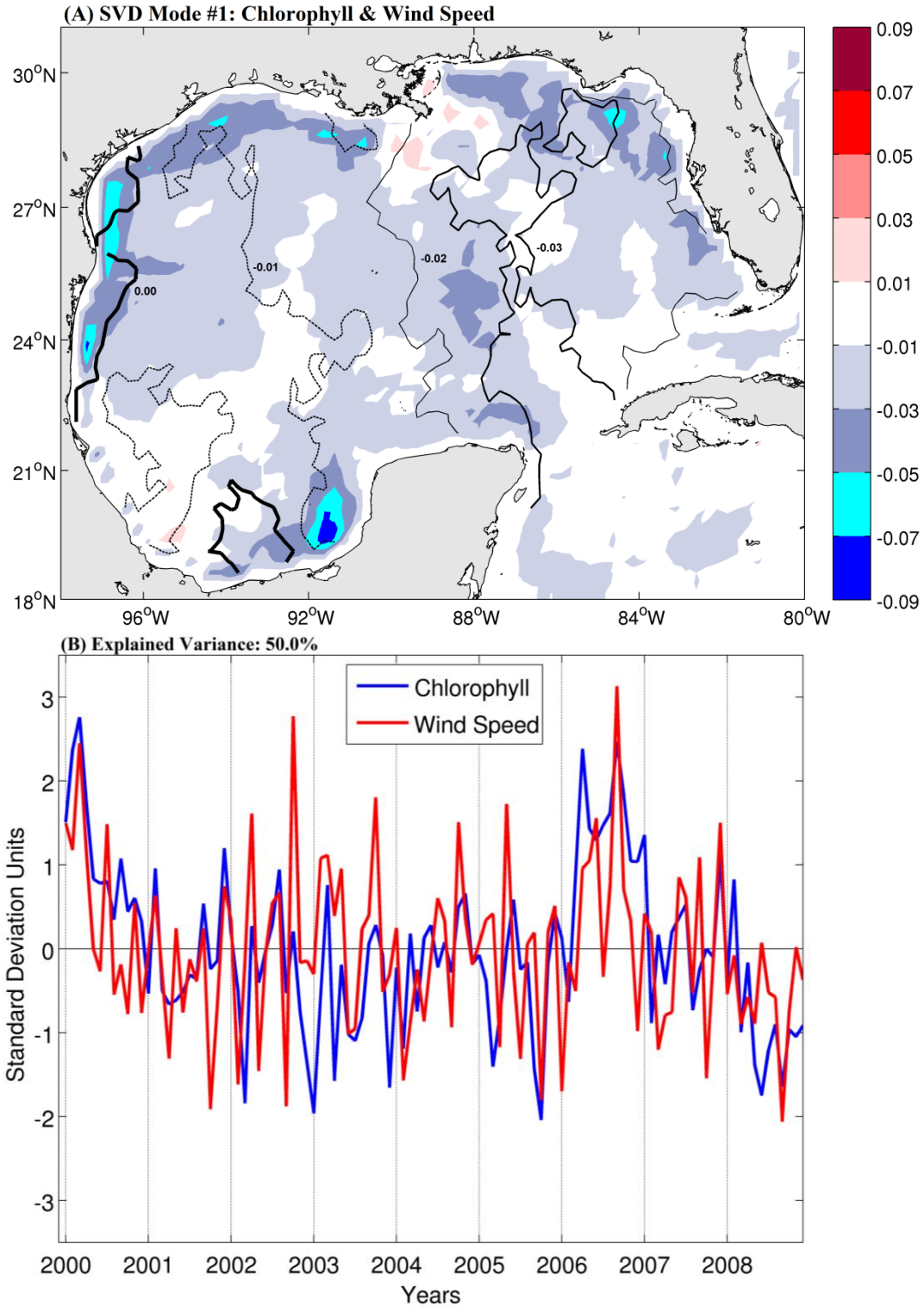


Fig. 4.16 (A) Spatial patterns of the first leading mode of a coupled SVD analysis for chlorophyll-*a* (color contours) and wind speed ( line contours). (B) The 9-year (2000-2008) time series of chlorophyll (blue) and wind speed (red) of expansion coefficients with the total square covariance accounting for 50% of the total variance.

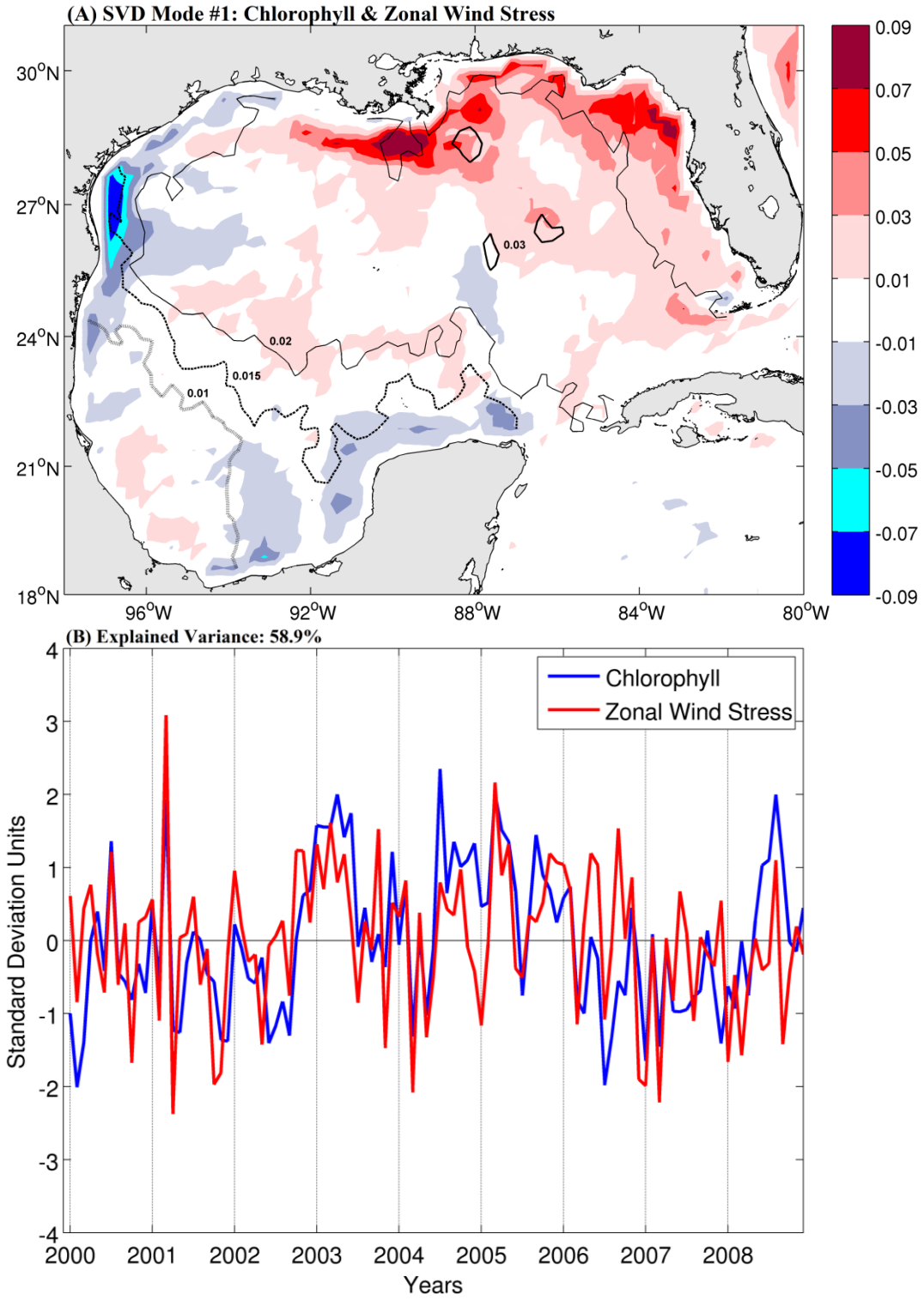


Fig. 4.17 (A) Spatial patterns of the first leading mode of a coupled SVD analysis for chlorophyll-*a* (color contours) and zonal wind stress (line contours). (B) The 9-year (2000-2008) time series of chlorophyll (blue) and zonal wind stress (red) of expansion coefficients with the total square covariance accounting for 58.9% of the total variance.

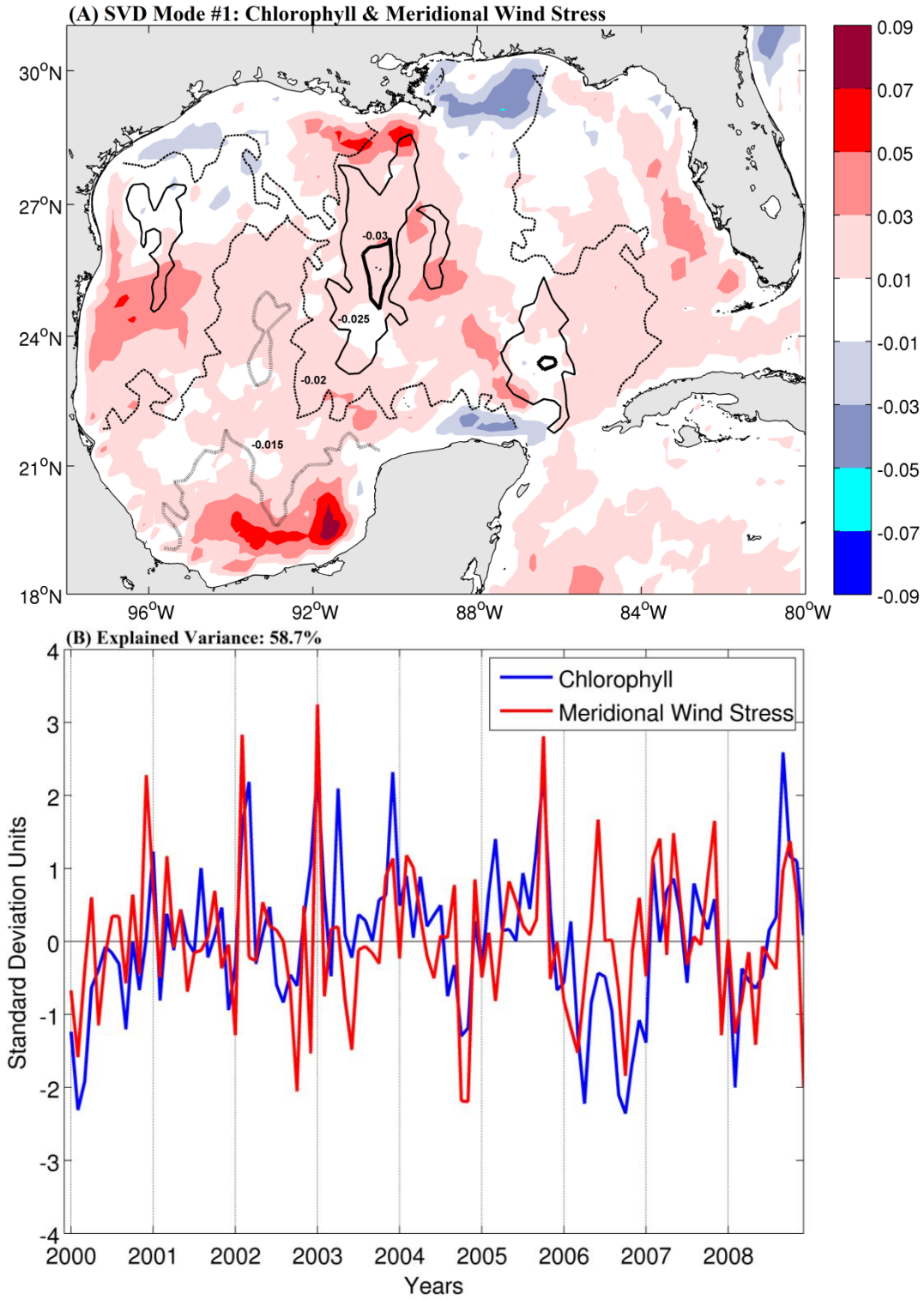


Fig. 4.18 (A) Spatial patterns of the first leading mode of a coupled SVD analysis for chlorophyll-*a* (color contours) and meridional wind stress (line contours). (B) The 9-year (2000-2008) time series of chlorophyll (blue) and meridional wind stress (red) of expansion coefficients with the total square covariance accounting for 58.7% of the total variance.

Discussion

The Mississippi River provides large fluxes of freshwater and associated dissolved particulate materials into the northern Gulf of Mexico (Lohrenz et al. 1999). The annual mean transport of Mississippi River water is westward towards the Louisiana-Texas shelf because of prevalent easterly wind conditions (e.g., Schiller et al. 2011, Chapter 3, this dissertation). Easterly winds predominate in the spring, fall and winter making the Louisiana-Texas shelf the most frequent plume pathway. Eastward plume transport is observed when persistent southerly southwesterly winds develop at the end of spring and during the summer. Westerly winds in the winter and fall can also induce eastward plume transport, but these have short durations because they are associated with intraseasonal variability (i.e., cold fronts) and not with the seasonal cycle of the wind field (Schiller et al. 2011). These intraseasonal fluctuations of the Mississippi River plume contribute to large non-seasonal chlorophyll variability in the northern Gulf (Fig. 4.1).

In this study, correlation and SVD analyses were used to investigate the association between non-seasonal surface chlorophyll and wind forcing in the Gulf of Mexico. The datasets used are the GlobColour merged ocean color product and QuikSCAT Level 3 data over a 9-year period (2000-2008). Results for the first mode of the coupled SVD analysis were 50% explained co-variability (chlorophyll and wind speed); 58.9% (chlorophyll and zonal wind stress); and 58.7% (chlorophyll and meridional wind stress). The fraction of cross-covariance explained by the leading modes of our SVD applications is comparable to those of other studies. For example, the leading SVD of South Atlantic sea surface temperature (SST) and sea level pressure (SLP) of Venegas et al. (1997) using 40 years of the Comprehensive Ocean-Atmosphere Data Set explained 63% of the cross-covariance, the fraction of the covariance between the two fields.

Similarly, Sterl and Hazeleger (2003) repeated the Venegas et al. (1997) SVD calculation but using 52 years of NCEP/NCAR reanalysis data of SST and SLP to find a leading mode that explained 38% of the cross-covariance. The main findings of this study are:

1) Increases (decreases) in non-seasonal wind speed anomalies are associated with non-seasonal increases (decreases) in surface chlorophyll over the Campeche Bank, Bay of Campeche, and West Florida continental shelf areas. The proposed mechanism for these associations is upward entrainment of nutrients by turbulent mixing.
2) Strengthening (weakening) of non-seasonal zonal easterly wind anomalies are associated with westward (eastward) movement of the Mississippi plume and the creation of positive (negative) non-seasonal chlorophyll anomalies in the western (northern) Gulf. This anomalous non-seasonal chlorophyll dipole pattern is similar to the seasonal dipole pattern (Chapter 3, this dissertation).
3) Northerly (southerly) non-seasonal meridional wind anomalies were associated with coastal upwelling (downwelling) in the Bay of Campeche shelf, offshore (inshore) advection of chlorophyll in the western Gulf, and an anomalous chlorophyll dipole pattern across the Mississippi River mouth with positive (negative) chlorophyll anomalies to the west and negative (positive) anomalies to the east.
4) The temporal character of the non-seasonal coupled patterns of chlorophyll and wind forcing is predominantly intraseasonal and coherent over large spatial scales although interannual modulations are also apparent.
5) No associations were found for non-seasonal anomalies of chlorophyll and wind stress curl indicating that Ekman pumping is not a significant driver of non-seasonal surface chlorophyll anomalies.

For the positive non-seasonal chlorophyll anomalies in the Tamaulipas region of the western Gulf, I suggested an association with advection of nutrient-rich Mississippi River waters from the north by anomalous northerly winds. For this mechanism to hold true, an offshore advection of chlorophyll between 24° and 26°N in Figure 12A needs to be invoked. Interestingly, Walker (2005) used satellite-tracked drifting buoys to investigate the wind and eddy-related processes in the northwestern Gulf of Mexico and detected a major pathway for the seaward transport of inner shelf water near 25°N during December 1993 and January 1994 (their plate 1b and Fig. 4a). She suggested wind stress or convergence of shelf flows as possible mechanisms for this cross-shore transport. In addition, Martínez-López and Zavala-Hidalgo (2009) presented evidence for an offshore transport of chlorophyll-rich waters in that region during May 2007 (their Fig. 13). While the most energetic northerly wind events and offshore chlorophyll transport in their Figure 12B occur during the winter, these events can be seen in other seasons.

References

Björnsson H, Venegas SA (1997) A manual for EOF and SVD analyses of climate data. McGill University, CCGCR Report No. 97-1, Montreal, Quebec, 52 pp

Campbell JW (1995) The lognormal distribution as a model for bio-optical variability in the sea. J Geophys Res 100:13237-13254

Davis RE (1976) Predictability of sea surface temperature and sea level pressure anomalies over the North Pacific Ocean. J Phys Oceanogr 6:249-266

Deser C, Blackmon ML (1993) Surface climate variations over the North Atlantic Ocean during winter: 1900-1989. J Climate 6:1743-1753

Enfield DB, Mayer DA (1997) Tropical Atlantic SST variability and its relation to El Niño-Southern Oscillation. J Geophys Res 102:929-945

Fang Z, Wallace JM (1994) Arctic sea ice variability on a timescale of weeks and its relation to atmospheric forcing. J Climate 7:1897-1913

Goldenberg SB, O'Brien JJ (1981) Time and space variability of tropical Pacific wind stress. Mon Wea Rev 109:1190-1207

Lanzante JR (1984) A rotated eigenanalysis of the correlation between 700 mb heights and sea surface temperature in the Pacific and Atlantic. Mon Wea Rev 112:2270-2280

Large WG, McWilliams JC, Doney SC (1994) Oceanic vertical mixing: A review and a model with a nonlocal boundary layer parameterization. Rev Geophys 32:363-403

Large WG, Pond S (1981) Open ocean momentumm flux measurements in moderate to strong winds. J Phys Oceangr 11:324-336

Large WG, Pond S (1982) Sensible and latent heat flux measurements over the ocean. J Phys Oceangr 12:464-482

Lohrenz SE, Fahnenstiel GL, Redalje DG, Lang GA, Dagg MJ, Whitledge TE, Dortch Q (1999) Nutrients, irradiance, and mixing as factors regulating primary production in coastal waters impacted by the Mississippi River plume. Cont Shelf Res 19:1113-1141

Maritorena S, Siegel DA, Peterson A (2002) Optimization of a semi-analytical ocean color model for global scale applications. Appl Opt 41:2705-2714

Maritorena S, Siegel DA (2005) Consistent merging of satellite ocean color data sets using a bio-optical model. Remote Sensing Env 94:429-440

Martínez-López B, Zavala-Hidalgo J (2009) Seasonal and interannual variability of cross-shelf transports of chlorophyll in the Gulf of Mexico. J Mar Sys 77:1-20

Müller-Karger FE, Walsh JJ, Evans RH, Meyers MB (1991) On the seasonal phytoplankton concentration and sea surface temperature cycles of the Gulf of Mexico as determined by satellites. J Geophys Res 96:12,645-12,665

Peng S, Fyfe J (1996) The coupled patterns between sea level pressure and sea surface temperature in the midlatitude North Atlantic. J Climate 9:1824-1839

Risien CM, Chelton DB (2008) A global climatology of surface wind and wind stress fields from 8 years of QuikSCAT scatterometer data. J Phys Oceangr 38:2379-2413

Schiller RV, Kourafalou VH, Hogan P, Walker ND (2011) The dynamics of the Mississippi River plume: Impact of topography, wind and offshore forcing on the fate of the plume waters. J Geophys Res 116:C06029, doi:10.1029/2010JC006883

Sterl A, Hazeleger W (2003) Coupled variability and air-sea interaction in the South Atlantic Ocean. Clim Dynam 21:559-571

Venegas SA, Mysak LA, Straub DN (1997) Atmosphere-ocean coupled variability in the South Atlantic. 10:2904-2920

Walker ND (2005) Wind and eddy-related shelf/slope circulation processes and coastal upwelling in the northwestern Gulf of Mexico. In: Sturges W, Lugo-Fernandez A (eds) Circulation in the Gulf of Mexico: observations and models. American Geophysical Union, Washington, DC, p 295-313

Wallace JM, Smith C, Jiang QR (1990) Spatial patterns of atmosphere-ocean interaction in the northern winter. J Climate 3:990-998

## SUMMARY

This dissertation characterizes the individual and coupled variability of surface chlorophyll and wind forcing on a seasonal and non-seasonal basis in the Gulf of Mexico.

Large fluctuations of the overall variability of surface chlorophyll were observed on the shelf or near the shelf break. For the seasonal analysis, chlorophyll "hotspots" exist on the West Florida continental shelf, the Mississippi River mouth, the Tamaulipas Shelf, and the Bay of Campeche. The most remarkable feature of the seasonal chlorophyll variability is an annual "seesaw" (dipole) pattern between the two extremes of the annual mean Mississippi River plume that is associated with simultaneous annual changes in the zonal wind stress. Strengthening of the zonal easterly winds during the winter is associated with increases in chlorophyll over the Western Shelf and decreases of chlorophyll near the Mississippi mouth. The opposite seasonal changes of chlorophyll and zonal winds occur during the summer. A similar relationship was observed during the non-seasonal analysis. Strengthening (weakening) of non-seasonal zonal easterly wind anomalies are associated with westward (eastward) movement of the Mississippi plume and the creation of positive (negative) non-seasonal chlorophyll anomalies in the western (northern) Gulf. The seasonal and non-seasonal dipoles appear to be driven by the zonal winds, however, bio-physical simulations would be needed to confirm these and other statistical relationships proposed in this study.

In the interior basin, the seasonal variability of chlorophyll has lower values during the summer and higher values during the winter. These annual fluctuations of chlorophyll are in phase with the seasonal cycle of wind speed (i.e., summer weakening and winter strengthening) over the Gulf. Wind speed can be considered as a proxy directly related to turbulent mixing, mixed layer depth, and entrainment of nutrients at the bottom of the mixed layer. Thus, this

direct seasonal association between chlorophyll and wind speed may be interpreted as increased (decreased) turbulent mixing/mixed layer depth during winter (summer). For non-seasonal wind speed, increases (decreases) in anomalies are associated with non-seasonal increases (decreases) in surface chlorophyll over the Campeche Bank, Bay of Campeche, and West Florida continental shelf areas. The proposed mechanism for these associations is upward entrainment of nutrients by turbulent mixing. Overall, wind speed is a factor for interior waters on a seasonal scale, but for shelf areas on a non-seasonal scale.

Meridional winds are important on a non-seasonal basis. Northerly (southerly) meridional wind anomalies are associated with coastal upwelling (downwelling) in the Bay of Campeche shelf and offshore (inshore) advection of chlorophyll in the western Gulf. A notable anomalous chlorophyll dipole pattern across the Mississippi River mouth with positive (negative) non-seasonal chlorophyll anomalies to the west and negative (positive) anomalies to the east results from northerly (southerly) non-seasonal wind anomalies. Although the mean zonal winds (trade winds) predominate in the Gulf of Mexico, it is the variability in the meridional winds that is more effective in driving localized changes in chlorophyll through associated ocean dynamics.

I have successfully applied the GlobColour merged satellite data product and QuikSCAT satellite winds to help quantify the seasonal and non-seasonal variability of surface phytoplankton biomass in the Gulf of Mexico. The relevant mechanisms driving the variability of phytoplankton biomass in the Gulf are coastal upwelling, horizontal advection, and turbulent vertical mixing. Each of these mechanisms involves the surface wind forcing and their importance in a given region depends on topographic features and atmospheric and oceanic circulation patterns.

Most researchers that use merged satellite color data products apply them on a global scale (e.g., Kahru et al. 2010, Maina et al. 2011, Cole et al. 2012). I have shown the potential success of using merged data on a smaller geographic area, such as the Gulf of Mexico. Previous chlorophyll research in the Gulf has been based on single-sensor data (e.g., SeaWiFS) to account for seasonal and interannual patterns (e.g., Martínez-López and Zavala-Hidalgo 2009, Salmerón-García et al. 2011). This study improves upon these by applying a merged product that provides better data coverage and by investigating the intraseasonal band. Some studies have used the coupled SVD technique to study coupling of oceanic and atmospheric variables on decadal time scales (e.g., Venegas et al. 1997, Sterl and Hazeleger 2003; both used sea surface temperature and sea level pressure). I utilized the SVD approach for nine years of chlorophyll and wind data. Future studies on chlorophyll-wind coupling, as multi-decadal data become available, should allow testing relationships similar to those proposed here on timescales beyond interannual. These future studies should stratify the data seasonally because I found clear differences in the chlorophyll-wind relationships between summer and winter.

References

Cole HS, Henson S, Martin A, Yool A (2012) Mind the gap: The impact of missing data on the calculation of phytoplankton phenology metrics. J Geophys Res 117:C08030, doi:10.1029/2012JC008249

Kahru M, Gille ST, Murtugudde R, Strutton PG, Manzano MS, Wang H, Mitchell BG (2010) Correlations between winds and ocean chlorophyll. J Geophys Res 115:C12040, doi:10.1029/2010JC006500

Maina J, McClanahan TR, Venus V, Ateweberhan M, Madin J (2011) Global gradients of coral exposure to environmental stresses and implications for local management. PLoS One 6:e23064, doi:10.1371/journal.pone.0023064

Martínez-López B, Zavala-Hidalgo J (2009) Seasonal and interannual variability of cross-shelf transports of chlorophyll in the Gulf of Mexico. J Mar Sys 77:1-20

Salmerón-García O, Zavala-Hidalgo J, Mateos-Jasso A, Romero-Centeno R (2011) Regionalization of the Gulf of Mexico from space-time chlorophyll-a concentration variability. Ocean Dynamics 61:439-448

Sterl A, Hazeleger W (2003) Coupled variability and air-sea interaction in the South Atlantic Ocean. Clim Dynam 21:559-571

Venegas SA, Mysak LA, Straub DN (1997) Atmosphere-ocean coupled variability in the South Atlantic. 10:2904-2920